

**UNIVERSIDAD AUTÓNOMA DE BAJA CALIFORNIA
INSTITUTO DE INGENIERÍA**



**MAESTRÍA Y DOCTORADO EN CIENCIAS E INGENIERÍA
ÁREA DE MEDIO AMBIENTE**

**DIFERENCIAS ENTRE LOS AMBIENTES SEDIMENTARIOS DEL
VALLE DE MEXICALI Y GRANÍTICO DE LAS SIERRAS
PENINSULARES DE BAJA CALIFORNIA: ANÁLISIS DE RUIDO Y
ESTRUCTURA DE CORTEZA**

TESIS

que para cubrir los requisitos necesarios para obtener el grado de

DOCTOR EN CIENCIAS

Presenta:

ERIK ESTEBAN RAMÍREZ RAMOS

Mexicali, Baja California, México, 2 de abril de 2019

TESIS DEFENDIDA POR
Erik Esteban Ramírez Ramos

Y APROBADA POR EL SIGUIENTE COMITÉ

Dr. Jorge Ramírez Hernández

Codirector del Comité

Dr. José Antonio Vidal Villegas

Codirector del Comité

Dra. Joann Miriam Stock

Miembro del Comité

Dr. Octavio Lázaro Mancilla

Miembro del Comité

Dr. Antonio González Fernández

Miembro del Comité

Dr. Jaime Alonso Reyes López

Miembro del Comité

Dra. Jesús Eliana Rodríguez Burgueño

Coordinador del Programa MYDCI

2 de abril de 2019

RESUMEN de la tesis de **ERIK ESTEBAN RAMÍREZ RAMOS**, presentada como requisito para la obtención del grado de DOCTOR EN CIENCIAS. Mexicali, Baja California, 2 de abril de 2019.

**DIFERENCIAS ENTRE LOS AMBIENTES SEDIMENTARIOS DEL
VALLE DE MEXICALI Y GRANÍTICO DE LAS SIERRAS
PENINSULARES DE BAJA CALIFORNIA: ANÁLISIS DE RUIDO Y
ESTRUCTURA DE CORTEZA**

Resumen aprobado por:

Dr. Jorge Ramírez Hernández

Codirector de Tesis

Dr. José Antonio Vidal Villegas

Codirector de Tesis

Se realizó un análisis de los niveles de ruido sísmico ambiental a partir de los registros de estaciones sísmicas ubicadas en el norte de Baja California, México. Se utilizaron los datos de las estaciones de la Red Sísmica del Noroeste de México (RESNOM) con el objetivo de caracterizar los espectros de ruido de cada estación. Las estaciones sísmicas están ubicadas en el ambiente sedimentario del Valle de Mexicali (VM) y en el granítico de las Sierras Peninsulares de Baja California (SPBC). El ruido ambiente se caracterizó usando la técnica densidad espectral de potencia (PSD, por sus siglas en inglés) propuesta por Peterson (1993). Se encontró que, a periodos entre 0.1 y 2 s, la mediana de los niveles de ruido (MNLs, por sus siglas en inglés) de estaciones ubicadas en el VM son hasta 25 dB mayores, y cercanas al nuevo modelo de ruido alto (NHNM, por sus siglas en inglés), que las MNLs de estaciones en las SPBC. Para periodos > 2 s, las MNLs son similares para ambas regiones y se encuentran entre el NHNM y el nuevo modelo de ruido bajo. Se encontraron diferencias en los niveles de ruido cuando los sensores sísmicos (diferentes marcas pero mismo ancho de banda) se intercambiaron. Para periodos < 1s, los MNLs calculado a partir de los registros de sensores Gürälps son ~20 dB más altos que los MNLs de sensores Nanometrics; para periodos > 10 s los MNLs de los sensores Nanometrics son ~20 dB más altos que los MNLs de sensores Gürälps. Se observaron variaciones diarias en el ruido de periodo corto, relacionado con la actividad humana, como niveles de ruido alto para periodos > 1 s durante el día en una estación en la ciudad de Mexicali. Al menos en dos Sitios, en y al sur del VM, hay una relación directa en las variaciones de presión atmosférica y temperatura con el ruido sísmico: presión alta y temperatura baja se relacionan con niveles de ruido alto en la banada de los 4 - 8.5 s, y vice versa. Para observar cualquier posible cambio en las velocidades sísmicas que se puedan relacionar con el cambio abrupto en la geología regional (roca granítica con sedimentos) se realizó un estudio de refracción sísmica en la región SPBC-suroeste Laguna Salada (LS). Se instalaron 30 estaciones sísmicas temporales de tres componentes, complementadas con dos estaciones permanentes de seis componentes pertenecientes a RESNOM. Las estaciones, espaciadas ~6 km a lo largo del perfil de refracción, grabaron dos explosiones: la explosión directa realizada al sur

de la ciudad de Ensenada y la explosión reversa al suroeste de LS (dirección suroeste-noreste). Se modelaron los rayos de las dos explosiones (con la teoría asintótica de rayos) para obtener un modelo de onda P a lo largo del perfil de refracción. Los resultados del modelado son los siguientes: en la sección suroeste del perfil se extiende una zona de baja velocidad de ~ 2 km/s entre las profundidades de 0 y 3.5 km; en la Sierra Juárez, la velocidad promedio de onda P es ~ 5.6 km.s entre las profundidades de 0 y 5 km; y en el suroeste de LS existe una capa de baja velocidad de ~ 2.5 km/s entre las profundidades de 0 y 3 km. Se modeló una capa de ~ 6.5 km/s entre los 4 y 12 km en la región Ensenada-Ojos Negros y entre las profundidades de 4 y 8 km bajo el suroeste de LS. Se modeló una zona de velocidad ~ 6.7 km/s, a distancias de 0 a 50 km del perfil, que aparece entre profundidades de 12 y 15 km.

Palabras Clave: Ruido sísmico ambiental, niveles de ruido, densidad espectral de potencia, redes sísmicas, RESNOM, sismómetro, refracción sísmica, modelo de corteza, norte de BC.

ABSTRACT of the thesis presented by **ERIK ESTEBAN RAMÍREZ RAMOS**, in fulfillment of the requirements of the degree of DOCTORATE IN SCIENCE. Mexicali, Baja California, 2 de abril 2019.

**DIFERENCES BETWEEN THE SEDIMENTARY MEXICALI VALLEY
AND THE GRANITICAL PENINSULAR RANGES OF BAJA
CALIFORNIA ENVIRONMENTS: NOISE ANALYSIS AND CRUSTAL
STRUCTURE**

Approved by:

Dr. Jorge Ramírez Hernández

Thesis Advisor

Dr. José Antonio Vidal Villegas

Thesis Advisor

A seismic ambient noise-level analysis was performed from records of seismic stations located in northern Baja California, Mexico. Data from stations of the Northwest Mexico Seismic Network (RESNOM) was used, with the goal to characterize the noise spectrum for each station. The seismic stations are located in the sedimentary environment of the Mexicali Valley (MV) and the granitic Peninsular Ranges of Baja California (PRBC). The ambient seismic noise was characterized using the power spectral density (PSD) technique (Peterson, 1993). It was found that, at periods between 0.1 and 2 s, the median noise levels (MNLs) of stations in the MV are up to 25 dB higher, and near the new high-noise model (NHNM), than MNLs of PRBC stations. For periods > 2 s, the MNLs are similar for both regions and are between the NHNM and new low-noise models. Differences were found in the noise levels when seismic sensors (different brands but same bandwidth) were interchanged. For periods < 1 s, the MNLs computed from records of Güralp sensors are ~20 dB higher than MNLs from Nanometrics sensors; for periods > 10 s the MNLs of Nanometrics sensors are ~20 dB higher than the MNLs from Güralp sensors. It was observed daily variations in short-period noise, related to human activity, such as higher noise levels for periods > 1 s at daylight in a station in the city of Mexicali. At least for two sites, in and south of MV, there is a direct relationship among variations of atmospheric pressure and temperature with seismic noise: high pressure and low temperature are related with high-noise levels in the 4.0 - 8.5 s period band and vice versa. To see any change in seismic velocities that may be associated with an abrupt change in the regional geology (granitic rock in contact with sediments), refraction seismic study was conducted in the PRBC, Mexico-southwestern Laguna Salada (LS) region. There were installed 30 three-component portable seismic stations, supplemented with two permanent six-component stations of RESNOM. The stations, spaced ~6 km along a refraction profile, recorded two blasts; these were the direct shot located to the south of the city of Ensenada and the reverse shot in

the southwestern LS (south-west-northeast direction). Rays from the two blasts were modeled (using asymptotic ray theory) to obtain a *P*-wave velocity model along the refraction profile. The modeling results are as follows: in the southwestern part of the profile a low-velocity zone of ~ 2 km/s exists between the depths of 0 and 3.5 km; in Sierra Juárez, the mean *P*-wave velocity is ~ 5.6 km/s between the depths of 0 and 5 km ; and in southwestern LS, a low-velocity layer of ~ 2.5 km/s exists between the depths of 0 and ~ 3 km. It was also modeled a layer of ~ 6.5 km/s between 4 and 12 km in the Ensenada-Ojos Negros region, and between the depths of 4 and 8 km below the southwestern LS. From a profile distance of 0 to 50 km, a velocity zone of ~ 6.7 km/s appears between the depths of 12 and 15 km.

Keywords: Ambient seismic noise, noise levels, power spectral density, seismic networks, RESNOM, seismometer, seismic refraction, crustal model, northern BC.

Agradecimientos

A Carolina Barajas por su apoyo durante todo el recorrido.

Al doctor Antonio Vidal por su ciega confianza en mí (contra marea) y por su constante guía y apoyo.

Al doctor Jorge Ramírez por confiar en mí y en esta empresa, además de su ferviente apoyo al proyecto.

Al Concejo Nacional de Ciencia y Tecnología (CONACYT) por otorgarme la beca de posgrado número 254218.

Al Instituto de Ingeniería de la Universidad Autónoma de Baja California por apoyar el proyecto doctoral, así como por facilitar el acceso y uso de sus instalaciones.

A la División de Ciencias de la Tierra del CICESE por facilitar el acceso y uso de sus instalaciones.

A los que apoyaron en la instalación y recolección de estaciones sísmicas temporales y permanentes que formaron parte de este estudio: Rogelio Arce, Francisco Méndez, Oscar Gálvez, Luis Orozco, Rogelio Reyes, German Martínez, Miguel Oliver, Leandro John y Martín Pacheco, de la División de Ciencias de la Tierra del CICESE; Frida Cital, Agustín Oropeza, Erick Jonathan Ramírez e Iván Ramrez del Instituto de Ingeniería de la UABC; y Jovanny Morán, del Instituto Tecnológico de Ensenada, Baja California,

México.

A José Acosta Chang, Euclides Ruiz y Gustavo Arellano por prestar equipo sísmico y por apoyar técnicamente con el mismo.

Al Sr. Rafael Barajas por proveer, sin costo, vehículos todo terreno para la instalación, recolección de estaciones sísmicas.

Al personal de Explosivos RIVADA por su apoyo y comprensión durante el proceso de la detonación necesaria para el estudio: Ingeniero Dagguer y Glenda Vázquez.

A las oficinas gubernamentales de los tres ordenes de gobierno que facilitaron los permisos necesarios para realizar el experimento sísmico: SEMARNAT, SEDENA, Gobierno del Estado de Baja California, el Municipio de Mexicali.

A Alejandra Nuñez, Sergio Arregui, Ignacio Méndez y Julia Sánchez, personal técnico de la División de Ciencias de la Tierra del CICESE.

Al Doctor Klaus Bataille de la Universidad de Concepción, Chile, por su contribución al proyecto por medio de una estancia de investigación en dicho país.

Al personal administrativo del Instituto de Ingeniería por su apoyo durante el transcurso doctoral, en especial al Dr. Marcos Coronado.

Contenido

	Página
Resumen en español	i
Resumen en inglés	iii
Dedicatoria	v
Agradecimientos	vi
Contenido	viii
Lista de Figuras	xi
Lista de Tablas	xiii
I. Introducción	1
I.1 Planteamiento del problema	1
I.1.1 Marco Geológico: Sierras Peninsulares de Baja California y Provincia Extensional del Golfo	1
I.1.2 Evaluación del funcionamiento de la red sísmica local	3
I.1.3 Modelo de estructura de velocidades apropiado para el norte de BC	4
I.2 Justificación	6
I.2.1 Niveles de ruido sísmico ambiental de las estaciones del norte de BC	6
I.2.2 Modelos de estructura de velocidades de corteza para el norte de BC	7
I.3 Objetivos	7
I.3.1 Objetivos generales	7
I.3.2 Objetivos particulares	8
I.4 Hipótesis	8
I.5 Responsabilidades de autorías en artículos	9
I.5.1 Artículo: <i>Seismic Noise Levels in Northern Baja California, Mexico</i>	9
I.5.2 Artículo: <i>A Crustal Velocity Model for the Peninsular Ranges of Baja California and Southwestern Laguna Salada, México.</i>	10
I.6 Revisión bibliográfica	11
I.6.1 Ruido sísmico ambiental del norte de BC	11
I.6.2 Estudios de refracción sísmica en el norte de BC	11
II. Presentación del estudio	14

Contenido (continuación)

	Página
II.1 Resultados: Niveles de ruido sísmico ambiental del norte de BC	14
II.2 Resultados: Modelo de estructura de corteza para el norte de BC	19
REFERENCIAS	22
III. Anexo 1: Seismic Noise Levels in Northern Baja California, Mexico	27
III.1 Introduction	29
III.2 Characteristics of the Instrumentation	30
III.3 Noise Data Processing	31
III.4 Noise Level Analysis	33
III.4.1 Short-Period Noise Analysis	35
III.4.2 Microseismic Noise Analysis	36
III.4.3 Meteorological Related Noise Levels	38
III.5 Conclusions	41
III.6 Data and Resources	42
III.7 Acknowledgments	43
III.8 Bibliography	44
III.9 Mailing Address	47
III.10 Tables	49
III.11 Figure Captions	50
III.12 Figures	53
III.13 Description of the Electronic Supplement	61
III.13.1 List of Figure Captions	61
III.13.2 Electronic Figures	61
IV. Anexo 2: Crustal Velocity Model, Refraction, Northern Baja California	63
IV.1 INTRODUCTION	65
IV.2 INSTRUMENTATION AND DATA	66
IV.3 DATA REDUCTION	67
IV.4 INTERPRETED PHASES	68
IV.5 MODELING TRAVEL TIMES AND AMPLITUDES	70
IV.5.1 Methodology	70
IV.5.2 Modeling Results	71
IV.6 DISCUSSION	73
IV.7 CONCLUSIONS	74
IV.8 DATA AND RESOURCES	76
IV.9 ACKNOWLEDGMENTS	76
IV.10 REFERENCES	77
IV.11 MAILING ADDRESS	82
IV.12 TABLES	84

Contenido (continuación)

	Página
IV.13 FIGURE CAPTIONS	85
IV.14 FIGURES	89

Lista de Figuras

Figura	Página
1 Mapa que muestra las dos principales provincias geológicas del norte de BC y la interacción entre las placas tectónicas del Pacífico y de Norteamérica (recuadro). El mapa detallado indica las fallas principales (líneas rojas, obtenidas de Seiler <i>et al.</i> (2010)). Los círculos grises indican la sismicidad $M \geq 3.5$, desde 1990 hasta la fecha, registrada por RESNOM. Las estaciones sísmicas permanentes de RESNOM son: Triángulos negros, sensores Güralf; triángulos invertidos verdes, sensores Nanometrics. Las estaciones meteorológicas de CONAGUA se representan por diamantes morados. El círculo negro indica la boyta Point Loama (46323). La estrella blanca es el sismo El Mayor-Cucapah del 4 de abril de 2010 $M_W 7.2$. Estudios previos de refracción sísmica son indicados como: Línea morada (Nava y Brune (1982)); línea azul (Nuñez Cornú <i>et al.</i> (1996)); línea naranja (Ramírez-Ramos <i>et al.</i> (2015)). Los triángulos invertidos negros indican el perfil de refracción sísmica. Las estrellas Amarilla y Azul indican la ubicación de las explosiones A y B, respectivamente. Las regiones indicadas en el mapa son: SEM, Sierra El Mayor; SC, Sierra Cucapah; SSF, Sierra San Felipe; SSP; SJ, Sierra Juárez.	5
2 (a-c) Mediana de curvas de ruido para las tres componentes de estaciones ubicadas en las regiones SPBC y VM (d-f). Curvas calculadas para cada estación (líneas grises) y Medianas de curvas de ruido (líneas negras). Las curvas de ruido propuestas por Peterson (1993) son las NLNM (líneas discontinuas) y NHNM (líneas punteadas).	15
3 Comparación de los niveles espectrales de ruido para las estaciones RMX, TKX y UABX, que fueron instrumentadas con diferentes sensores: (a-c) para el año 2013, con sensores CMG-3ESPC; (d-f) para el año 2015, con sensores Trillium Compact. Líneas punteadas y discontinuas hacen referencia a los niveles de ruido, NHNM y NLNM (Peterson (1993)), respectivamente.	16
4 Gráficas que muestran los valores promedio de los PSD (líneas grises) durante el 2013 de (a-c) UABC y (d-f) CPX. Líneas negras indican MNL; líneas rojas, NHNM; líneas azules, NLNM. Se muestran los espectrogramas horarios de los PSD de los siete días analizados para (g) UABX y (h) CPX. Las barras de color vertical indican el nivel del PSD. El eje x de (g,h) indica el tiempo local (UTC-7) en el formato hh:mm dd/mm/aa.	17

Lista de Figuras (continuación)

Figura	Página
5 Comparaciones de los espectrogramas a partir de los MNL de las estaciones (a) SFX y (b) UABX con los registros de presión atmosférica (línea verde) y temperatura ambiente (línea azul) de las estaciones meteorológicas TO55 y 24, respectivamente (gráficas abajo de espectrogramas). Gráficas azules indican la temperatura promedio por día, mientras que las gráficas verdes indican la presión atmosférica promedio diaria.	18
6 Modelo de velocidades de corteza para las SPBC y el suroeste de LS del perfil de refracción sísmica (Fig. 1). (a) Profundidad total del modelo, (b) profundidad del basamento de las capas de baja velocidad en el modelo de Ensenada, (c) velocidad al basamento de las capas de baja velocidad al suroeste de LS. Las líneas punteadas indican las fronteras de capas inferidas. La barra de colores lateral derecha indica la velocidad de onda P	20
7 (a) Modelos de capas planas resultantes del modelado para las regiones de Ensenada y Sierra Juárez (EM18 y SJ18, respectivamente) y su comparación con el modelo propuesto por Nava y Brune (1982) (NB82). (b) Modelo de capas planas resultante del proceso de modelado para la región de LS (LS18) y su comparación con modelos usados en la región: MVM, propuesto por Fabriol y Munguía (1997); SMVM, propuesto por Ramírez-Ramos <i>et al.</i> (2015).	22

Lista de Tablas

Capítulo I

Introducción

I.1 Planteamiento del problema

La región norte de Baja California (BC) existe un importante sistema de fallas geológicas que constituyen un segmento de la frontera entre las placas tectónicas del Pacífico y Norte América (Recuadro Fig. 1), frontera delimitada por el sistema de fallas San Andrés - Golfo de California (Atwater, 1970). La actividad sísmica generada por este sistema de fallas puede alcanzar valores de magnitud de 7.2 (Vidal-Villegas *et al.*, 2018).

Para estimar la localización hipocentral (epicentro y profundidad) de la sismicidad de la región es esencial contar con una red sísmica operando en óptimas condiciones (McNamara y Buland, 2004) y un modelo de estructura de velocidades de corteza apropiado para la región (Ramírez-Ramos *et al.*, 2015).

I.1.1 Marco Geológico: Sierras Peninsulares de Baja California y Provincia Extensional del Golfo

La región norte de BC se caracteriza por dos subregiones de geología y topografía contrastantes:

- Las Sierras Peninsulares de Baja California (SPBC, Fig. 1), caracterizadas por rocas de tipo granítico con algunas zonas donde existe cierto grado de metamorfismo

(Gastil, 1975). Esta subregión está formada por sierras que alcanzan alturas de hasta de 2800 m sobre el nivel medio del mar, al como la Sierra San Pedro Mártir (SSP, Fig. 1). Las principales fallas de esta región (Fig. 1) son: falla Vallecitos (FV), falla Tres Hermanos (FTH), falla San Miguel (FTH), falla Agua Blanca (FAB), falla Sierra Juárez (FSJ) y falla San Pedro Mártir (FSPM). La sismicidad en las SPBC se asocia principalmente al sistema de fallas San Miguel-Vallecitos (González y Suárez, 1984). Las magnitudes más altas de sismos registradas instrumentalmente son: M_L 5.8 en 1963, en el la unión fallas San Miguel y Vallecitos (Leeds, 1979); seis sismos M_L 6.0 ocurridos en 1954 y 1956, en la sección SE de la falla San Miguel (Shor Jr y Roberts, 1958; Leeds, 1979); M 5.7 en 1949, en la falla Vallecitos (Frez *et al.*, 2000).

- La Provincia Extensional de Golfo (PEG, zona gris del recuadro de Fig. 1) que se extiende hacia el este del Escarpe Principal del Golfo (Díaz-Torres *et al.*, 2012) a lo largo de la parte oriental del norte de la Península de Baja California. Ésta presenta una topografía de cuencas (Laguna Salada y Valle de Mexicali) y sierras (El Mayor, Cucapah, p. e.) (Stock *et al.*, 1991). Los sedimentos depositados en las cuencas por el Golfo de California y el Río Colorado son de origen marino y continental, respectivamente. Tienen espesores de 4 a 6 km y sub-yacen en un basamento (Puente y De La Peña, 1979; Abdeslem *et al.*, 2001). Las principales fallas en la región del Valle de Mexicali (VM) son (Fig. 1): falla Laguna Salada (FLS); falla Cucapah (FC); falla Cañón Rojo (FCR); falla Imperial (FI), falla Cerro Prieto (FCP), falla Detachment Cañada David (FDCC) y falla Indiviso (FIn). El sistema de fallas Cerro Prieto - Imperial y el centro de dispersión Cerro Prieto, así como el sistema de fallas Cucapah - Laguna Salada, concentran la mayor parte de la sismicidad del VM (Fig 1). Las magnitudes más altas de

sismos registradas son (Frez *et al.*, 2000): M 7.0 - 7.5 en 1892, en falla Laguna Salada (estimada por Strand, 1980); M_W 7.2 en 2010, ocurrido en la vecindad de la falla Cucapah; M_L 7.1 y 9.8 en 1940 y 1979, respectivamente, asociados a la falla Imperial; M 6.5 y 7.1 en 1934 asociados a la falla Cerro Prieto.

I.1.2 Evaluación del funcionamiento de la red sísmica local

Dada la ocurrencia de sismos en el norte de BC, que van desde M 1.0 (microsismisidad) hasta M 7.2, la Red Sísmica del Noroeste de México (RENSOM) opera desde finales de la década de los 70's (Vidal-Villegas *et al.*, 2018). Al presente, dicha red opera estaciones sismológicas integradas por sensores de banda ancha (120 s - 50 Hz) y acelerómetros con digitalizadores de 24 bits. La operación apropiada de la red sísmica para el registro y localización de sismos requiere de: grabación y transmisión de datos continua; calibración de equipo; buena relación señal a ruido, entre otros. Para evaluar la relación señal a ruido es necesario realizar un análisis de ruido sísmico ambiental en los sitios de observación.

La caracterización del ruido sísmico ambiental grabado por redes sísmicas se realiza basado en la metodología propuesta por Peterson (1993), estudio que caracterizó los niveles de ruido de estaciones sísmicas distribuidas en el mundo. Basado en la densidad espectral de potencia (PSD, por sus siglas en inglés), el autor definió los nuevos modelos de niveles de ruido alto (NHNM, por sus siglas en inglés) y bajo (NLNM, por sus siglas en inglés), los cuales se han convertido en un estándar en la comparaciones de niveles de ruido (Custódio *et al.*, 2014). McNamara y Buland (2004) propone una nueva metodología de análisis de los niveles de ruido basada en Peterson (1993), la cual es útil para la caracterización del desempeño de la red sísmica (Custódio *et al.*, 2014), para detectar problemas con las estaciones (instrumentales o relacionadas con el sitio). Los

principales resultados de estudios de ruido sísmico ambiental realizados en el mundo (Marzorati y Bindi, 2006; Sheen *et al.*, 2009; Evangelidis y Melis, 2012; Rastin *et al.*, 2012) destacan (Custódio *et al.*, 2014): ruido cultural/antrpogénico, provenientes de fuentes de periodo corto, con fuertes variaciones diurnas/nocturnas; ruido microsísmico (3 - 20 s) afectado fuertemente por variaciones por estaciones, correlacionadas con condiciones oceánicas; ruido de periodo largo, afectado por el tipo de instalación y por las condiciones de aislamiento (térmico).

Debido a lo anterior, se requiere evaluar y comparar los resultados de las estaciones ubicadas en los distintos ambientes geológicos. Así mismo, es necesario analizar el posible efecto sobre los niveles de ruido de factores como: las mareas del Océano Pacífico y el Golfo de California; la temperatura y presión atmosférica; la actividad antropogénica; maquinaria cercana a la estación sísmica (aires acondicionados, generadores, subestaciones eléctricas, etc.). Aunado a eso, dado a que las estaciones sísmicas se encuentran ubicadas a lo largo de los ambientes geológicos contrastantes del norte de BC (VM y SPBC), es necesario evaluar los niveles de ruido sísmico ambiental de cada una de las estaciones para compararlas con los niveles de ruido alto y bajo, NHNM y NLNM, respectivamente, definidos por Peterson (1993).

I.1.3 Modelo de estructura de velocidades apropiado para el norte de BC

El marco tectónico activo del norte de BC genera la importante sismicidad regional (desde longitud 31° a 32.5 ° N) que incluye sismos M_w 7.2 (El Mayor - Cacapah de 4 de abril de 2010). Dicha sismicidad es registrada por RESNOM y para ser localizada

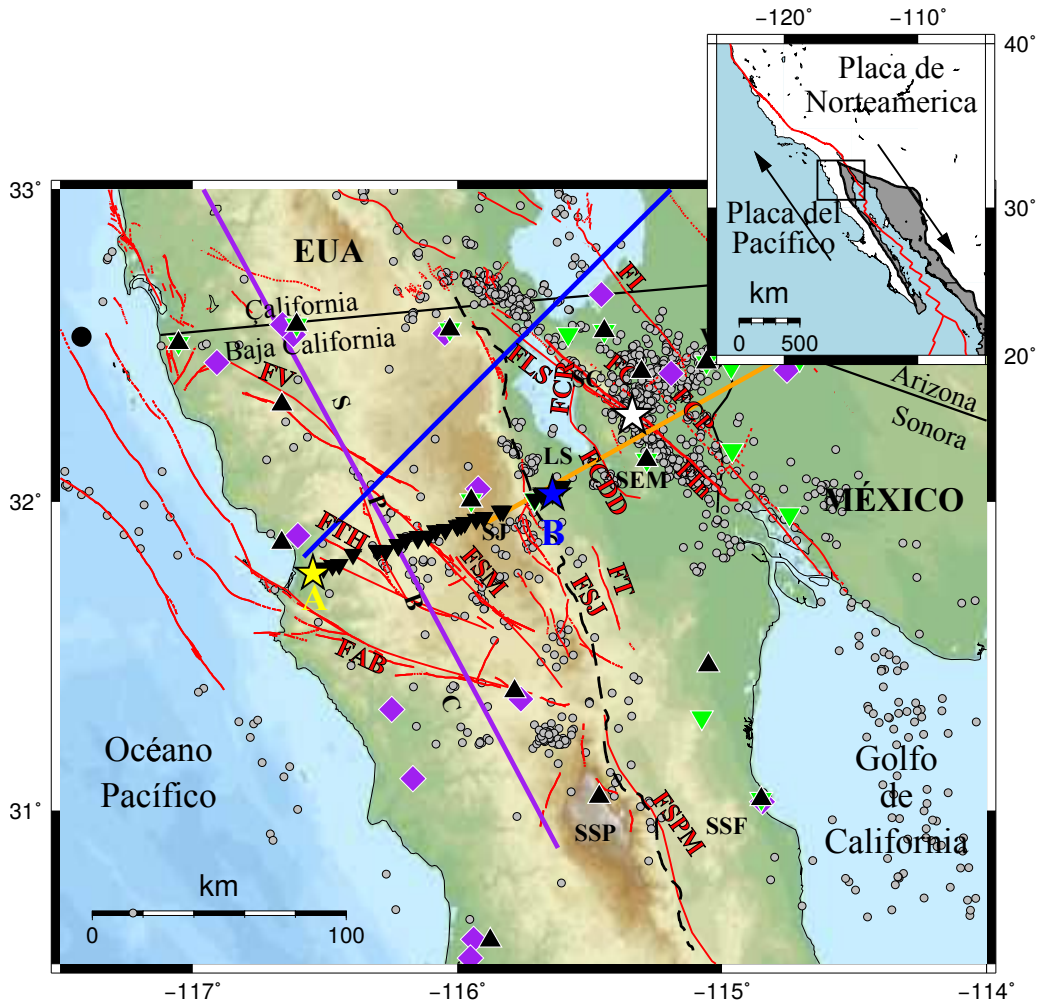


Figura 1: Mapa que muestra las dos principales provincias geológicas del norte de BC y la interacción entre las placas tectónicas del Pacífico y de Norteamérica (re-cuadro). El mapa detallado indica las fallas principales (líneas rojas, obtenidas de Seiler *et al.* (2010)). Los círculos grises indican la sismicidad $M \geq 3.5$, desde 1990 hasta la fecha, registrada por RESNOM. Las estaciones sísmicas permanentes de RESNOM son: Triángulos negros, sensores Guralp; triángulos invertidos verdes, sensores Nanometrics. Las estaciones meteorológicas de CONAGUA se representan por diamantes morados. El círculo negro indica la boya Point Loama (46323). La estrella blanca es el sismo El Mayor-Cucapah del 4 de abril de 2010 $M_W 7.2$. Estudios previos de refracción sísmica son indicados como: Línea morada (Nava y Brune (1982)); línea azul (Nuñez Cornú *et al.* (1996)); línea naranja (Ramírez-Ramos *et al.* (2015)). Los triángulos invertidos negros indican el perfil de refracción sísmica. Las estrellas Amarilla y Azul indican la ubicación de las explosiones A y B, respectivamente. Las regiones indicadas en el mapa son: SEM, Sierra El Mayor; SC, Sierra Cucapah; SSF, Sierra San Felipe; SSP; SJ, Sierra Juárez.

hipocentralmente requiere de un modelo de estructura de velocidades de corteza detallado y adecuado para la región.

Actualmente, la red sísmica utiliza esencialmente dos modelos de velocidades para la localización hipocentral: el de capas planas propuesto por Nava y Brune (1982) para la región de las SPBC; el de capas planas propuesto por Fabriol y Munguía (1997) (derivado del propuesto por McMechan y Mooney, 1980), para la región del Valle de Mexicali.

I.2 Justificación

Dadas las características geológicas contrastantes del norte de BC, ambientes sedimentario (VM) y granítico (SPBC), es necesario tener una evaluación de las características sísmicas de la región: niveles de ruido sísmico ambiental y la estructura de velocidades de corteza. En las siguientes secciones se detallará la justificación de cada uno de los dos estudios necesarios.

I.2.1 Niveles de ruido sísmico ambiental de las estaciones del norte de BC

Debido a la ausencia de estudios de ruido sísmico ambiental en el norte de BC y a la actualización de la instrumentación de las estaciones de la red sísmica (reemplazo de sismómetros de periodo corto con grabadoras de 12 bits por sismómetros de banda ancha y grabadoras de 24 bits) es necesario un análisis de esta naturaleza. Este análisis tiene dos vertientes, por un lado, analizar el funcionamiento de los nuevos equipos de

registro, y por el otro, caracterizar cuantitativamente los niveles de ruido ambiental en las estaciones sísmicas de la red. Lo cual permitirá evaluar las ventajas de los nuevos equipos y deará mayor robustez a la red.

I.2.2 Modelos de estructura de velocidades de corteza para el norte de BC

Dado que no existe un estudio de Refracción Sísmica apropiado para ambas provincias geológicas (VM y SPBC), que cuente con al menos 2 explosiones (directa y reversa; Fig. 1) en los extremos del perfil de análisis, se pretende realizar un estudio como parte del análisis estructural del norte del Baja California para determinar la estructura de velocidades de la corteza, encontrar posibles fallas geológicas y establecer, si es posible, la profundidad al Moho.

Contar con un modelo de estructura de velocidades de corteza apropiado podría mejorar la localización hipocentral de la sismicidad regional, lo cual ayudaría, por ejemplo, a delimitación de zonas sismogénicas que puedan trazar posibles fallas o ambientes de dispersión de corteza, y estudios de peligro sísmico del norte de BC.

I.3 Objetivos

I.3.1 Objetivos generales

Caracterizar sísicamente los ambientes sedimentario del Valle de Mexicali, BC, y granítico de las Sierras Peninsulares de Baja California.

I.3.2 Objetivos particulares

- Calcular las curvas de ruido sísmico ambiental de las estaciones de banda ancha ubicadas en el norte de BC y compararlas con los niveles de ruido alto y bajo (NHNM y NLNM, respectivamente), propuestos por Peterson (1993), para evaluar su funcionamiento.
- Realizar un modelado de corteza del norte de BC con la técnica de Refracción Sísmica: usar los tiempos de arribo de explosiones grabadas a lo largo de un perfil de estaciones sísmicas con la teoría asintótica de rayos.

I.4 Hipótesis

- Se espera que los niveles de ruido sísmico ambiental de las estaciones de banda ancha del norte de BC sean: i) en las estaciones ubicadas en el Valle de Mexicali, cercanos, o mayores, a la curva del NHNM; ii) en estaciones ubicadas en las SPBC, cercanos a la curva del NLNM.
- Esperaría que el Moho debajo de las SPBC sea profunda (que alcance profundidades de ~ 40 km) mientras que bajo Laguna Salada (LS) y en el Valle de Mexicali el Moho se encuentre a ~ 25 km. Indicando un adelgazamiento de corteza en dirección este.
- Las velocidades de corteza en las SPBC son mayores a las velocidades de corteza del VM y LS.

I.5 Responsabilidades de autorías en artículos

I.5.1 Artículo: *Seismic Noise Levels in Northern Baja California, Mexico*

1. Erik E. Raírez: Autor principal del texto. Acomodó la base de datos continuos, de las estaciones de banda ancha de RESNOM. Realizó todos los cálculos computacionales, así como todas las figuras del artículo.
2. J. Antonio Vidal-Villegas: Facilitó ordenadores para el computo de gran volumen realizado. Apoyó en la edición del manuscrito. Gestionó parte de los fondos para cubrir el costo de la publicación.
3. M. Alejandra Nuñez-Leal: Proporcionó, en el formato solicitado (mseed), los datos de las estaciones de banda ancha de RESNOM. Generó las curvas de los niveles de ruido de cada estación usando PQLX para la comparación con las curvas generadas por el primer autor. Escribió la sección correspondiente a las características de la instrumentación sísmica y de RESNOM.
4. Jorge Ramírez-Hernandez: Facilitó los datos meteorológicos usados en la publicación. Apoyó en la edición del manuscrito. Gestionó parte de los fondos para cubrir el costo de la publicación.
5. Adán Mejía-Trejo: Facilitó los datos de los niveles de marea del Océano Pacífico en la región norte de BC. Contribuyó en la sección en la que se describe el comportamiento de la marea del Océano Pacífico y del Golfo de California.
6. Eliana Rosas-Verdugo: Consiguió los mapas geológicos del noroeste de México a través de la base de datos del INEGI. Dibujó el mapa de las unidades geológicas

descritas por el INEGI y las relacionó con la ubicación de las estaciones sísmicas de RESNOM y de las meteorológicas de CONAGUA.

I.5.2 Artículo: *A Crustal Velocity Model for the Peninsular Ranges of Baja California and Southwestern Laguna Salada, México.*

1. Erik E. Ramírez: Instaló la mayoría de las estaciones, en dos campañas, de los dos perfiles sísmicos de refracción. Extrajo y armó la base de datos. Modeló de manera directa los datos del perfil de refracción sísmica. Escribió la mayoría del manuscrito. Elaboró todas las gráficas y mapas.
2. J. Antonio Vidal-Villegas: Gestionó los recursos necesarios para la perforación del pozo en Laguna Salada, la compra y detonación de explosivos. Además de gestionar recursos para cubrir parte de los viáticos, gasolina y renta de vehículos necesarios para la instalación de las estaciones sísmicas. Facilitó equipo computacional para el proceso de modelado. Apoyó en la edición del manuscrito. Gestionó fondos para cubrir parte del costo de la publicación.
3. Jorge Ramírez-Hernandez: Gestionó los recursos necesarios para cubrir parte de los viáticos y gasolina, además de facilitar vehículos necesarios para la instalación de las estaciones sísmicas. Apoyó en la edición del manuscrito. Gestionó fondos para cubrir parte del costo de la publicación.
4. Antonio González-Fernández: Apoyó en el proceso de modelado directo de corteza usando el software RAYINVR, ajustando los tiempos de arribo y amplitudes relativas.
5. Joann M. Stock: Prestó equipo sísmico de banda ancha para el estudio de re-

fracción sísmica. Apoyó en el proceso de escritura, así como en la edición del manuscrito.

I.6 Revisión bibliográfica

I.6.1 Ruido sísmico ambiental del norte de BC

Para la evaluación del sitio de ubicación de una estación sísmica se calcula la densidad espectral de potencia (PSD, por sus siglas en inglés) como estándar de calidad (McNamara y Buland (2004)). Para la evaluación del PSD, Peterson (1993) definió los Nuevos Modelos de Ruido Alto y Bajo usando los niveles de ruido registrados en estaciones sísmicas ubicadas en todo el mundo.

Se han realizado estudios evaluando el PSD, p.e. en el territorio continental de EUA, para caracterizar el ruido ambiental registrado por redes sísmicas (McNamara y Buland, 2004). Así mismo, trabajos como los de Diaz *et al.* (2010) y Custódio *et al.* (2014) han reportado relaciones entre la geología de los sitios observados y los niveles de ruido sísmico: en ambientes sedimentarios los niveles de ruido tienden al NHNM, mientras que en sitios rocosos los niveles de ruido tienden al NLNM.

I.6.2 Estudios de refracción sísmica en el norte de BC

Durante la primera mitad de la década de los 70's se realizó un estudio de refracción sísmica para la región de las SPBC usando una explosión en Corona, California, EUA (como tiro directo) y el sismo de Pino Solo, Baja California, ocurrido el 17 de julio de 1975 con M_L 5.1 (como tiro reverso). A partir del análisis de estos registros, Nava y Brune (1982) proponen un modelo de tres capas, el cual ubica la discontinuidad Corteza

- Manto a 42 km de profundidad (Tabla 1 y Fig. 1).

Nuñez Cornú *et al.* (1996) realizaron un estudio de refracción sísmica (no reverso) usando la explosión de Blythe, Arizona, EUA, en un perfil de ~ 300 km de longitud, orientado en la dirección NE-SO, terminando en Ensenada, BC (Fig. 1). En este estudio, los autores proponen una intrusión del manto superior debajo de la región del Valle de Mexicali a una profundidad de 17 km.

Para el Valle de Mexicali existe un modelo de 7 capas (Tabla 1), el cual es una versión modificada por Fabriol y Munguía (1997) del propuesto por McMechan y Mooney (1980) para el Valle Imperial (contiguo hacia el norte del VM, del lado de EUA). En este modelo la discontinuidad Corteza-Manto se ubica a 20 km de profundidad.

Para la región del sur del VM, BC, Ramírez-Ramos *et al.* (2015) propusieron un modelo de estructura de velocidades de tres capas planas (Tabla 1), con una profundidad del Moho de 15 km, usando una explosión realizada en el sur de Arizona (como tiro directo) y un sismo relocalizado en la región de El Mayor, BC (Fig. 1).

Comparado la profundidad del Moho con el modelo de las SPBC apreciamos un adelgazamiento de la corteza en la dirección este.

La determinación del modelo de estructura de velocidades del perfil sísmico de refracción se obtuvo a partir de la modelación de los tiempos de arribo y amplitudes relativas utilizando los programas RAYINVR y TRAMP, respectivamente. A su vez, los sismogramas sintéticos se generaron con el programa PLTSYN utilizando Teoría Asintótica de Rayos (Zelt y Smith, 1992). Lo anterior, para determinar el modelo de estructura

Tabla I: Modelos de estructura de velocidades de onda P en capas planas, resultado de estudios previos para la región norte de BC: el modelo para las SPBC propuesto por Nava y Brune (1982) (NB82); el modelo de Fabriol y Munguía (1997) para el VM (MVM; *Mexicali Valley Model*); el modelo propuesto por Ramírez-Ramos *et al.* (2015) para el sur del VM (SMVM; *Southern Mexicali Valley Model*).

Modelos					
NB82		MVM		SMVM	
Profundidad (km)	Velocidad P promedio (km/s)	Profundidad (km)	Velocidad P promedio (km/s)	Profundidad (km)	Velocidad P (km/s)
0.0 - 5.0	5.6	0.0 - 0.1	1.7	0.00 - 1.23	1.90 - 3.81
5.0 - 19.8	6.6	0.1 - 0.7	2	1.23 - 5.60	4.77 - 6.30
19.8 - 41.8	7	0.7 - 1.8	2.3	5.60 - 15.25	6.54 - 7.18
41.8 -	8	1.8 - 2.9	2.6	15.27 -	7.65
		2.9 - 5.6	3		
		5.6 - 10.0	5		
		10.0 - 20.0	6		
		20 -	7.8		

de velocidades del perfil sísmico de refacción.

Capítulo II

Presentación del estudio

Los métodos, resultados y conclusiones de este estudio son presentados en los artículos contenidos en los anexos de esta disertación. El siguiente es un resumen de las contribuciones más importantes de esta investigación.

II.1 Resultados: Niveles de ruido sísmico ambiental del norte de BC

Se analizaron 19 estaciones permanentes equipadas con sensores de banda ancha (Güralp CMG-3ESPC, CMG 40-T y Nanometrics Trillium Compact) y acelerómetros Episensor FBA ES-T. La base de datos consistió de tres años de registro continuo (100 muestras/s) ordenada en 24 archivos de una hora de longitud. Para caracterizar el ruido sísmico ambiental de cada estación sísmica se calculó el PSD de acuerdo a lo propuesto por Peterson (1993). Para el análisis estadístico de las estaciones (e.j. variaciones, diurnas, mensuales, anuales) se calcularon los niveles de ruido medio (MNL, por sus siglas en inglés) de cada día en cada estación sísmica.

Como primer resultado importante de esta sección se tienen los derivados de la comparación de las MNL de tres años de datos continuos de las estaciones ubicadas en las SPBC y en el VM (Fig. 2). Se calcularon, por cada componente del sismómetro (Z, vertical; N-S, Norte-Sur; E-O, Este-Oeste), las MNL de cada una de las estaciones

ubicadas en las SPBC y se agruparon (Fig. 2a-c) para a partir de esas curvas obtener un MNL representativo de la región (línea negra de Fig. 2a-c). Lo mismo se realizó para las estaciones del VM (Fig. 2d-f). Las comparaciones de las MNL de las estaciones ubicadas en el VM se caracterizan por tener valores hasta 20dB más altos, a periodos < 1 s, con respecto a las estaciones ubicadas en las SPBC.

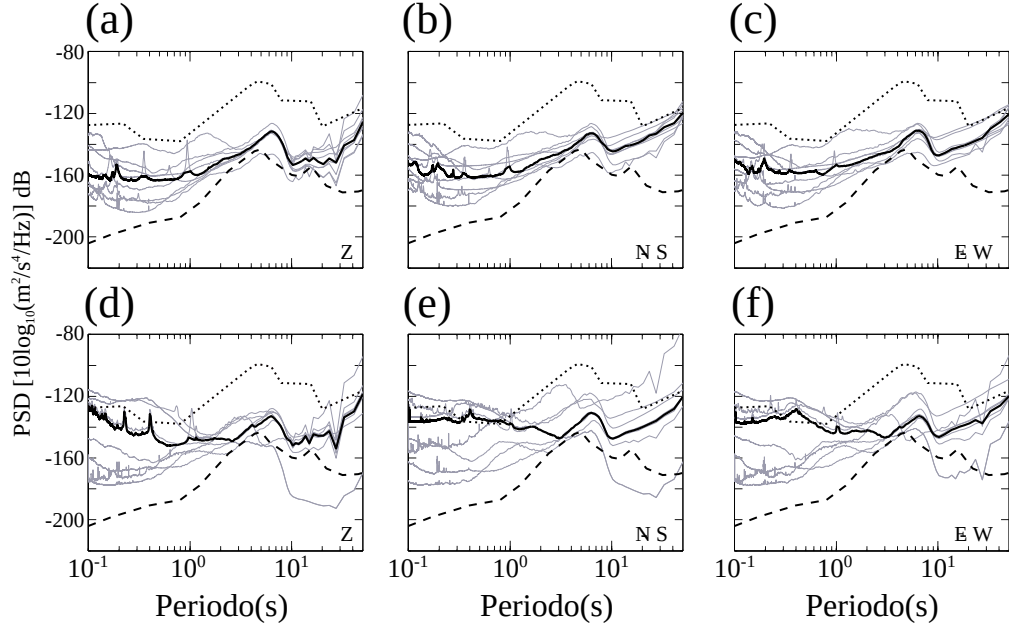


Figura 2: (a-c) Mediana de curvas de ruido para las tres componentes de estaciones ubicadas en las regiones SPBC y VM (d-f). Curvas calculadas para cada estación (líneas grises) y Medianas de curvas de ruido (líneas negras). Las curvas de ruido propuestas por Peterson (1993) son las NLNM (líneas discontinuas) y NHNM (líneas punteadas).

Dado que en 5 estaciones sísmicas de RESNOM se realizó un cambio en los sensores de banda ancha (CMG-3ESPC por Trillium Compact), se analizaron los datos de 3 estaciones (RMX, TKX, UABX) por un periodo de tiempo de un año, del 1 de enero de 2013 al 31 de diciembre de 2013 (Fig. 3a-c), cuando las estaciones tenían sensores CMG-3ESPC; durante el periodo del 1 de enero de 2015 al 31 de diciembre de 2015 (Fig. 3d-f) cuando las estaciones contaron con sensores Trillium Compact.

De comparar los MNL del PSD debido a cambios en los sensores (ambos del mismo ancho de banda: 120 s - 50 Hz) se aprecian variaciones en los niveles de ruido. Para periodos menores a 1 s, los resultados del PSD de estaciones con sensores CMG-3ESPC tienden al NHNM; a periodos entre 2 y 20 s los PSD de ambos sensores son similares; a periodos largos los PSD de los sensores Trillium Compact tienen un comportamiento bimodal.

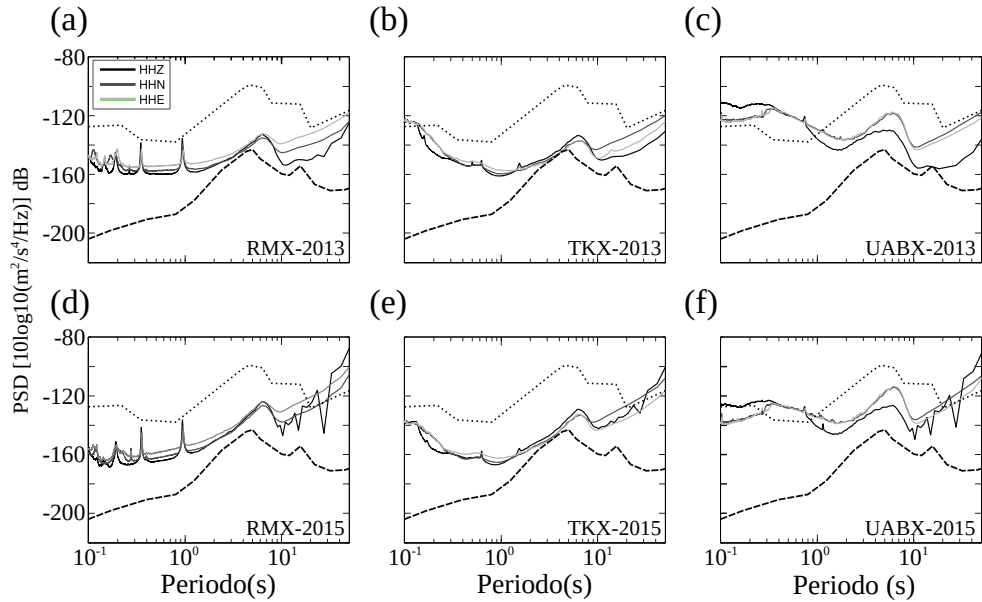


Figura 3: Comparación de los niveles espectrales de ruido para las estaciones RMX, TKX y UABX, que fueron instrumentadas con diferentes sensores: **(a-c)** para el año 2013, con sensores CMG-3ESPC; **(d-f)** para el año 2015, con sensores Trillium Compact. Líneas punteadas y discontinuas hacen referencia a los niveles de ruido, NHNM y NLNM (Peterson (1993)), respectivamente.

Para cuantificar la influencia del ruido sísmico cultural se calcularon los MNL de las estaciones UABX y CPX ubicadas en la subregión del VM. La estación UABX se encuentra dentro de la zona urbana de la ciudad de Mexicali, BC, mientras que la estación CPX se encuentra en la zona agrícola del VM ubicada al sur de la ciudad de Mexicali (Fig. 1). El análisis se realizó usando 7 días de registro continuo en cada una de las tres componentes de la estación UABX (Fig. 4a-c) y CPX (Fig. 4c-f). De los

espectrogramas de ambas estaciones se aprecia que los niveles de ruido <1 s son altos y marcados durante el día (Fig. 4g), alrededor del horario de actividades humanas, mientras que en los espectrogramas de la estación CPX no se aprecian de manera tan marcada (Fig. 4h). Ejemplificando así la influencia del ruido cultural (antropogénico) en las estaciones sísmicas.

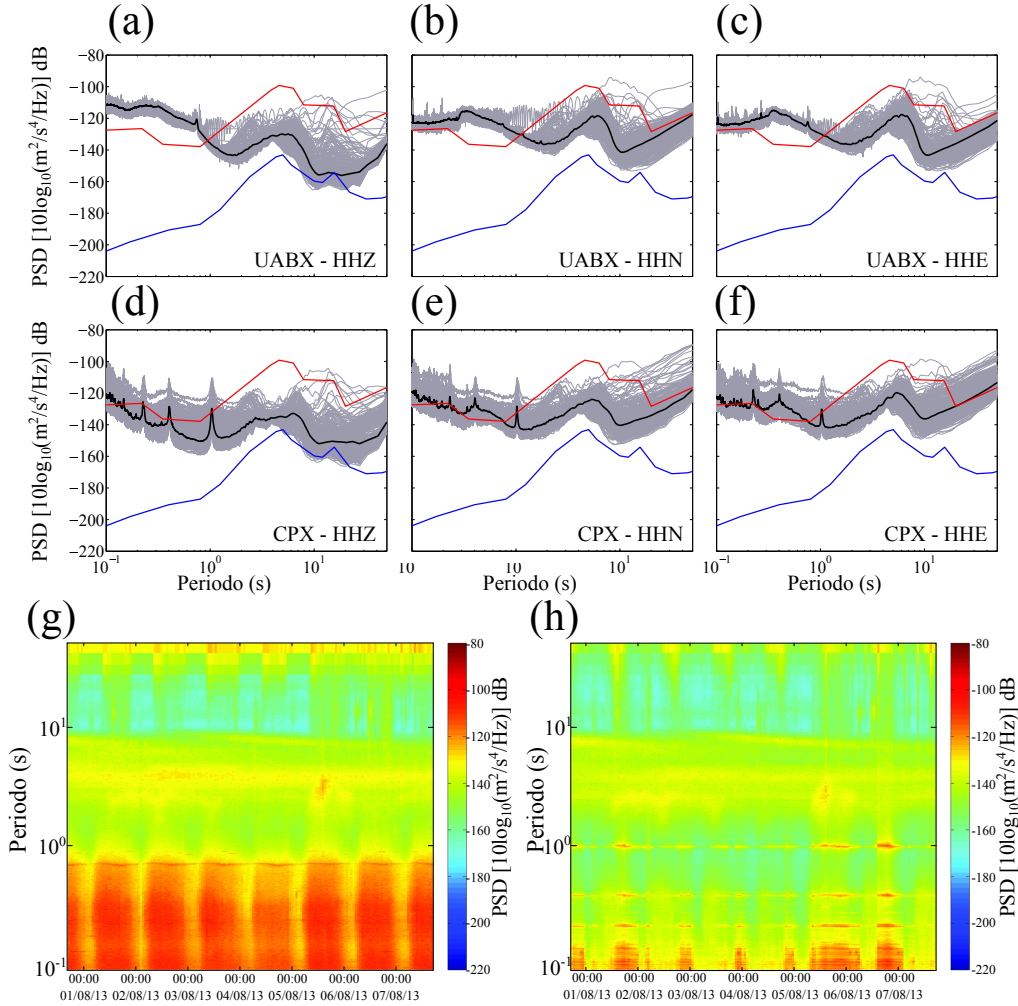


Figura 4: Gráficas que muestran los valores promedio de los PSD (líneas grises) durante el 2013 de **(a-c)** UABC y **(d-f)** CPX. Líneas negras indican MNL; líneas rojas, NHNM; líneas azules, NLNM. Se muestran los espectrogramas horarios de los PSD de los siete días analizados para **(g)** UABX y **(h)** CPX. Las barras de color vertical indican el nivel del PSD. El eje x de **(g,h)** indica el tiempo local (UTC-7) en el formato hh:mm dd/mm/aa.

Al comparar los registros de presión atmosférica y temperatura de las estaciones de CONAGUA (Fig. 1) con los espectrogramas de la componente vertical de dos estaciones (SFX y UABX, Fig. 5) en el VM (donde se alcanzan temperaturas de hasta 50°), se aprecia lo siguiente: una relación entre el ciclo de temperatura anual y los cambios en los niveles de ruido (en la banda de entre los 4.0 y 8.5 s) para estaciones que están expuestas a temperaturas ambiente, a diferencia de estaciones que están en ambientes con temperatura controlada; en la banda de entre los 4.0 y 8.5 s se aprecia un aumento en los niveles de ruido al elevarse los niveles de presión atmosférica.

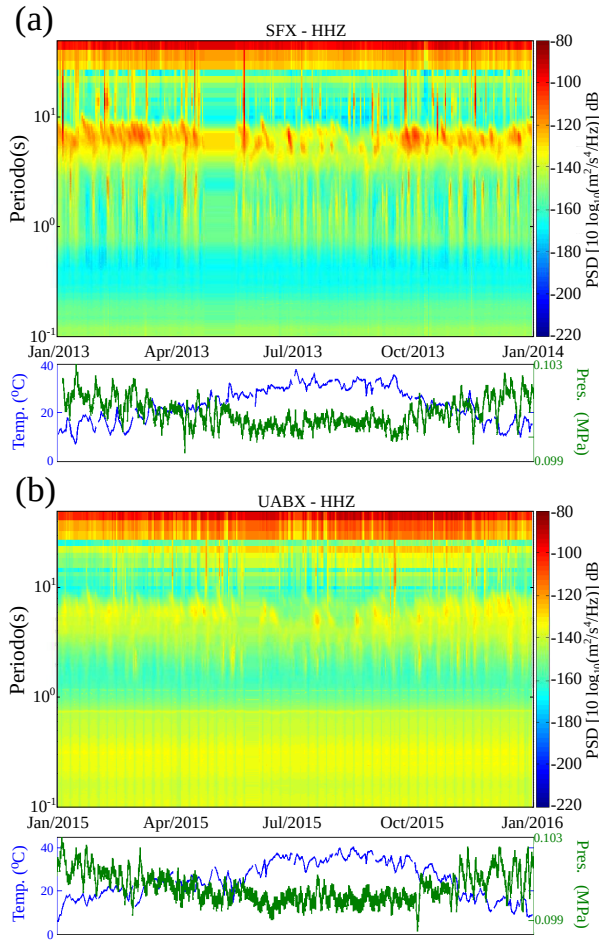


Figura 5: Comparaciones de los espectrogramas a partir de los MNL de las estaciones (a) SFX y (b) UABX con los registros de presión atmosférica (línea verde) y temperatura ambiente (línea azul) de las estaciones meterológicas TO55 y 24, respectivamente (gráficas abajo de espectrogramas). Gráficas azules indican la temperatura promedio por día, mientras que las gráficas verdes indican la presión atmosférica promedio diaria.

II.2 Resultados: Modelo de estructura de corteza para el norte de BC

El modelo resultante del trazado de rayos y ajuste de tiempos de arribo, para el perfil sísmico SPBC-suroeste LS (Fig. 1), observados vs. calculados se aprecia en la Fig. 6.

Debido a las contrastantes características del modelo, p.e. capa de baja velocidad en la región de Ensenada y en LS (Fig. 6), se construyeron 3 modelos de capas planas (promedios de profundidad y velocidades de cada interfáz) de la siguiente manera:

- EM18: Modelo de cuatro capas para la región de Ensenada (distancias < 22 km).

La velocidad promedio de la primera capa es de 4.1 km/s, donde la profundidad de la primera interfáz es de \sim 1.4 km con velocidades superior e inferior de 5.3 y 6.4 km/s, respectivamente. La segunda capa se extiende hasta \sim 6.6 km de profundidad con una velocidad promedio de 6.5 km/s. La segunda interfáz tiene velocidades de 6.6 y 6.8 km/s en la parte alta y baja, respectivamente. La tercera capa tiene una velocidad promedio de 6.9 km/s y alcanza una profundidad de \sim 10.9 km. La tercera interfáz tiene velocidades arriba y abajo de 7.0 y 7.2 km/s, respectivamente. La cuarta capa tiene una velocidad promedio de 7.3 km/s. La interfáz de la cuarta capa con el semiespacio (velocidad de 8.0 km/s) se infiere a una profundidad de \sim 35.4 km.

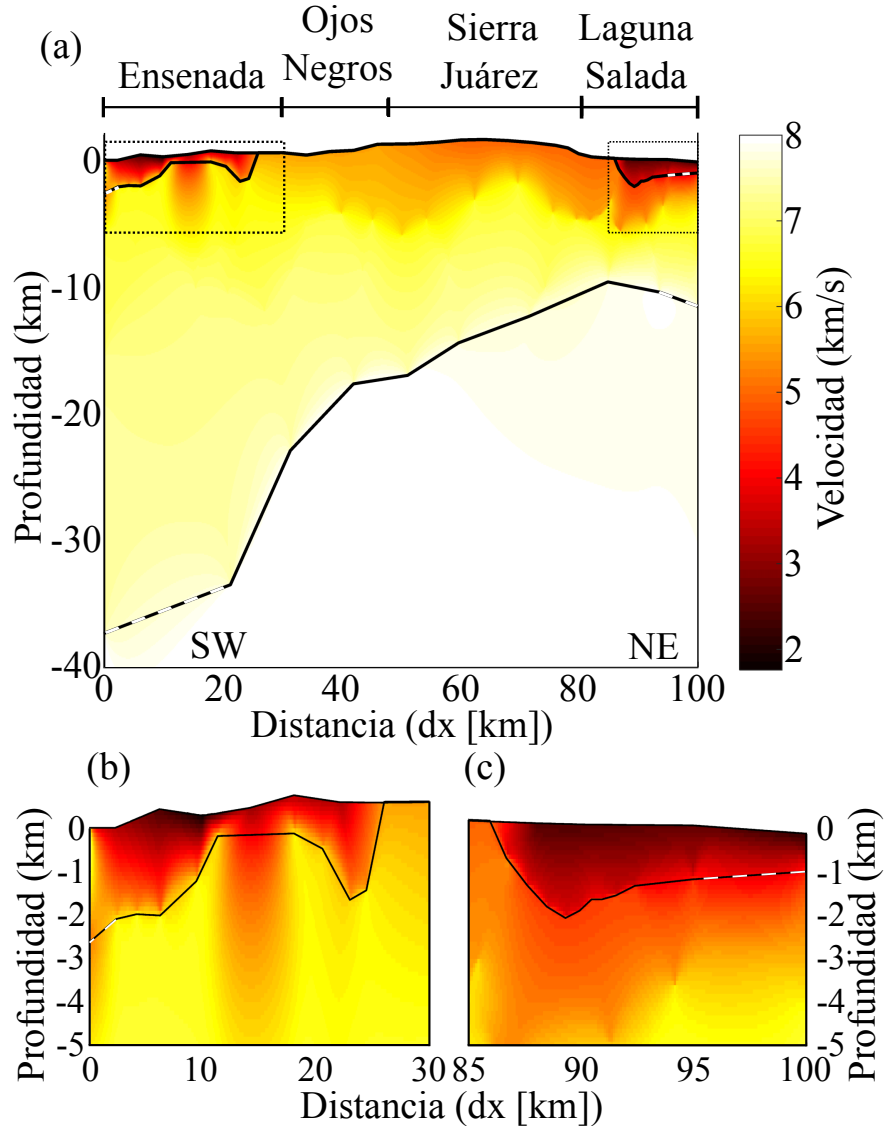


Figura 6: Modelo de velocidades de corteza para las SPBC y el suroeste de LS del perfil de refracción sísmica (Fig. 1). (a) Profundidad total del modelo, (b) profundidad del basamento de las capas de baja velocidad en el modelo de Ensenada, (c) velocidad al basamento de las capas de baja velocidad al suroeste de LS. Las líneas punteadas indican las fronteras de capas inferidas. La barra de colores lateral derecha indica la velocidad de onda P .

- SJ18: Para la región del Valle de Ojos Negros y Sierra Juárez, a distancias de entre 22 y 87 km del perfil, se modelaron 3 capas. La primera alcanza una profundidad de ~ 4.5 km con una velocidad promedio de 5.6 km/s; y velocidades arriba y abajo de la interfáz de 5.3 y 6.0 km/s, respectivamente. La segunda capa se ubica entre profundidades de ~ 4.5 y ~ 9.5 km y tiene una velocidad promedio

de 6.8 km/s; con velocidades arriba y abajo de la interfáz de 6.6 y 7.0 km/s, respectivamente. La tercera capa tiene una velocidad promedio de 7.3 km/s y se extiende desde \sim 9.5 km hasta 18.2 km de profundidad; tiene velocidades arriba y abajo de interfáz de 7.2 y 7.5 km/s, respectivamente. La última capa se encuentra sobre un semiespacio con velocidad promedio de 7.9 km/s.

- LS18: Para la región de LS, a distancias 87 km, se modeló la cuenca LS con una velocidad promedio de 3.0 km/s alcanzando una profundidad de \sim 1.6 km. La primera interfáz (basamento) tiene velocidades arriba y abajo de 3.7 y 4.6 km/s, respectivamente. La segunda capa tiene una velocidad promedio de 5.0 km/s y alcanza una profundidad de \sim 4.8 km; con velocidades arriba y abajo de la interfáz de 5.4 y 6.3 km/s, respectivamente. La tercera capa tiene una velocidad promedio de 6.6 km/s alcanzando una profundidad de \sim 8.0 km; con velocidades arriba y abajo de la interfáz de 7.0 y 7.3 km/s, respectivamente. La cuarta capa tiene una velocidad promedio de 7.4 km/s y se encuentra sobre un semiespacio de velocidad 7.8 km/s a una profundidad de \sim 11.3 km.

La Fig. 7 muestra la comparación de los tres modelos resultantes (EM18, SJ18 y LS18) con los que se tienen para cada subregión del norte de BC: SPBC (Fig. 6a) y VM (Fig. 6b). La diferencia principal de los tres modelos entre sí es el límite de la última interfáz, que profundiza en dirección suroeste, desde \sim 11 km (LS) hasta la inferencia de \sim 35 km (sur de la ciudad de Ensenada) de profundidad. La otra diferencia es que los modelos EM18 y LS18 presentan una capa de baja velocidad en la cima que no está presente en SJ18.

Con respecto a las diferencias de velocidad con los modelos previos de la región, los modelos EM18 y SJ18 presentan velocidades de \sim 1 km/s más altas que las que tiene el

modelo NB82 (Nava y Brune, 1982). Por otro lado, el modelo LS18 tiene valores de velocidad ~ 2 km/s mas altos que los que tiene el modelo MVM (Fabriol y Munguía, 1997).

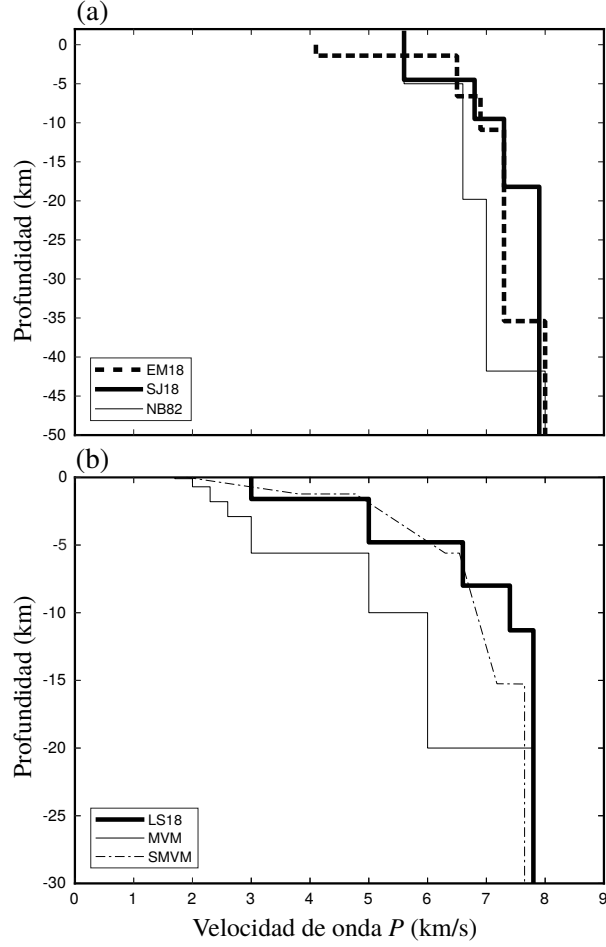


Figura 7: (a) Modelos de capas planas resultantes del modelado para las regiones de Ensenada y Sierra Juárez (EM18 y SJ18, respectivamente) y su comparación con el modelo propuesto por Nava y Brune (1982) (NB82). (b) Modelo de capas planas resultante del proceso de modelado para la región de LS (LS18) y su comparación con modelos usados en la región: MVM, propuesto por Fabriol y Munguía (1997); SMVM, propuesto por Ramírez-Ramos *et al.* (2015).

Para mayor detalle en cuanto a los datos utilizados, metodología, resultados, análisis y conclusiones ver sección de Anexos.

Referencias

- Abdeslem, J. G., Cardeña, J. M. E., Orozco, L. M., Ortega, V. M. W., y Hernández, J. R. (2001). Crustal structure from 2-D gravity and magnetic data modeling, magnetic power spectrum inversion, and seismotectonics in the Laguna Salada basin, northern Baja California, Mexico. *Geofísica Internacional*, **40**(2): 67–85.
- Atwater, T. (1970). Implications of plate tectonics for the Cenozoic tectonic evolution of western North America. *Geological Society of America Bulletin*, **81**(12): 3513–3536.
- Custódio, S., Dias, N. A., Caldeira, B., Carrilho, F., Carvalho, S., Corela, C., Díaz, J., Narciso, J., Madureira, G., Matias, L., *et al.* (2014). Ambient noise recorded by a dense broadband seismic deployment in western Iberia. *Bulletin of the Seismological Society of America*, **104**(6): 2985–3007.
- Díaz, J., Villaseñor, A., Morales, J., Pazos, A., Córdoba, D., Pulgar, J., García-Lobón, J. L., Harnafi, M., Carbonell, R., Gallart, J., *et al.* (2010). Background noise characteristics at the IberArray broadband seismic network. *Bulletin of the Seismological Society of America*, **100**(2): 618–628.
- Díaz-Torres, J. J., Fletcher, J. M., Spelz-Madero, R. M., Martín-Barajas, A., y Suárez-Vidal, F. (2012). Geomorfometría del escarpe principal del golfo de California. Análisis comparativo entre dos segmentos del rift: Sierra San Pedro Martir y Sierra Juarez, Baja California, México. *Revista mexicana de ciencias geológicas*, **29**(3): 590–610.
- Evangelidis, C. y Melis, N. (2012). Ambient noise levels in Greece as recorded at the Hellenic Unified Seismic Network. *Bulletin of the Seismological Society of America*, **102**(6): 2507–2517.

- Fabriol, H. y Munguía, L. (1997). Seismic activity at the Cerro Prieto geothermal area (México) from August 1994 to December 1995, and its relationship with tectonics and fluid exploitation. *Geophysical Research Letters*, **24**(14): 1807–1810.
- Frez, J., González, J., Acosta, J., Nava, F., Méndez, I., Carlos, J., García-Arthur, R., y Alvarez, M. (2000). A detailed microseismicity study and current stress regime in the Peninsular Ranges of northern Baja California, Mexico: The Ojos Negros region. *Bulletin of the Seismological Society of America*, **90**(5): 1133–1142.
- Gastil, R. G. (1975). Reconnaissance geology of the state of Baja California. *The Geological Society of America, Inc. Memoir*, **40**: 139–143.
- González, J. J. y Suárez, F. (1984). Geological and seismic evidence of a new branch of the Agua Blanca fault. *Geophysical Research Letters*, **11**(1): 42–45.
- Leeds, A. L. (1979). *Relocation of M 5.0 northern Baja California earthquakes using SP times*. University of California, San Diego.
- Marzorati, S. y Bindi, D. (2006). Ambient noise levels in north central Italy. *Geochemistry, Geophysics, Geosystems*, **7**(9).
- McMechan, G. A. y Mooney, W. D. (1980). Asymptotic ray theory and synthetic seismograms for laterally varying structures: theory and application to the Imperial Valley, California. *Bulletin of the Seismological Society of America*, **70**(6): 2021–2035.
- McNamara, D. E. y Buland, R. P. (2004). Ambient noise levels in the continental United States. *Bulletin of the seismological society of America*, **94**(4): 1517–1527.
- Nava, A. y Brune, J. N. (1982). An earthquake-explosion reversed refraction line in the

Peninsular Ranges of southern California and Baja California Norte. *Bulletin of the Seismological Society of America*, **72**(4): 1195–1206.

Nuñez Cornú, F., Frez-Cárdenas, J., Montana, C., Munguía, L., Nava, F. A., González-García, J. J., Mendoza, L., Aragón, M., Sánchez-Mora, C., Morandi, M., Madrid, J., y et al. (1996). Un modelo de la estructura de corteza para el sistema de fallas de San Andrés en la zona fronteriza México-EEUU. *Geotermia*, **12**(1): 43–51.

Peterson, J. (1993). Observations and modeling of seismic background noise.

Puente, C. I. y De La Peña, L. A. (1979). Geology of the Cerro Prieto geothermal field. *Geothermics*, **8**(3-4): 155–175.

Ramírez-Ramos, E. E., Vidal-Villegas, A., González-Fernández, A., y Stock, J. M. (2015). A crustal velocity model for the southern Mexicali Valley, Baja California, México. *Seismological Research Letters*, **86**(1): 181–191.

Rastin, S., Unsworth, C., Gledhill, K., y McNamara, D. (2012). A detailed noise characterization and sensor evaluation of the north Island of New Zealand using the PQLX data quality control system. *Bulletin of the Seismological Society of America*, **102**(1): 98–113.

Seiler, C., Fletcher, J. M., Quigley, M. C., Gleadow, A. J., y Kohn, B. P. (2010). Neogene structural evolution of the Sierra San Felipe, Baja California: Evidence for proto-gulf transtension in the Gulf Extensional Province? *Tectonophysics*, **488**(1-4): 87–109.

Sheen, D.-H., Shin, J. S., y Kang, T.-S. (2009). Seismic noise level variation in South Korea. *Geosciences Journal*, **13**(2): 183–190.

- Shor Jr, G. G. y Roberts, E. (1958). San Miguel, Baja California Norte, earthquakes of February, 1956: A field report. *Bulletin of the Seismological Society of America*, **48**(2): 101–116.
- Stock, J. M., Martín, A. B., Suárez, F. V., y Miller, M. M. (1991). Miocene to Holocene extensional tectonics and volcanic stratigraphy of NE Baja California, Mexico.
- Strand, C. L. (1980). *Pre-1900 earthquakes of Baja California and San Diego County*. Tesis de doctorado, San Diego State University, Department of Geological Sciences.
- Vidal-Villegas, J. A., Munguía, L., González-Ortega, J. A., Nuñez-Leal, M. A., Ramírez, E., Mendoza, L., Castro, R. R., y Wong, V. (2018). The Northwest Mexico Seismic Network: Real-Time Seismic Monitoring in Northern Baja California and Northwestern Sonora, Mexico. *Seismological Research Letters*, **89**(2A): 324–337.
- Zelt, C. y Smith, R. (1992). Seismic traveltimes inversion for 2-D crustal velocity structure. *Geophysical journal international*, **108**(1): 16–34.

Anexo 1: Seismic Noise Levels in Northern Baja California, Mexico

Erik E. Ramírez[1]

J. Antonio Vidal Villegas[2]

M. Alejandra Nuñez-Leal[2]

Jorge Ramírez-Hernández[1]

Adan Mejía-Trejo[3]

Eliana Rosas-Verdugo[2]

[1] Universidad Autónoma de Baja California (UABC), Instituto de Ingeniería. Calle de la Normal S/N, Insurgentes Este, 21280, Mexicali, Baja California, México.

[2]Centro de Investigación Científica y de Educación Superior de Ensenada (CICESE), División de Ciencias de la Tierra. Carretera Ensenada-Tijuana 3918, Zona Playitas, 22860, Ensenada, Baja California, México.

[3] Universidad Autónoma de Baja California (UABC), Instituto de Investigaciones Oceanológicas (IIO). Carretera Ensenada-Tijuana 3917, Fraccionamiento Playitas, 22860, Ensenada, Baja California, México.

Abstract

We performed a seismic noise level analysis from records of seismic stations located in Northern Baja California, Mexico. We used data from stations of the Northwestern Mexico Seismic Network; with the goal to characterize the noise spectrum for each station as a function of time. The seismic stations are located in the sedimentary environment of the Mexicali Valley (MV) and the granitic Peninsular Ranges of Baja California (PRBC). The ambient seismic noise was characterized using the Power Spectral Density (PSD) technique (Peterson, 1993). We found that, at periods between 0.1 and 2 s, the Median Noise Levels (MNLs) of stations in the MV are up to 25 dB higher, and near the New High Noise Model, than MNLs of PRBC stations. For periods > 2 s, the MNL are similar for both regions and are between the New High and Low Noise Models. We found differences in the noise levels when seismic sensors (different brands but same bandwidth) were interchanged. For periods < 1 s the MNLs computed from records of Güralp sensors are ~ 20 dB higher than MNLs from Nanometrics sensors; for periods > 10 s the MNLs of Nanometrics sensors are ~ 20 dB higher than the MNLs from Güralp sensors. We observed daily variations in short period noise, related to human activity, such as higher noise levels for periods < 1 s at daylight in a station in the city of Mexicali. No influence of variations of the sea level of the Pacific Ocean on the PSD of stations of North Baja California was observed. At least for two sites, in and south of MV, there is a direct relationship among variations of pressure and temperature with seismic noise: high pressure and low temperature are related with high noise levels in the 4.0 to 8.5 s period band, and vice versa.

III.1 Introduction

Northern Baja California, Mexico (NBC) consists mainly of two different geological regions, which are divided by the Main Gulf Escarpment (Fig. 1): the granitic Peninsular Ranges of Baja California (PRBC) and the sedimentary environment of the Mexicali Valley (MV) (Lomnitz *et al.*, 1970). The MV is composed of two basins: the Laguna Salada and the Mexicali Valley. The boundary of these two basins is the Cucapah and El Mayor mountain ranges, located in the northwest of the Gulf Extensional Province (Surez-Vidal *et al.*, 2008). The Mexicali Valley basin (5-6 km thick, Pelayo *et al.*, 1991) lies east of the Cucapah and El Mayor mountains.

In Northern Baja California, earthquakes ranging from microseismicity (M 1.0) to major earthquakes (M 7.2) occur and, as a result, the Northwestern Mexico Seismic Network (RESNOM) operates (Vidal-Villegas *et al.*, 2018). An example of the need for proper operation of this network is the Mw 7.2 El Mayor- Cucapah earthquake, which occurred on 4 April 2010 (Hauksson *et al.*, 2011). This earthquake ruptured a series of faults including the Indiviso fault (Gonzalez-Ortega *et al.*, 2014). The occurrence of the El Mayor-Cucapah earthquake motivated efforts to improve the instrumentation of the RESNOM network (from a short period to broadband seismometers, for instance). Proper operation of this network requires continuous operation, good signal to noise ratio, sites of lower levels of noise and continuous transmission to the processing center. To evaluate a site for a seismic station, the power spectral density from ambient noise (PSD) has become a standard tool. In this technique, new low and high noise models are defined (NLNM and NHNM, respectively [Peterson, 1993]) using noise levels recorded by seismic stations located worldwide. Based on the computation of the probabilistic power spectral densities (PPSDs), McNamara and Buland (2004) proposed a new approach to assess the background seismic noise levels of seismic stations. Studies

in other regions (e.g., continental USA, McNamara and Buland, 2004) have characterized the ambient noise recorded by seismic networks. Also, there are reports of regions where a relationship between the geology and the noise levels has been observed; in sedimentary environments PPSDs are high, and in rock sites, PPSDs are low (Díaz *et al.*, 2010, and Custódio *et al.*, 2014).

Because of the absence of these kinds of studies in NBC, and the improvement of the instrumentation of the RESNOM stations (by replacing short period seismometers/12-bit recorders with broadband seismometers/24-bit recorders), a study of ambient seismic noise levels was necessary. Therefore, this study aims to assess the functioning of RESNOM stations and to characterize, from a statistical analysis, the noise levels of the MV and PRBC regions.

III.2 Characteristics of the Instrumentation

Currently, NBC is covered by 26 RESNOM stations instrumented with broadband seismometers and accelerometers (Table 1, Fig. 1). The instrumentation of these seismic stations is as follows: eleven stations with Güralp CMG-3ESPC/Reftek 130 recorders (configured from 120 s to 50 Hz); one station with a Güralp CMG-40T/Reftek 130 and another one with Güralp CMG-40T/Reftek 71A-07 (flat from 30 s to 50 Hz); 13 stations with Nanometrics Trillium Compact/Reftek 130 (120 s to 50 Hz). The criteria for choosing the sites for permanent stations are as follows: to reduce the geographical gaps between stations; to be as distant as possible from cultural noise sources, to be installed on bedrock outcrops and to follow security procedures. In the mountain range environment, sensors were installed on a concrete base over solid rock; in the sedimentary environment, on a concrete base over compact sediments; and in urban areas, for

safety reasons, inside schools or government facilities. The RESNOM stations use two types of shelters: (1) Container-type, a concrete base with metal lid. (2) Concrete-type, with a concrete pillar installed directly into the soil and independent of the concrete wall structure. High-density insulation walls were installed inside station shelters (Foamular 250, from Owens Corning) to avoid temperature variations; additionally, thermal insulation boxes, using the same material, covered the seismic sensors.

III.3 Noise Data Processing

To characterize the background seismic noise of the Northwestern Mexico region, we calculated the PPSDs of each component of the seismic stations. To calculate the PPSDs we followed the methodology proposed by McNamara and Buland (2004), and we used the software PQLX by Richard Boaz. In addition to the use of this software, we wrote MATLAB (<https://www.mathworks.com/products/matlab.html>, last accessed November 2018) scripts to calculate the PSD and to statistically analyze three years (2013-2015) of seismic noise data (Fig. 2). The whole database was separated into two 1-year sections (January to December; 2013 and 2015; skipping 2014, in some stations, due to gaps in the recordings), so that we could analyze variations in the PSDs due to changes in instrumentation. For instance, stations RHX, RMX, TJX, TKX, UABX initially operated with CMG-3ESPC, but now operate with Trillium Compact sensors (Table 1). For each day, the database consisted of 24 records (1 hour-length of 3-component data), in mseed format. We ordered the files into Julian day folders for each station. Preprocessing the signal included the segmentation of the 1-hour records into windows of 16384 samples (163.84 s) with 50% of overlap. This overlap was designed to reduce the effects of earthquake signals in the PSD results (Burtin *et al.*,

2008). A 30% cosine taper was applied to eliminate possible corner effects. Then, we calculated the fast Fourier transform for each overlapped segment. Next, derivation was performed to obtain acceleration spectra. At this point, we computed the PSD and then converted to decibels (dB) relative to $1 \text{ (m}^2/\text{s}^4\text{)}/\text{Hz}$. By averaging each one-hour PSD segment, we generated one file with the PSD of each component. Next, we calculated the average PSD file per day from the 24-hour PSD files. To analyze how often an amplitude is observed for each period of acceleration, we plotted histograms of the amplitudes calculated at each period based on the PSD. Finally, we computed the median of the PSD for each component (median noise level, MNL), for each 1-year period, to get a representative noise curve for each station. We chose the median, instead of the average, because the median is less sensitive to outliers.

For comparison purposes, for the vertical component of the SJX station (for instance), we computed the PPSDs using PQLX (Fig. 3a), and the PSD obtained using our scripts (Fig. 3b). In both figures, 3a and 3b, the median noise levels are similar. In this case, as in all other stations, data gaps due to power breakdown (e.g., bottom of Fig. 3b), data transmission interruption, updates, and maintenance in the network were eliminated. The effects produced by the rejected signals can be appreciated in the differences between Fig. 3a and 3b. Although the PPSDs look spread between the NLNM and above the NHNM, and there is a thick line (produced by electronic noise due to an absence of seismometer signal) at -200 dB, (Fig. 3a), the PSD is more concentrated around the MNL (Fig. 3b). To avoid these effects, and to have the possibility of modifying our programs to process the useful signals, we used our scripts.

III.4 Noise Level Analysis

We compared noise levels based on the seismic records of stations located in MV or PRBC. For this, we computed the Median Noise Levels (MNLs) for a three-year period record of each station. Next, we grouped the MNLs according to the location of the station and calculated the MNL for stations deployed on the PRBC (Fig. 4a-c) or on the MV (Fig. 4d-f). For periods shorter than 2 s, the three-component MNLs for stations in PRBC lie between the NHNM and NLNM (Fig. 4a-c); while the MNLs for stations in MV trend to the NHNM (Fig. 4d-f). For periods greater than 2 s, the MNLs of the two regions have a similar trend; for periods between 2 and 20 s, the MNLs trend to the NLNM, and for periods greater than 20 s the MNL curves trend to the NHNM.

As previously noted, instruments from stations RHX, RMX, TJX, TKX, and UABX were changed in the middle of 2014 (Fig. 1 and Table 1). Because of this, we had the opportunity to assess possible variations in the noise levels due to the use of different instruments, but with the same bandwidth. The changes made were from Güralp CMG-3ESPC (120 s - 50 Hz) to Nanometrics Trillium Compact (NTC, 120 s - 50 Hz). All the five stations recorded for a 3-year period (from 2013 to 2015); since the sensors were changed in June 2014, we compared the noise levels in periods of one year: 2013 with Güralp CMG-3ESPC and 2015 with NTC. For 2013 we calculated the 3-component MNLs of RMX, TKX, and UABX stations (Fig. 5a-c), initially instrumented with Güralp CMG-3ESPC sensors. For 2015, we also obtained the MNL curves for the same stations, but now instrumented with NTC sensors (Fig. 5d-f). In the computation of MNLs curves, proper instrumental constants for each station were considered.

The results indicate that the Güralp and NTC sensors respond differently to the ambient noise, which we assume has effectively the same characteristics in each of the years studied. The first general difference between Güralp and NTC sensors are the "negative

“spikes” presented in the vertical component of NTC sensors (bimodal behavior, Govoni *et al.*, 2017) at periods higher than ~ 10 s (RMX and UABX, mainly [Fig. 5d and 5f]). The NTC sensors are more sensitive to temperature variations (residual thermal response at long periods), in both cases, due to the proximity of air-conditioned devices to the sensors. The “negative spikes” are not a characteristic of the ambient noise; rather, they are due to the bimodal behavior of the NTC sensor at high temperatures. We understand the bimodal behavior as the probability that, at long periods, the PSD could have two contrasting values at some period. In computing the median, this behavior is shown as “negative spikes”. We also observed that for NTC sensors the MNLs are higher than the NHNM curve (for periods > 20 s). For the UABX station and Güralp sensor, the lower MNL curve for the vertical component relative to the two horizontal ones is noticeable (Fig. 5c), suggesting that the sensor was not well leveled. In the case of periods between 1 and 10 s, for RMX and TKX stations with Güralp and NTC sensors, the MNLs are similar and close to the NLNM (Figs. 5a, b, d, and e). However for the UABX station, the MNLs trend to the NHNM curve (Fig. 5c). Finally, for periods < 1 s in the RMX station three noticeable spikes at around 1 s, 0.35 s, and 0.2 s (Fig. 5a and 5d) are observed. We identify these peaks as due to the vibration produced when the air conditioning starts to operate. This station is installed inside a government building, where the temperature is regulated. Due to these effects, this station will be relocated. In general for TKX and UABX stations (Fig. 5b and 5c), in the 2013-year that functioned with Güralp sensors (and periods < 1 s), the spectral noise levels trend to the NHNM curve and are higher than the spectral levels computed from noise recorded by NTC sensors. To correct the anomalous spikes, at short periods, in RMX and UABX we will reinstall the sensors in sites far from the air-conditioning devices and reinforce the thermal insulation around the sensors.

The long-period behavior of the NTC sensor is due to its sensitivity to thermal changes.

Govoni *et al.* (2017) observed that the small size and light weight might contribute to signal pollution due to the high thermal capacity of the aluminum case and to the strain of the cable. Therefore, an extra layer of thermal insulation was added to stations that presented this long-period behavior and a reduction in the noise level was obtained (up to 20 dB). Further experiments (using a shake table) are needed to explain MNLs offset between sensors at periods $< \sim 1$ s.

III.4.1 Short-Period Noise Analysis

For Short-Periods (SP), less than 1 s, noise levels vary mostly depending on whether the stations are in the MV or the PRBC. Short period records are affected by local sources of noise, which are dominated by cultural noise (McNamara and Buland, 2004). MNLs of the MV stations are higher than those at the PRBC stations; differences are up to 30 dB for the vertical component at periods less than 1 s (Fig. 4). The MNL for PRBC is comprised between the NHNM and NLNM, whereas the MNL for MV is close to the NHNM. To illustrate the observed SP noise daily variations due to human activity, we computed MNLs and spectrograms from records of UABX and CPX stations (Fig. 6), both located in the MV (Fig. 1). The UABX station is located inside the city of Mexicali, while CPX (on the Cerro Prieto volcano) is located 20 km away from the outskirts of the city. From the data of the 2013 year, MNLs obtained (Fig. 6a-f) show that, for periods < 1 s, the differences vary from 5 to 10 dB; the MNLs of the UABX station are higher than those of the CPX station. Also noticeable are the spikes such as those reported for the RMX station. The CPX station has similar conditions of operation as those of the RMX station (Fig. 5a, d). For periods > 1 s, UABX and CPX stations have similar MNLs (Fig. 6a-f). We also calculated vertical-component spectrograms for one week (August 1st to 7th, 2013) of the PSD for each hour of noise signal recorded at

UABX and CPX stations (Fig. 6g, h, respectively). The date (x-axis in spectrograms) was adjusted 7 hours to get the local time (UTC-7), showing the daily variation (Fig. 6g, h). The spectrograms of UABX (Fig. 6g) show strong daily variations in SP noise levels: from -130 dB at midnight to \sim -100 dB in the daytime. At station CPX (Fig. 6h) these SP variations (-140 to -120 dB) are less than in UABX, showing that, for these two cases, the SP changes in noise levels are due to human activities.

III.4.2 Microseismic Noise Analysis

Northern Baja California, Mexico, has two long coastal shorelines (Fig. 1). To the west is the Pacific Ocean, while to the east is the Gulf of California. The wave climate variability and trends for the Eastern Tropical Pacific, analyzed from a 19-year period (using high-resolution wave hindcast), show that the ocean adjacent to the Baja California Peninsula has a seasonal variability in wave height and period (Garcia Nava *et al.*, 2015). The Pacific coast of the peninsula is dominated by swell generated from the extratropical North Pacific and extratropical South Pacific (Alves, 2006). Buoy observations and hindcast show a seasonal pattern with the highest mean sea wave height (the average of the highest one-third of all of the wave heights during the 20-minute sampling period) of about 2.5 m for the Pacific coast while in the Gulf of California values are below 1 m (Garcia Nava *et al.*, 2015). Generation of waves in the Gulf of California is due to local phenomena (wind) and can reach high values when tropical storms in the Pacific ocean enter and propagate into the Gulf.

To analyze the effect on noise levels, we used records of the Pacific Ocean Sea Levels (POSL) of the buoy 46232, located in Point Loma, Southern California, U.S.A. (Fig. 1), of the National Data Buoy Center; National Oceanic and Atmospheric Administration, U.S.A. We first analyzed the Average and Dominant Periods of the POSL to have a

notion of the range of periods (generated by the Pacific Ocean) that could appear in the MNL curves. The mean Average Period calculated from the buoy records, from 2013 to 2015, is 7.8 s (E Fig. S1a). The Mean Dominant Period, during the same time interval, is 13.4s (E Fig. S1b). In the spectrograms, we appreciate variations between 4.5 and 8.5 s (pink rectangle of E Fig. S2) from 2013 to 2015. The spectrogram of station CBX (which provided most of the data) was plotted alongside with the POSL, for the 2013 period (E Fig. S2).

Regarding the relationship between seismic noise levels and ocean conditions, we followed the methodology described in Custodio et al. (2014) to analyze the vertical component time evolution at selected periods (Fig. 7a) and the POSL (the significant wave height [WVHT]), from 2013 to 2015 (Fig. 7b). To examine the possible effect of POSL in seismic noise, we stacked the PSD of all RESNOM stations for selected periods (1, 6.06, 7.12, 14.24, and 17.24 s) during the three-year period and plotted them alongside the POSL variations (Fig. 7b). In the POSL records, we observe three peaks in the sea level: 08/04/2013, 01/03/2014, and 16/11/2016 with peak values at 4.2, 4.5, and 5.1 m, respectively (indicated by circles in Figure 7b and marked as dotted lines in Figure 7a). The first two peaks of the sea level, maximum of 4.2 and 4.5 m, are reflected slightly in variations of the stacked MNLs at 6.06 and 7.12 s (Fig. 7a), while for the 17.24 s stacked period, the two events are not reflected in the stacked MNLs (Fig. 7a). For stacked PSD periods of 1.00, 14.24, and 17.24 s, the three major sea rising events are not reflected in PSD variations (Fig. 7a). The last peak of the sea level (at 16/11/2015) does not appear at any stacked period. For the three-year analyzed period, we did not observe any influence of narrow variations of the POSL on the vertical-component noise recorded in Northern Baja California. The rising sea level does not appear evident (Fig. 7b); it is just observed as three narrow peaks (Fig. 7b) associated with storms of 2-to-3 days duration.

III.4.3 Meteorological Related Noise Levels

In Northern Baja California, the PRBC and MV present a considerable range of temperatures. For atmospheric analysis, we chose the following meteorological stations as representatives of different natural environments: Station 28, Pacific coast of PRBC, at 174 m above mean sea level (m.a.m.s.l.); station 160, inland the PRBC, in the Main Gulf Escarpment (Fig. 1), at 1576 m.a.m.s.l.; station 24, located in the MV, at 2 m.a.m.s.l.. Meteorological Stations (Table 2 and Fig. 1) of the National Water Commission, Mexico (CONAGUA) provided us with meteorological records. From these records (Fig. 8), we observed that temperatures in the PRBC vary from a minimum of ~ -2 to a maximum of $\sim 35^\circ \text{ C}$ in the Pacific Coast (e.g. MSs 28, 16, 161, 44, and 100), and from ~ -7 up to $\sim 40^\circ \text{ C}$ inland PRBC (e.g. MSs 160, 22, 155, and 84). In the MV (MSs 24, TO40, 59, 162, and TO55) temperatures vary from 0 up to 50° C . Variations of temperature between winter and summer are: $\sim 15^\circ \text{ C}$ (Fig. 8a) for stations in the Pacific coast of the PRBC, showing a more stable temperature controlled by the sea; $\sim 20^\circ \text{ C}$ (Fig. 8b) for stations inland the PRBC; $\sim 30^\circ \text{ C}$ (Fig. 8c) for stations in the MV region, where the differences are due to the weather of the Sonora Desert (Fig. 1). To reduce the influence of the temperature changes on the seismic signals, all broadband sensors are covered with a box made of high-density insulation material (Foamular 250, from Owens Corning). In stations where ambient temperatures are high (MV region) a double-layer insulation box was installed, as well as an internal insulation cover for the container box.

To see possible effects of temperature during the year, we compared the noise levels histograms, for stations where temperatures reach up to 50° C (MV region), with the temperature recordings for stations SFX and UABX (Fig. 9), stations outside and

inside of government buildings, respectively. In this comparison, for station SFX (Fig. 9) we observed that: from around May to October (time period of the highest temperatures, $\sim 39^\circ \text{ C}$) the levels of noise are between -130 and -115 dB; for the other months (time period of the lower temperatures, $\sim 16^\circ \text{ C}$), the levels of noise are high (-115 to around -90 dB). In the case of UABX, although the surrounding temperature is regulated, we observe (but not as evident as at station SFX) the same behavior: high outside temperatures against lower levels of noise (-150 to -130 dB), and less outside temperatures against levels of noise high (but trending to be constant, at around -130 dB). This implies that the sensor is sensitive to the outside temperatures.

The temperature data were collected from the MSs TO55 and 24 (adjacent to the seismic stations, Fig. 1). In this comparison, we observed that, when the temperature reaches 40° C , and remains this high for around three months, temperature levels are correlated with low noise levels of station SFX in the 4.0 - 8.5 s period band (Figure 9a). While at station UABX, with near the same outside temperature range but inside a temperature-regulated building, the relationship between temperature and noise levels (from 4 to 8.5 s period band) is not obvious as at station SFX.

We selected meteorological records of a three-year period (January 2013 to December 2015) to analyze a possible effect of atmospheric pressure in the noise levels recorded. We observed that station 28 shows a $\sim 0.001 \text{ MPa}$ variation (between ~ 0.099 and 0.1005 MPa) of pressure levels (Fig. 8a), with maxima during winter and minima during summer, and a mean level of $\sim 0.1 \text{ Mpa}$ (Fig. 8a). For station 24 we observed a $\sim 0.025 \text{ MPa}$ variation (from ~ 0.100 to 0.125 Mpa) pressure levels recorded during winter and summer, respectively; mean levels are varying around 0.1125 MPa (Fig. 8c). For station 160 we do not observe substantial variations during winter and summer, but atmospheric pressure levels are $\sim 0.084 \text{ MPa}$ (Fig. 8b). Comparing these values with those of the other two MS, we observe that they are ~ 0.016 and $\sim 0.0284 \text{ MPa}$

lower than pressure recordings of stations 28 and 24, respectively.

To analyze the possible atmospheric pressure relationship with noise levels, we compared the PSD derived from SFX and UABX records, which are close to the MS that present the highest pressure variations (24 and TO55, respectively). The period band of noise level spectrograms affected by the atmospheric pressure is between 4 and 8.5 s. At station SFX (Fig. 9a) the relationships between noise levels and atmospheric pressure are as follows: i) from January to July and from October to December pressure levels are high (~ 0.1025 MPa) and MNLs rise between -110 and -90 dB; ii) from July to October pressure levels are low (~ 0.1 MPa) and noise levels descend to ~ -140 dB. This represents a ~ 40 dB noise level variation related to a ~ 0.0025 MPa atmospheric pressure variation. At station UABX (Fig. 9b) we see a similar behavior: i) from January to July and from October to December, when atmospheric pressure levels are high (~ 0.1025 MPa), the MNLs vary from -140 to -120 dB; ii) from July to October, when pressure recordings are low (~ 0.1 MPa), noise levels descend between -160 and -140 dB. This represents a ~ 40 dB noise level variation related to a ~ 0.0025 MPa atmospheric pressure variation.

Therefore, from at least for these two sites, there is a direct relationship between the variation of pressure and seismic noise for the station outside of temperature-regulated environments: higher pressure values are related to an increase of noise levels, low pressure corresponds to a decrease of noise levels. Also, the relationship with the temperature and the noise levels are inversely proportional for stations outside of temperature-regulated environments: low temperature is related to high noise levels, high temperature corresponds to a decrease of noise levels. For the station inside of a temperature-regulated, the relationships between temperature and noise levels is inversely. Similar behaviors were observed by Stutzmann *et al.* (2000, 2012).

It is hard to differentiate the influence of temperature or pressure on seismic noise.

It would be necessary to have a single parameter well controlled (the temperature for instance) to determine the influence, or not, of the other parameter. This is approximately satisfied at station UABX, where the ambient temperature is regulated.

III.5 Conclusions

We characterized ambient seismic noise levels of northern Baja California using continuous noise records and the PSD technique. Based on the PSD Median Noise Level results, we show that the Mexicali Valley is characterized by levels of noise (up to 20 dB at periods less than 1 s) higher than those of the Peninsular Ranges of Baja California. This difference in the PSD Median Noise levels is explained in terms of the influence of cultural noise. For security reasons, among others, most of our stations on the Mexicali valley are located close or inside human facilities.

We found variations in the PSD Median Noise Level values due to changes of seismometers (from Güralp CMG-3ESPC to Nanometrics Trillium Compact, both with the same bandwidth) at three sites. For periods less than 1 s the PSD results derived from Güralp records trend to the NHNM, at periods between 2 and 20 s the results are similar, and at long periods the PSD results suggest a bimodal behavior of the NTC sensor. Based on these results, and due to the maximum temperatures in the MV region (up to 50° C) for the three stations, we conclude that, at least for NBC, the best results are obtained using Güralp sensors.

Since northern Baja California, Mexico has long shorelines with the Pacific Ocean (west coast) and the Gulf of California (east coast), we analyzed the possible influence of variations of sea level on the ambient noise. We did not find evidence of a correlation between stacked PSDs (at selected periods) and the Pacific Ocean Sea Level data.

So, we conclude that there is no obvious influence of variations of the sea level on the ambient noise analized.

Regarding the meteorological influence (temperature and pressure on noise) for stations in MV, where a wide range of temperatures occurs, we did find a relation between the annual temperature cycle and changes in the noise levels (in the 4.0 to 8.5 s period band) for stations that are exposed to outside temperature; stations that are not inside of temperature-regulated environments (buildings). Concerning the influence of atmospheric pressure on the noise, in the 4.0 to 8.5 s period band, an increase of atmospheric pressure led to an increase of noise levels and vice versa.

Because the noise spectral levels lie between the NHNM and NLNM, we concluded that the functioning of RESNOM is overall good.

III.6 Data and Resources

Data from the Northwestern Mexico Seismic Network are available, since September 10, 2014, from the Incorporated Research Institutions for Seismology Data Management Center (IRIS-DMC) at <http://ds.iris.edu/mda/BC> (last accessed on November 2018). The 2013-up-to-September 9, 2014 data used in this study are available upon request to M. A. N-L. (anunez@cicese.mx).

INEGI provided the geological data for the Northern Baja California at <http://www.beta.inegi.org.mx/temas/mapas/geologia/> (last accessed on November 2018).

Meteorological recordings of Northern Baja California were provided by CONAGUA, <http://smn.cna.gob.mx/es/pronosticos/8-smn-general/38-estaciones-meteorologicas-automaticas-emas> (last accessed on November 2018) and by request to the General Coordination of the National Weather Service (CGSMN).

We obtained POSL of buoy 46232 from the National Data Buoy Center; NOAA, [http://www.ndbc.noaa.gov/stationpage.php?station = 46232](http://www.ndbc.noaa.gov/stationpage.php?station=46232) (last accessed on November 2018).

Some plots were made using the Generic Mapping Tools version 5.3.1 <http://gmt.soest.hawaii.edu/> (last accessed on November 2018).

Plots of Figure 3b were computed using PQLX by Boaz Consultancy, <https://ds.iris.edu/ds/nodes/dmc/software/downloads/pqlx/> (last access on November 2018).

III.7 Acknowledgments

The first author was supported by the National Council of Science and Technology (CONACYT) under the scholarship number 254218. The Northwest Mexico Seismic Network is funded and operated by the Department of Seismology of CICESE under project no. 643118. This work was performed using the facilities of CICESE. The publishing charges were funded by PRODEP 2019 program at the Universidad Autónoma de Baja California, Instituto de Ingeniería. We acknowledge the personnel of RESNOM who are in charge of the installation, maintenance and administration of the seismic network: Luis Orozco, Oscar Gálvez, Ignacio Méndez, Francisco Farfán, Sergio Arregui, Guillermo Díaz, and Julia Sánchez. Sergio Arregui also provided the main script used for generating the maps using the Generic Mapping Tools software, and he wrote the programs to access and download the seismic records from the RESNOM database. We thank Raúl R. Castro and Joann Stock for reviewing the manuscript and helping us to improve it. The comments and suggestions provided by the Editor-in-Chief Thomas Pratt, the associate editor Cleat Zeiler, and the two anonymous reviewers substantially improved the content of this paper. INEGI provided vectorial data for the geological

map of Northern Baja California. Manuel E. Colima-Sánchez provided temperature data from Technical Management of the Peninsula Basin Baja California, CONAGUA. The General Coordination of the National Weather Service (CGSMN) of CONAGUA provided pressure and temperature data of some meteorological stations. We obtained the Pacific Sea Levels from the National Data Buoy Center; National Oceanic and Atmospheric Administration (NOAA).

III.8 Bibliography

Alves, J. H. G. M. (2006). Numerical modeling of ocean swell contributions to the global wind-wave climate, *Ocean Model.*, 11(1), 98-122, <https://doi.org/10.1016/j.ocemod.2004.11.007>.

Burtin, A., L. Bollinger, J. Vergne, R. Cattin, and J. L. Nábělek (2008). Spectral analysis of seismic noise induced by rivers: A new tool to monitor spatiotemporal changes in stream hydrodynamics, *J. of Geophys. Res.: Solid Earth* 113 (B015301), <https://doi.org/10.1029/2007JB005034>.

Custódio, S., N. A. Dias, B. Caldeira, F. Carrilho, S. Carvalho, C. Corela, L. Mtias, C. Haberland, and the WILAS Team (2014). Ambient noise recorded by a dense broadband seismic deployment in western Iberia, *Bull. Seismol. Soc. Am.* 104 (6) 2985-3007, <https://doi.org/10.1785/0120140079>.

Díaz, J., A. Villasenor, J. Morales, A. Pazos, D. Cordoba, J. Pulgar, J. L. García-Lobn, M. Harnafi, R. Carbonell, J. Gallart, and TopoIberia Seismic Working Group (2010).

Background noise characteristics at the IberArray broadband seismic network, Bull. Seismol. Soc. Am. 100 (2) 618-628, <https://doi.org/10.1785/0120090085>.

Garcia Nava H., B. Esquivel Trava, and A. Ruiz de Alegria Arzaburu (2015). Climatología, variabilidad y tendencia del oleaje en la zona del pacífico mexicano, presented in the 2015 UGM Annual Meeting, november 2015.

Gonzalez-Ortega, A., Y. Fialko, D. Sandwell, A. F. Nava-Pichardo, J. Fletcher, J. Gonzalez-Garcia, and G. Funning (2014). El Mayor-Cucapah (Mw 7.2) earthquake: Early near-field postseismic deformation from InSAR and GPS observations, J. Geophys. Res.: Solid Earth 119 (2) 1482-1497, <https://doi.org/10.1002/2013JB010193>.

Govoni, A., L. Bonatto, M. Capello, A. Cavaliere, C. Chiarabba, E. D'Alema, S. Danesi, S. Lovati, L. Margheriti, M. Massa, S. Mazza, F. Mazzarini, S. Monna, M. Moretti, A. Nardi, D. Piccinini, C. Piromallo, S. Pondrelli, S. Salimbeni, E. Serpelloni, S. Solarino, M. Vallocchia, M. Santulin and the AlpArray Working Group (2017). AlpArray-Italy: Site description and noise characterization, Adv. Geosci. 43 39-52, <https://doi.org/10.5194/adgeo-43-39-2017>.

Hauksson, E., J. Stock, K. Hutton, W. Yang, J. Antonio Vidal-Villegas, and H. Kanamori (2011). The 2010 Mw 7.2 El Mayor-Cucapah earthquake sequence, Baja California, Mexico and Southernmost California, USA: Active seismotectonics along the Mexican Pacific Margin, Pure. Appl. Geophys. 168 (8/9) 1255-1277, <https://doi.org/10.1007/s00024-010-0209-7>.

Lomnitz, C., C. R. Mooser, C. R. Allen, J. N. Brune, and W. Thatcher (1970). Seismic-

ity and tectonics of the northern Gulf of California region, México, preliminary results, Geofs. Int. 10 37-48.

McNamara, D. E. and R. P. Buland (2004). Ambient noise levels in the continental United States, Bull. Seismol. Soc. Am. 94 (4) 1517-1527, <https://doi.org/10.1785/012003001>.

Pelayo, A., L. A. Razo, N. L. C. A. Gutiérrez, G. F. Arellano, J. M. Espinoza, and J. L. Quijano (1991). Main geothermal fields of Mexico: Cerro Prieto geothermal field, Baja California, Geological Society of America, The Geology of North America, Vol. P-3, Economic Geology (Editor Guillermo P. Salas), México, 23-58.

Peterson, J. (1993). Observations and modeling of seismic background noise, U.S. Geol. Surv. Open-File Rept., 93-322.

Seiler, C., J. M. Fletcher, M. C. Quigley, A. J. Gleadow, and B. P. Kohn (2010). Neogene structural evolution of the Sierra San Felipe, Baja California: Evidence for proto-gulf transtension in the Gulf Extensional Province?, Tectonophysics 488 (1) 87-109, <http://dx.doi.org/10.1016/j.tecto.2009.09.026>.

Stutzmann, E., G. Roult, and L. Astiz (2000). GEOSCOPE station noise levels, Bull. Seismol. Soc. Am. 90 (3) 690-701, <https://doi.org/10.1785/0119990025>.

E. Stutzmann, F. Arduin, M. Schimmel, A. Mangeney, G. Patau (2012). Modelling long-term seismic noise in various environments, Geophys. J. Int. 191 (2) 707-722, <https://doi.org/10.1111/j.1365-246X.2012.05638.x>.

Suárez-Vidal, F., R. Mendoza-Borunda, L. M. Nafarrete-Zamarripa, J. Ramírez, and E. Glowacka (2008). Shape and dimensions of the Cerro Prieto pull-apart basin, Mexicali, Baja California, Mexico, based on the regional seismic record and surface structures, Int. Geol. Rev. 50 636-649, doi:10.2747/0020-6814.50.7.636.

Vidal-Villegas, J. A., L. Munguía, J. A. González-Ortega, M. A. Nuñez-Leal, E. Ramírez, L. Mendoza, R. R. Castro, and V. Wong (2018). The Northwest Mexico Seismic Network: Real-Time Seismic Monitoring in Northern Baja California and Northwestern Sonora, Mexico, Seismol. Res. Lett. 89 (2A) 324-337, doi: 10.1785/0220170183.

III.9 Mailing Address

Erik E. Ramirez - ramirez.erik@uabc.edu.mx

Universidad Autónoma de Baja California (UABC), Instituto de Ingeniería. Calle de la Normal S/N, Insurgentes Este, 21280, Mexicali, Baja California, México.

J. Antonio Vidal-Villegas - vidalv@cicese.mx

Centro de Investigación Científica y de Educación Superior de Ensenada, Baja California (CICESE) División Ciencias de la Tierra. Carretera Ensenada-Tijuana 3918, Zona Playitas, 22860, Ensenada, Baja California, México.

M. Alejandra Nuñez-Leal - anunez@cicese.mx

Centro de Investigación Científica y de Educación Superior de Ensenada, Baja California (CICESE) División Ciencias de la Tierra. Carretera Ensenada-Tijuana 3918, Zona

Playitas, 22860, Ensenada, Baja California, México.

Jorge Ramírez-Hernandez - jorger@uabc.edu.mx

Universidad Autónoma de Baja California (UABC), Instituto de Ingeniería. Calle de la Normal S/N, Insurgentes Este, 21280, Mexicali, Baja California, México.

Adán Mejía-Trejo - amejia@uabc.edu.mx

Universidad Autónoma de Baja California (UABC), Instituto de Investigaciones Oceanológicas (IIO). Carretera Ensenada-Tijuana 3917, Fraccionamiento Playitas, 22860, Ensenada, Baja California, México.

Eliana Rosas-Verdugo - eliana.rosas@uabc.edu.mx

Centro de Investigación Científica y de Educación Superior de Ensenada, Baja California (CICESE) División Ciencias de la Tierra. Carretera Ensenada-Tijuana 3918, Zona Playitas, 22860, Ensenada, Baja California, México.

III.10 Tables

Tabla I: Characteristics of Northwest Mexico Seismic Network(RESNOM) stations: Their instrumentation and the site geology.

Station Code	Seismometer Accelerometer	Operation period (°) (mm/yyyy)	Latitude (°)	Longitude	Altitude (m)	Site Geology †
ALAMX*	CMG-3ESPC <i>FBA ES-T</i>	11/2015 - today	32.0075	-115.7081	314	Intrusive igneous acid rock (Mesozoic, Cretaceous).
CBX	CMG-40T <i>FBA ES-T</i>	06/2001 - today	32.3131	-116.6636	1250	Intrusive igneous, intermediate rock (Mesozoic, Cretaceous).
CCX	CMG-3ESPC <i>FBA ES-T</i>	06/2011 - today	31.8678	-116.6645	33	Extrusive igneous, intermediate rock (Mesozoic, Cretaceous).
CHX	CMG-40T CMG-3ESPC <i>FBA ES-T</i> 03/2016 - today	11/2012 - 03/2016 03/2016 - today	31.4721	-115.0521	49	Intrusive igneous, acid rock (Cenozoic, Neogene).
CPX	CMG-3ESPC <i>FBA ES-T</i>	05/2012 - today	32.4195	-115.3050	179	Extrusive igneous, basic (Cenozoic, Quaternary).
DOCX*	NTC - 120s <i>FBA ES-T</i>	06/2014 - today	31.9594	-114.7451	13	Soil (Cenozoic, Quaternary).
GUVIX	NTC - 120s <i>FBA ES-T</i>	06/2014 - today	32.3029	-115.0762	14	Soil (Cenozoic, Quaternary).
JARAX*	NTC - 120s <i>FBA ES-T</i>	06/2015 - today	32.5378	-115.5815	5	Soil (Cenozoic, Quaternary).
PESCX	NTC - 120s <i>FBA ES-T</i>	06/2015 - today	32.4338	-114.9649	23	Soil (Cenozoic, Quaternary).
PIX	CMG-3ESPC <i>FBA ES-T</i>	07/2011 - today	31.5629	-113.4599	72	Metamorphic, Gneiss rock (Precambrian, N/D).
RHX	CMG-3ESPC NTC - 120s <i>FBA ES-T</i> 06/2014 - today	07/2013 - 06/2014 06/2014 - today	32.1350	-115.2843	16	Soil (Cenozoic, Quaternary).
RITX*	NTC - 120s <i>FBA ES-T</i>	06/2015 - today	32.1659	-114.9613	14	Soil (Cenozoic, Quaternary).
RMX	CMG-3ESCP NTC - 120s <i>FBA ES-T</i> 06/2014 - today	11/2011 - 06/2014 11/2011 - today	32.5535	-116.0290	1265	Intrusive igneous, acid rock (Mesozoic, Cretaceous).
SFX	CMG-3ESCP <i>FBA ES-T</i>	06/2012 - today	31.0376	-114.8510	48	Metamorphic metasedimentary rock (Paleozoic, N/D).
SJX	CMG-3ESCP <i>FBA ES-T</i>	03/2012 - today	32.0048	-115.9480	1609	Intrusive igneous, acid rock (Mesozoic, Cretaceous).
SLRCX	NTC - 120s <i>FBA ES-T</i>	06/2014 - today	32.4579	-114.7058	49	Soil (Cenozoic, Quaternary).
SPX	CMG-3ESPC <i>FBA ES-T</i>	05/2011 - 08/2015	31.0451	-115.4660	2790	Metamorphic Gneiss (Mesozoic, N/D).
SQX	CMG-3ESCP <i>FBA ES-T</i>	12/2011 - today	30.5762	-115.8758	101	Conglomerate sedimentary rock (Cenozoic, Tertiary).
SVX*	NTC - 120s	05/2015 - today	31.3271	-116.2510	111	Intrusive igneous, acid rock (Mesozoic, Cretaceous).
TJX	CMG-3ESCP NTC - 120s <i>FBA ES-T</i> 06/2014 - today	06/2011 - 06/2014 06/2011 - today	32.5102	-117.0543	198	Soil (Cenozoic, Quaternary).
TKX	CMG-3ESCP NTC - 120s <i>FBA ES-T</i> 06/2014 - today	11/2011 - 06/2014 11/2011 - today	32.5687	-116.6075	535	Intrusive igneous, acid rock (Mesozoic, Cretaceous).
TLX	CMG-40TD	05/2013 - today	32.448	-115.109	17	Soil (Cenozoic, Quaternary).
TPICX*	CMG-3ESCP <i>FBA ES-T</i>	09/2014 - today	21.483	104.848	923	Soil.
UABX	CMG-3ESCP NTC - 120s <i>FBA ES-T</i> 06/2014 - today	07/2011 - 06/2014 07/2011 - today	32.6316	-115.4447	5	Soil (Cenozoic, Quaternary).
VTX	CMG-3ESCP <i>FBA ES-T</i>	11/2011 - today	31.3914	-115.784	746	Soil (Cenozoic, Quaternary).
YACAX*	NTC - 120 s <i>FBA ES-T</i>	06/2015 - today	32.6054	-115.0938	21	Soil (Cenozoic, Quaternary).

* Not included in this study because there was not enough data (more than 1 year).

† Site geology was taken from geology maps (National Institute of Statistics and Geography [INEGI]: 1:250 000).

Tabla II: Meteorological stations of the National Water Commission, Mexico (CONAGUA)

Name (Station Code)	Latitude ($^{\circ}$)	Longitude ($^{\circ}$)	Altitude (m)	Site geology*
Ensenada (16)	31.1041	-116.1683	147	Intermediate Igneous Extrusive (Mesozoic, Cretaceous).
Tecate (22)	32.5411	-116.0475	1245	Intrusive Igneous Acid (Mesozoic, Cretaceous).
Las Escobas (23)	30.5797	-115.9386	27	Soil (Cenozoic, Quaternary).
Mexicali (24)	32.665	-115.4558	2	Soil (Cenozoic, Quaternary).
P. A. L. Rodriguez (28)	32.4476	-116.9091	174	Soil (Cenozoic, Quaternary).
San Vicente (44)	31.3288	-116.2484	113	Intrusive Igneous Acid (Mesozoic, Cretaceous).
Valle de las Palmas (56)	32.5369	-116.62	667	Intrusive Igneous Acid (Mesozoic, Cretaceous).
San Luis (59)	32.4229	-114.7544	32	Soil (Cenozoic, Quaternary).
Ej. Vale de la Trinidad (84)	31.3622	-115.76	763	Soil (Cenozoic, Quaternary).
Ej. Nuevo B. C. (100)	30.5188	-115.9504	13	Soil (Cenozoic, Quaternary).
P. P. Cuchuma (155)	32.569	-116.6611	551	Intrusive Igneous Acid (Mesozoic, Cretaceous).
Constitucion 1857 (160)	32.0416	-115.9216	1576	Intrusive Igneous Acid (Mesozoic, Cretaceous).
P. Lopez Zamora (161)	31.8913	-116.603	32	Intrusive Igneous Acid (Mesozoic, Cretaceous).
El Pinacate (162)	31.6797	-113.3044	99	Soil (Cenozoic, Quaternary).
Nuevo Leon (TO40)	32.4127	-115.1919	12	Soil (Cenozoic, Quaternary).
San Felipe (TO55)	31.0285	-114.8467	149	Soil (Cenozoic, Quaternary).

* Site geology was taken from geology maps (National Institute of Statistics and Geography [INEGI]: 1:250 000).

III.11 Figure Captions

Figure 1. Map showing the two main geological provinces of northwestern Mexico and the tectonic interaction between the North American and Pacific plates (inset). The gray area of inset shows the Gulf Extensional Province (Suárez-Vidal *et al.*, 2008). The detailed map shows the main faults (red lines) of the Northern Baja California and southern California regions, and the locations of the permanent seismic stations deployed in Northern Baja California, Mexico, and southern California, USA: RESNOM, black triangles (CMG-3ESPC and CMG-40T sensors) and inverted blue triangles (Trillium Compact sensors); Southern California Seismic Network, white triangles; Servicio Sismológico Nacional, blue diamonds; purple diamonds, meteorological stations with station code in purple. The black circle indicates the location of the Point Loma buoy (46232). The white star denotes the epicenter of the El Mayor - Cucapah earthquake (April 2010) Mw 7.2. The black dashed line represents the Main Gulf Escarpment. Abbreviations: MV, Mexicali Valley; PRBC, Peninsular Ranges of Baja California; LS,

Laguna Salada; EMM, El Mayor Mountains; CM, Cucapah Mountains; SJM, Sierra Járez Mountains, SPM; San Pedro Mártir Mountains; SFM, San Felipe Mountains. Faults (in red): SPMF, San Pedro Mrtir fault; ABF, Agua Blanca fault; SDF, San Diego fault; SCF, San Clemente fault; THF, Tres Hermanos fault; SMF, San Miguel fault; VF, Vallecitos fault; SJF, Sierra Juárez fault; TF, Tinajas fault; CDDF, Cañada David detachment fault; CRF, Cañon Rojo fault; LSF, Laguna Salada fault; CF, Cucapah fault; InF, Indiviso fault; CPF, Cerro Prieto fault; IF, Imperial fault; AF, Algodones fault; EF, Elsinore fault. The locations of the plotted main faults were obtained from Seiler *et al.* (2010) and Gonzalez-Ortega *et al.* (2014).

Figure 2. The plot to illustrate the availability of data from RESNOM stations from 2013 to 2016. Data recorded by the network are from the following sensors: Black, CMG-40T, and CMG-3ESPC; gray, NTC-120s; white, FBA ES-T.

Figure 3. (a) Power Spectral Density computed from the vertical component of background seismic noise at station SJX during 2013. The median noise level is shown in black, and the vertical color scale to the right indicates the probability of the presence of amplitudes. (b) The gray lines and the black line denotes the Average Power Spectral Density values, and the median value, respectively. In both figures, blue and red lines indicate the NLNM and the NHNM models. The bottom plot indicates data availability for the 2013 calendar year period; the data gap (May 2013) is due to loss of satellite connection.

Figure 4. (a, b, c) Three-component median noise curves for PRBC and (d, e, f) MV regions. Noise spectral levels computed for each station (gray lines), and median noise level (black line). The Peterson noise curves are NLNM (dashed line) and NHNM (dotted-line).

Figure 5. Noise spectral levels comparison for stations RMX, TKX, and UABX, which were instrumented with different sensors: for the 2013 year, with CMG-3ESPC sensors,

(a, b, c); for the 2015 year with NTC sensors, (d, e, f). Dotted and dashed lines indicate the reference spectral noise levels, NHNM and NLNM, respectively.

Figure 6. Average values of PSD (gray lines) during 2013 of UABX (a to c) and CPX (d to f) and the MNLs (black line), NHNM (red line) and NLNM (blue line). Also, shown is the hourly spectrogram of PSD for seven days for UABX (g) and CPX (h). Vertical color bar indicates the PSD level. The x-axis of (g) and (h) indicates time, in the local time zone (UTC-7), in the hh:mm DD/MM/YYYY format.

Figure 7. (a) Vertical component of stacked PSD for selected ground-motion periods (labels on the right side) of all RESNOM stations. (b) POSL elevation at the Point Loma buoy. Sea level peaks (circles) are projected onto stacked PSD (dotted vertical lines).

Figure 8. Daily average temperature (black line) and atmospheric pressure (gray line) recorded by CONAGUA stations. Plots for stations 28 (a) and 24 (c) correspond to a three-year period, and plot for station 160 (b) is for a two-year period.

Figure 9. Comparison of MNLs spectrograms of stations SFX (a) and UABX (b) against atmospheric and temperature recordings (plots below spectrograms) of TO55 and 24 (Fig. 1), respectively. Right color bars indicate the PSD level in dB. Blue plots indicate the average temperature recordings per day, while green plots indicate the atmospheric pressure. In spectrograms of (a), effects due to changes in temperature are visible between 4 and 8.5 s. In the period band between 4 and 8.5 s of the spectrograms, we identify a relationship with the atmospheric pressure, inverse to ambient temperature: high levels of noise are related to high-pressure levels, and vice versa.

III.12 Figures

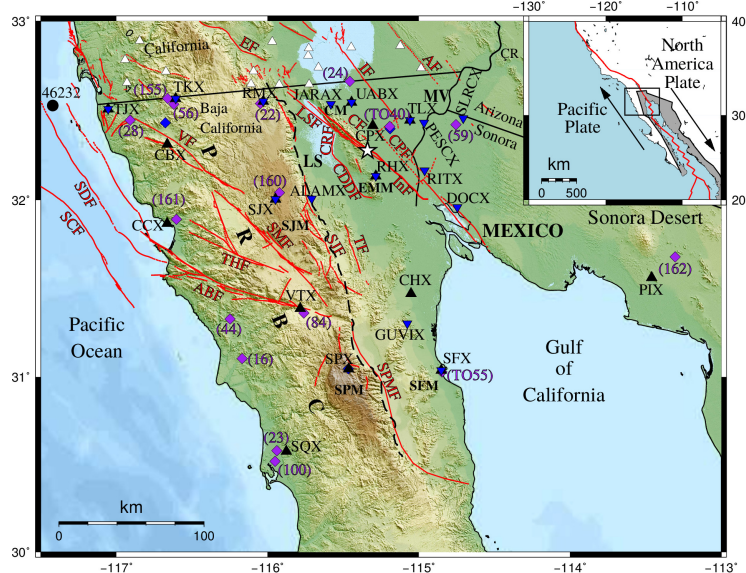


Figura 1: Map showing the two main geological provinces of northwestern Mexico and the tectonic interaction between the North American and Pacific plates (inset). The gray area of inset shows the Gulf Extensional Province (Suárez-Vidal *et al.*, 2008). The detailed map shows the main faults (red lines) of the Northern Baja California and southern California regions, and the locations of the permanent seismic stations deployed in Northern Baja California, Mexico, and southern California, USA: RESNOM, black triangles (CMG-3ESPC and CMG-40T sensors) and inverted blue triangles (Trillium Compact sensors); Southern California Seismic Network, white triangles; Servicio Sismológico Nacional, blue diamonds; purple diamonds, meteorological stations with station code in purple. The black circle indicates the location of the Point Loma buoy (46232). The white star denotes the epicenter of the El Mayor - Cucapah earthquake (April 2010) Mw 7.2. The black dashed line represents the Main Gulf Escarpment. Abbreviations: MV, Mexicali Valley; PRBC, Peninsular Ranges of Baja California; LS, Laguna Salada; EMM, El Mayor Mountains; CM, Cucapah Mountains; SJM, Sierra Járez Mountains, SPM; San Pedro Martir Mountains; SFM, San Felipe Mountains. Faults (in red): SPMF, San Pedro Martir fault; ABF, Agua Blanca fault; SDF, San Diego fault; SCF, San Clemente fault; THF, Tres Hermanos fault; SMF, San Miguel fault; VF, Vallecitos fault; SJF, Sierra Juárez fault; TF, Tinajas fault; CDDF, Cañada David detachment fault; CRF, Cañon Rojo fault; LSF, Laguna Salada fault; CF, Cucapah fault; InF, Indiviso fault; CPF, Cerro Prieto fault; IF, Imperial fault; AF, Algodones fault; EF, Elsinore fault. The locations of the plotted main faults were obtained from Seiler *et al.* (2010) and Gonzalez-Ortega *et al.* (2014).

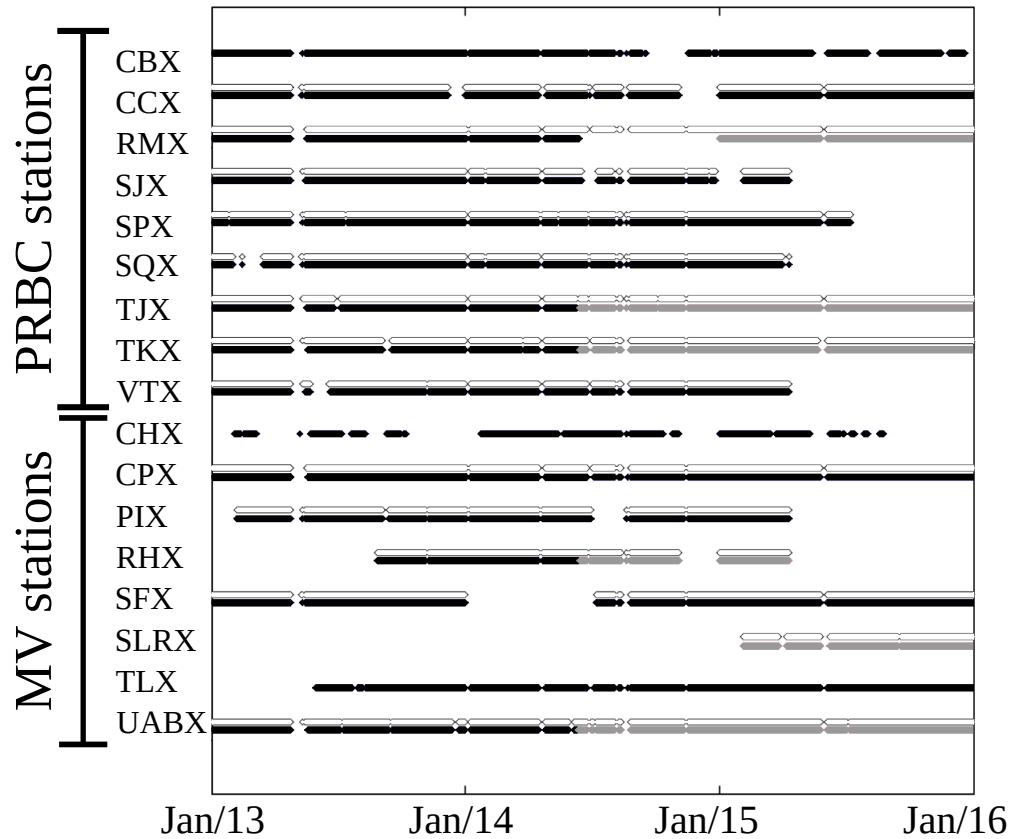


Figura 2: The plot to illustrate the availability of data from RESNOM stations from 2013 to 2016. Data recorded by the network are from the following sensors: Black, CMG-40T, and CMG-3ESPC; gray, NTC-120s; white, FBA ES-T.

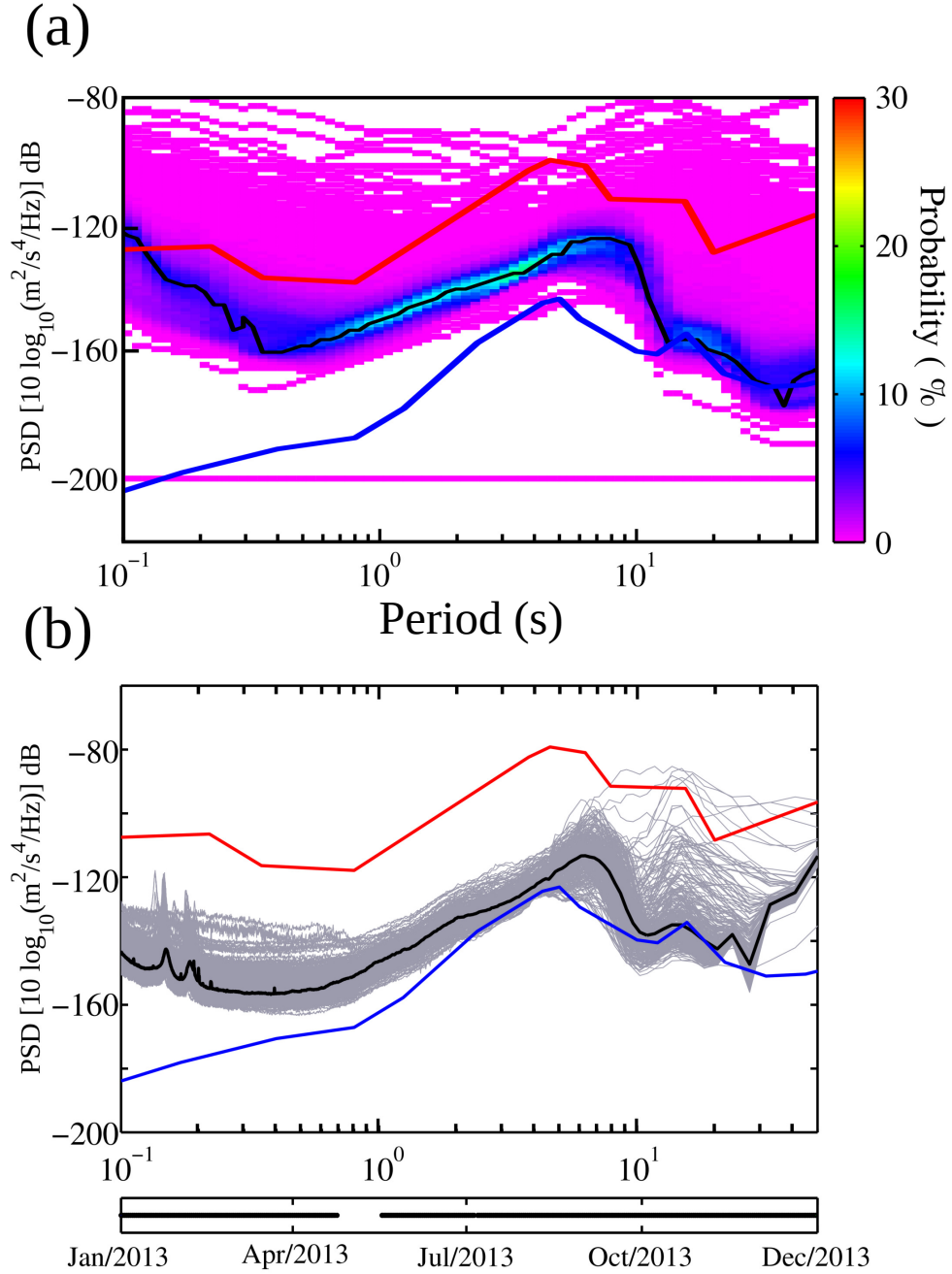


Figura 3: (a) Power Spectral Density computed from the vertical component of background seismic noise at station SJX during 2013. The median noise level is shown in black, and the vertical color scale to the right indicates the probability of the presence of amplitudes. (b) The gray lines and the black line denotes the Average Power Spectral Density values, and the median value, respectively. In both figures, blue and red lines indicate the NLNM and the NHNM models. The bottom plot indicates data availability for the 2013 calendar year period; the data gap (May 2013) is due to loss of satellite connection.

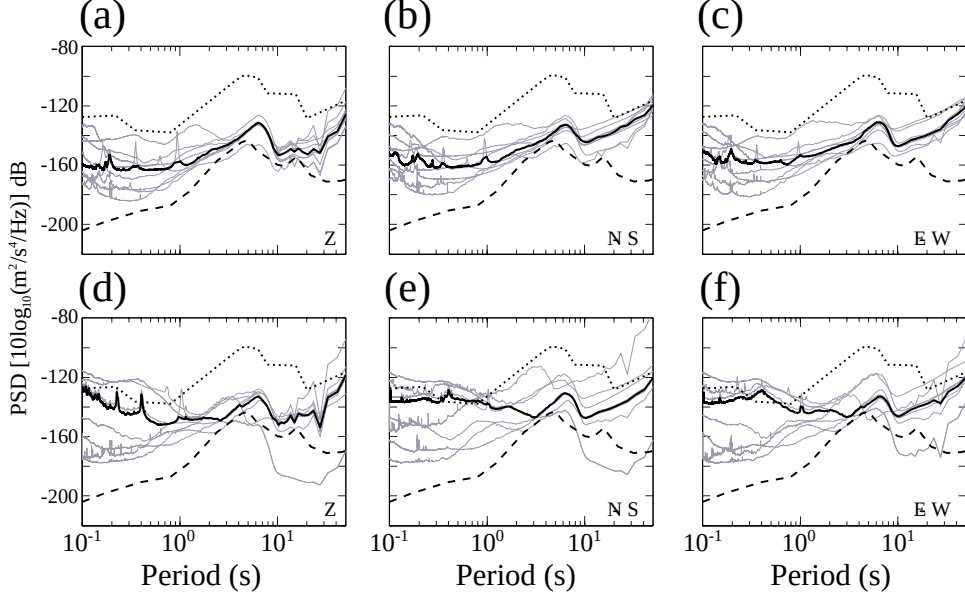


Figura 4: (a, b, c) Three-component median noise curves for PRBC and (d, e, f) MV regions. Noise spectral levels computed for each station (gray lines), and median noise level (black line). The Peterson noise curves are NLNM (dashed line) and NHNM (dotted-line).

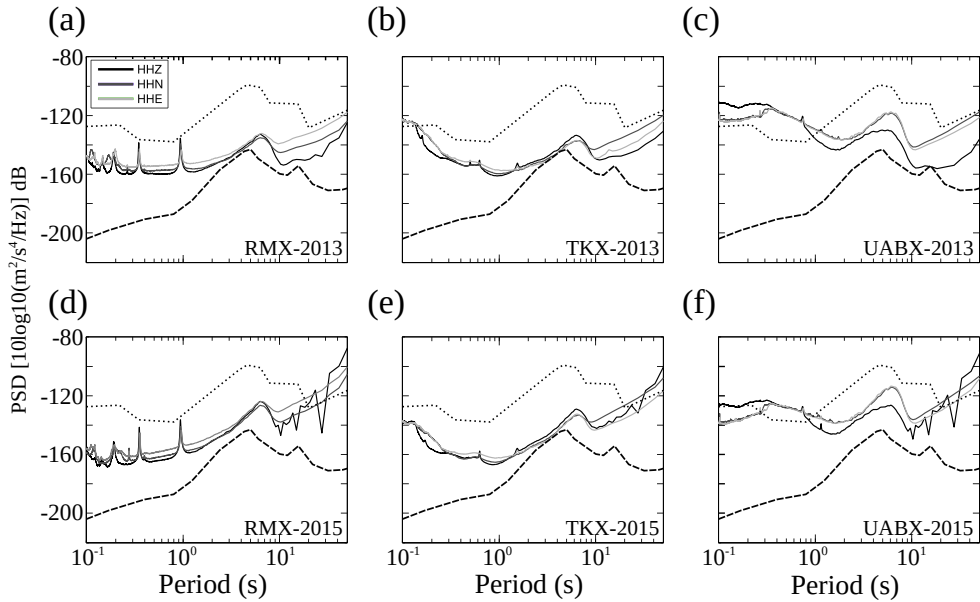


Figura 5: Noise spectral levels comparison for stations RMX, TKX, and UABX, which were instrumented with different sensors: for the 2013 year, with CMG-3ESPC sensors, (a, b, c); for the 2015 year with NTC sensors, (d, e, f). Dotted and dashed lines indicate the reference spectral noise levels, NHNM and NLNM, respectively.

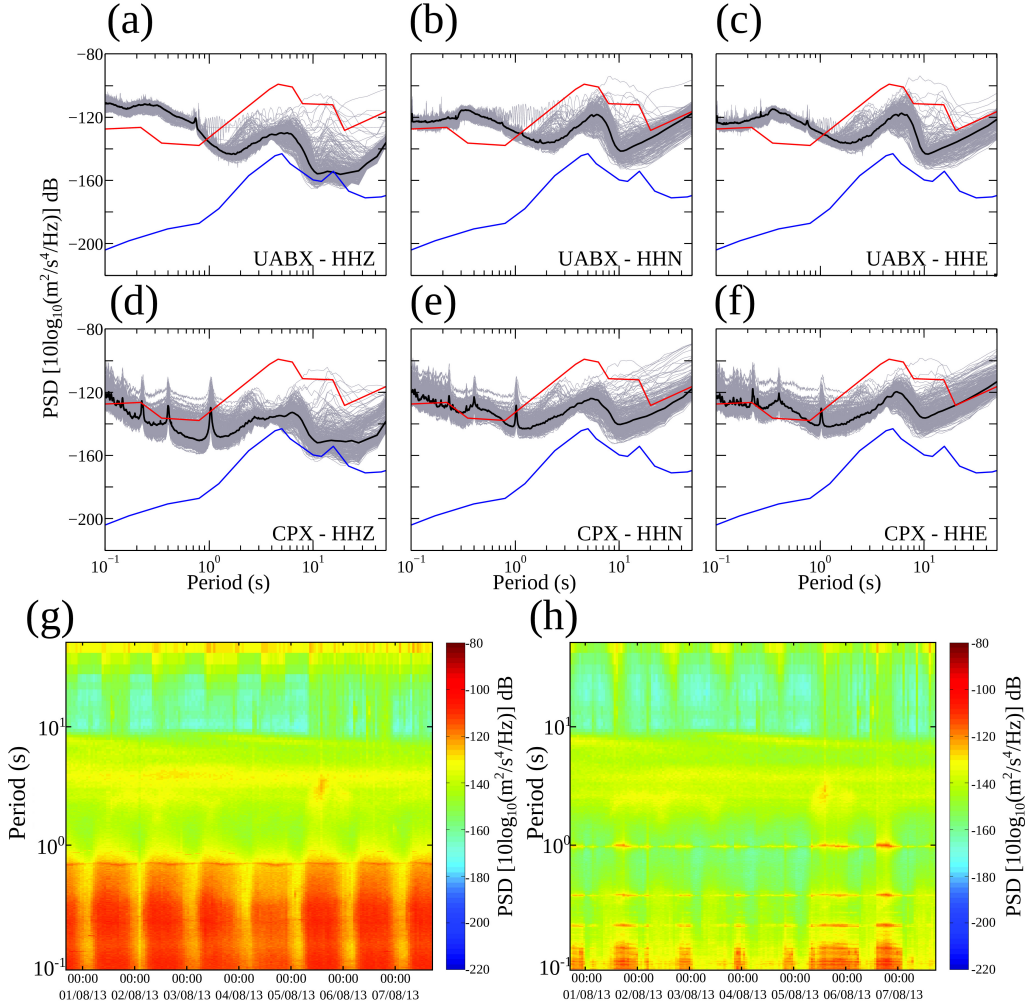


Figura 6: Average values of PSD (gray lines) during 2013 of UABX (a to c) and CPX (d to f) and the MNLs (black line), NHNM (red line) and NLNM (blue line). Also, shown is the hourly spectrogram of PSD for seven days for UABX (g) and CPX (h). Vertical color bar indicates the PSD level. The x-axis of (g) and (h) indicates time, in the local time zone (UTC-7), in the hh:mm DD/MM/YYYY format.

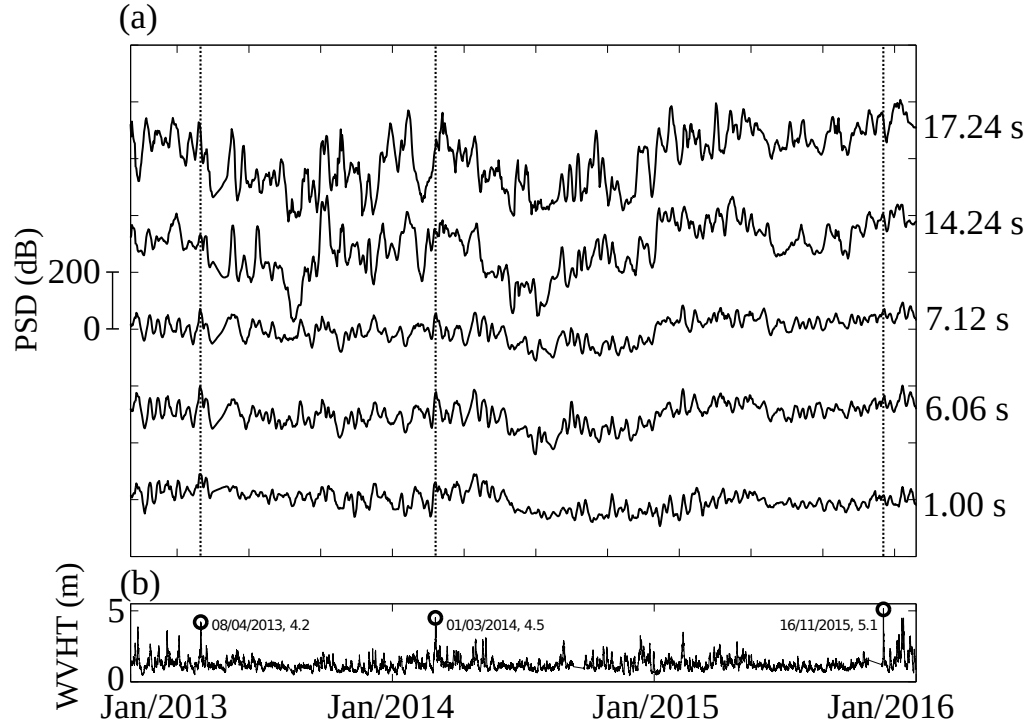


Figura 7: (a) Vertical component of stacked PSD for selected ground-motion periods (labels on the right side) of all RESNOM stations. (b) POSL elevation at the Point Loma buoy. Sea level peaks (circles) are projected onto stacked PSD (dotted vertical lines).

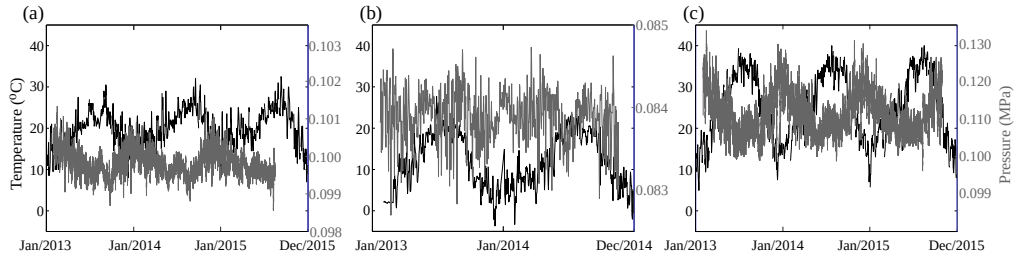


Figura 8: Daily average temperature (black line) and atmospheric pressure (gray line) recorded by CONAGUA stations. Plots for stations 28 (a) and 24 (c) correspond to a three-year period, and plot for station 160 (b) is for a two-year period.

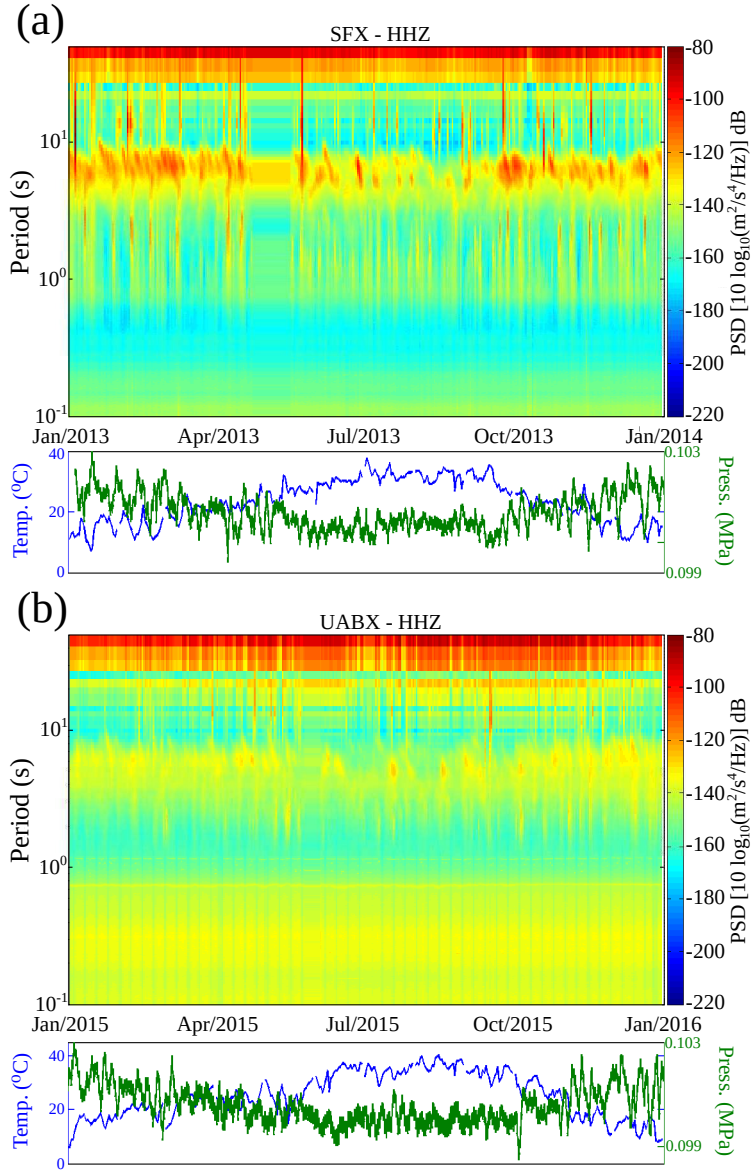


Figura 9: Comparison of MNLs spectrograms of stations SFX (a) and UABX (b) against atmospheric and temperature recordings (plots below spectrograms) of TO55 and 24 (Fig. 1), respectively. Right color bars indicate the PSD level in dB. Blue plots indicate the average temperature recordings per day, while green plots indicate the atmospheric pressure. In spectrograms of (a), effects due to changes in temperature are visible between 4 and 8.5 s. In the period band between 4 and 8.5 s of the spectrograms, we identify a relationship with the atmospheric pressure, inverse to ambient temperature: high levels of noise are related to high-pressure levels, and vice versa.

III.13 Description of the Electronic Supplement

This supplemental material is related to: 1) Plots of the period records in the Pacific Ocean, recorded in the Point Loma buoy, and the averages values in the period and dominant period variation. 2) Indicates the variations in the MNL between 4.5 and 8.5 s in the CBX station and its comparison with the Pacific Ocean Sea Levels during 2013.

III.13.1 List of Figure Captions

Figure S1. Period records of the Point Loma buoy (46232). (a) Indicates the average period variation, during the 2013 - 2016 period. (b) Shows the dominant period variation during the same period of time. Both plots indicate the average value in red line and in text as: Mean Average Period (MAP) and Mean Dominant Period (MDP).

Figure S2. (a) Spectrogram of the CBX station during the 2013, the pink rectangle indicates a 4.5 to 8.5 s section where fluctuations in the MNL are visible. (b) Height variations of the Pacific Ocean during 2013, recorded by the Point Loma buoy. Right color bar indicate the PSD level.

III.13.2 Electronic Figures

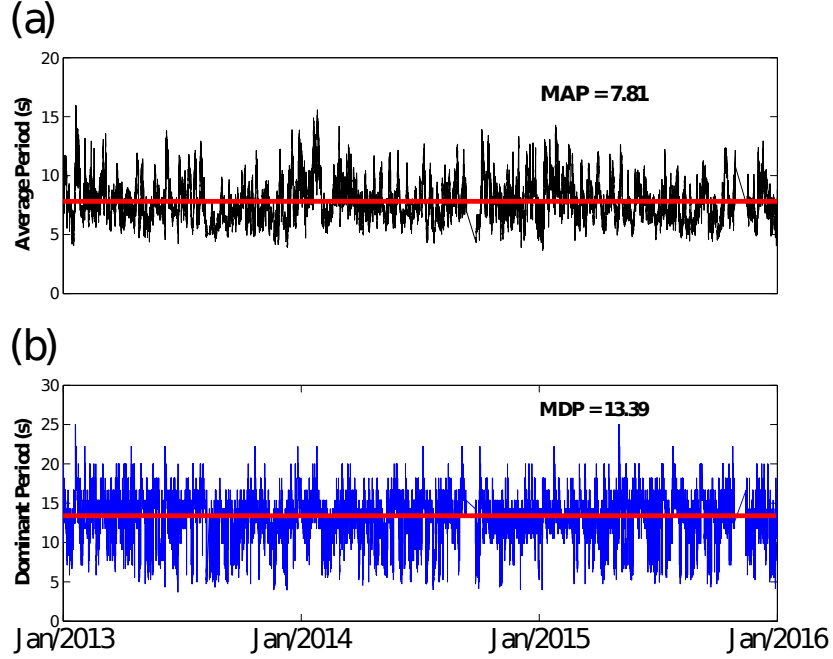


Figura 10: Figure S1. Period records of the Point Loma buoy (46232). (a) Indicates the average period variation, during the 2013 - 2016 period. (b) Shows the dominant period variation during the same period of time. Both plots indicate the average value in red line and in text as: Mean Average Period (MAP) and Mean Dominant Period (MDP).

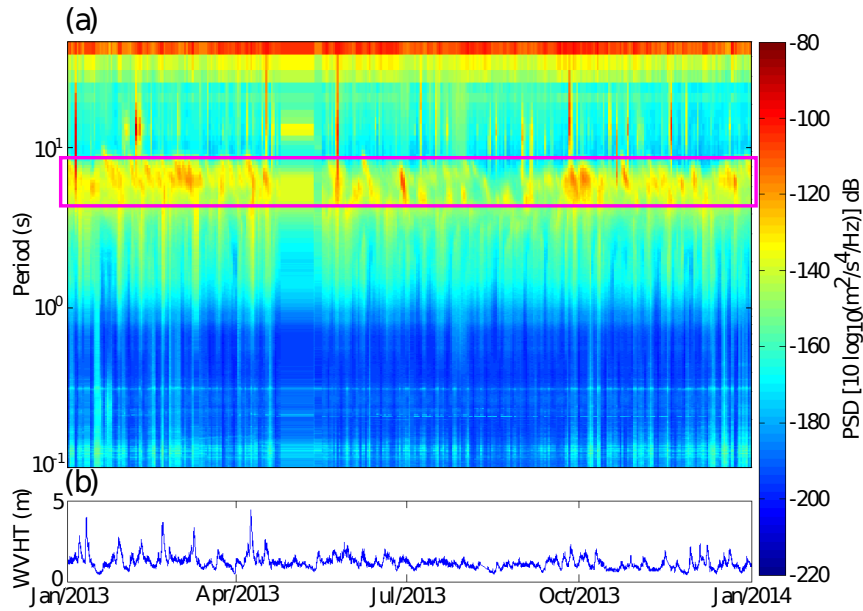


Figura 11: Figure S2. (a) Spectrogram of the CBX station during the 2013, the pink rectangle indicates a 4.5 to 8.5 s section where fluctuations in the MNL are visible. (b) Height variations of the Pacific Ocean during 2013, recorded by the Point Loma buoy. Right color bar indicate the PSD level.

Anexo 2: Crustal Velocity Model, Refraction, Northern Baja California

Erik E. Ramírez[1]

J. Antonio Vidal Villegas[2]

Jorge Ramírez-Hernández[1]

Antonio González-Fernández[3]

Joann M. Stock[4]

[1] Universidad Autónoma de Baja California (UABC), Instituto de Ingeniería. Calle de la Normal S/N, Insurgentes Este, 21280, Mexicali, Baja California, México.

[2] Centro de Investigación Científica y de Educación Superior de Ensenada (CICESE), Departamento de Sismología, División de Ciencias de la Tierra. Carretera Ensenada-Tijuana 3918, Zona Playitas, 22860, Ensenada, Baja California, México.

[3] Centro de Investigación Científica y de Educación Superior de Ensenada (CICESE), Departamento de Geología, División de Ciencias de la Tierra. Carretera Ensenada-Tijuana 3918, Zona Playitas, 22860, Ensenada, Baja California, México.

[4] California Institute of Technology (Caltech), Seismological Laboratory, Division of Geological and Planetary Sciences. Pasadena, CA 91125, USA.

Abstract

To see any change in seismic velocities associated with an abrupt change in the regional geology (granitic rock in contact with sediments), we conducted a refraction seismic study in the Peninsular Ranges of Baja California, Mexico-southwestern Laguna Salada region. We installed 30 three-component portable seismic stations, supplemented with two permanent 6-component stations of the Northwest Mexico Seismic Network. The stations spaced \sim 6 km along a refraction profile recorded two blasts: the direct shot located to the south of the city of Ensenada, and the reverse shot in the southwestern Laguna Salada (SW - NE direction). Record sections show seismograms with impulsive P arrivals at nearby stations. Rays from the two blasts were modeled (using asymptotic ray theory) to obtain a P-wave velocity model from 0 to \sim 15 km depth along the refraction profile. Our modeling results are as follows: in the southwestern part of the profile (0 to 25 km distance), a low-velocity zone of \sim 2 km/s from 0 - 3.5 km depth; in Sierra Juárez the mean P-wave velocity is \sim 5.6 km/s from 0 to 5 km depth; in southwestern Laguna Salada a low-velocity layer of \sim 2.5 km/s from 0 to \sim 3 km depth. We also modeled a layer of \sim 6.5 km/s from 4 to 12 km in the Ensenada-Ojos Negros region, and from 4 to 8 km depth below southwestern Laguna Salada. From 0 - 50 km profile distance, a velocity zone of \sim 6.7 km/s appears from 12 to 15 km depth.

Key words:

Crustal Velocity Model, Refraction, Northern Baja California.

IV.1 INTRODUCTION

The transtension due to relative plate motion of Pacific and North America generates normal and strike-slip faults in northern Baja California (BC; Stock *et al.*, 1991). The plate boundary, continues northwest with mainly right lateral movement (Fig. 1, inset) on the San Andreas fault system (Axen and Fletcher, 1998; Suárez-Vidal *et al.*, 2007; SuÁrez-Vidal *et al.*, 2008; Armstrong *et al.*, 2010; Wei *et al.*, 2011; Oskin *et al.*, 2012). In addition to the faults in northern Baja California (Fig. 1), México, two different geological domains are present: the granitic Peninsular Range of Baja California (PRBC), and the sedimentary environment of the Mexicali Valley region (MV; Lomnitz *et al.*, 1970). The Main Gulf Escarpment (dashed line in Fig. 1) separates these two regions. The sedimentary environment of the Mexicali Valley region is comprised of two basins: Laguna Salada (LS) and Mexicali Valley (MV) basins. The boundary between these basins is the Cucapah and El Mayor mountain ranges, located in the northwestern Gulf Extensional Province (Suárez-Vidal *et al.*, 2008). The Laguna Salada basin is 20 km wide and 100 km long in the north-northwest direction (García-Abdeslem *et al.*, 2001). It is bordered to the west by the Main Gulf Escarpment (Angelier *et al.*, 1981; Henry, 1989) and by the Cucapah and El Mayor mountain ranges to the east. Sediments thickness in the eastern part of LS is around 720 m to 1500 m, based on data from the ELS-3 well and the 4965 seismic reflection profile, respectively (Fig. 1; Gonzalez-Escobar *et al.*, 2016), and increases eastward reaching a thickness of 3 km (García-Abdeslem *et al.*, 2001).

In northern Baja California (BC) refraction studies have been carried out to estimate crustal velocity models of different geological regions:

- (1) Nava and Brune (1982) estimated a crustal velocity model for the PRBC using the 1975 Corona, CA, quarry-blast and a well-located ML 5.1 Pino Solo earthquake (17

July 1975) in a 400 km long NW-SE refraction profile. This model is composed of 4 horizontal layers, and the Moho depth is \sim 42 km.

(2) Nun \tilde{n} ez-Corn \acute{u} *et al.* (1996) performed an unreversed refraction study using a blast located in Blythe, Arizona, as one end of a \sim 300 km long profile oriented in the NE-SW direction, ending at Ensenada, B.C., M \acute{e} xico.

(3) Ram \acute{I} rez-Ramos *et al.* (2015) developed a three flat-layer velocity model (for the southern MV) with a proposed Moho depth at 15 km, using a blast in southern Arizona and a well-located earthquake (from San Luis Rio Colorado to the El Mayor mountains, Fig. 1).

Because of the active tectonic environment of northern BC, as well as the significant seismicity from 31° N to 32.5° N (recorded by the Northwest Mexico Seismic Network, RESNOM), and the occurrence of the 2010 Mw 7.2 El Mayor-Cucapah earthquake (e.g. Hauksson *et al.*, 2011, Gonzalez-Ortega *et al.*, 2014), it is necessary to have detailed velocity models for PRBC and Mexicali Valley. Based on a refraction study, using a profile of \sim 90 km-length, our purpose was to estimate a crustal *P*-wave velocity model beneath the PRBC-southwestern LS (reaching 15-to-20 km depth). The obtained velocity model can be used to improve the locations of earthquakes in the region.

IV.2 INSTRUMENTATION AND DATA

We deployed a temporary seismic refraction profile in May, 2015 and in December, 2016 to record two quarry blasts (Table 1): one at San Carlos, south of the city of Ensenada, BC (blast A) and one located southwestern LS, BC (blast B). Temporary seismic stations were installed along the refraction profile with an approximate spacing between stations of 6-7 km (Table 2 and 3). Instrumentation included: 20 three-component

short-period stations (Geospace Technologies HS-1 [2 Hz] seismometers - 24-bit SARA recorders SL06); one intermediate-band station (PMD [15 s] seismometer - 24-bit PMD recorder); three broadband stations (Nanometrics Trillium Compact [120 s] - 24-bit Nanometrics Taurus recorders). Finally, we also installed six accelerometer stations (two Nanometrics Titan - 24-bit Nanometrics Centaur, and four Kinematics Episensor ES-T and 24-bit REFTEK DAS-130 recorders).

Our dataset also includes recordings from two permanent RESNOM broadband stations: equipped with CMG-3ESPC seismometer, a Kinematics FBA ES-T accelerometer, and 6-channel Reftek 130 recorders (white diamonds in Fig. 1).

IV.3 DATA REDUCTION

Raw vertical-component data from the aforementioned explosions were extracted from recorders, converted to miniSEED format, and used to build a database. Instrument corrections were not applied since the frequency response of the instruments is linear in the frequency range of our interest ($> \sim 1.8$ Hz). Seismograms corresponding to the blast A and recorded by the broadband stations were filtered from 1 - 10 Hz; for the other seismic stations, the P-wave arrivals were clear (good signal-to-noise ratio), so filtering was not necessary.

For the modeling process, we included topography every 1 km (Fig. 2a). The profile crosses, from west to east, different geological settings: Ensenada Mountains, from 10 to 800 m above mean sea level (a.m.s.l.); Ojos Negros Valley, ~ 750 m a.m.s.l.; Sierra Juárez (SJ), maximum of 1780 m a.m.s.l.; the Main Gulf Escarpment, from 1700 to 250 m a.m.s.l.; LS, from ~ 200 to 10 m a.m.s.l.. The extents of the Ojos Negros Valley and LS basins were geographically located, along the refraction profile, and included in the

modeling process.

IV.4 INTERPRETED PHASES

Correlations between arrival times and distances, to each station of the profile, were made using a series of Matlab (<https://www.mathworks.com/products/matlab.html>, last accessed February 2019) scripts written for this purpose; these programs plotted distance against reduced travel-time vertical component seismograms of the A and B blasts (Fig. 2b and 2c). The following vertical components were not used because the *P* arrivals were not clear: from blast B, SS146 and SS136; from blast A, VS132. Instead, E-components (stations SS146 and SS136) and N-component (station VS132) were used. Record sections (Fig. 2b) and (Fig. 2c) were plotted with a reduced velocity of 6.4 km/s, which is the average crustal P-wave velocity in northern BC.

The interpreted phases (Fig. 2b) from the direct shot (A, Table 1) are the following:

- a direct P wave (PA1,1 wave, P wave traveling through sediments) from blast A to an offset distance of \sim 10 km (westeast direction), with a mean velocity of 2.8 km/s;
- a reflected phase (PA1,2), in the crystalline basement, that appears from an offset distance of 5 to 10 km. This phase has an apparent velocity of 5.3 km/s;
- the refracted phase observed in distances between 5 and 58 km is denoted as PA2,1, and this phase has an apparent velocity of 6.3 km/s;
- we identified reflections, in distances between 5 and 54 km, as PA2,2, with an apparent velocity of 6.6 km/s;

- a reflected phase is observed from \sim 10 to 40 km and is identified as PA3,2 with an apparent velocity of 7.0 km/s; and
- a reflection (PA4,2) is observed in the record section in distances between 24 and 58 km and has an apparent velocity of 7.4 km/s.

For the reverse shot (B, Table 1), we identify the following P-wave phases from seismograms (the distances are relative to position of blast A, Fig. 2c):

- a direct *P*-wave (PB1,1) at distances between \sim 90 and 86 km that travels through sediments of eastern LS. The apparent velocity of the shallow sediments is 2.4 km/s.
- a refracted P wave (PB3,1) that appears in the record section between distances of \sim 72 and 46 km, with an apparent velocity of 6.4 km/s;
- the refracted phase (PB4,1) with an apparent velocity of 7.2 km/s, which appears in the record section in the distances between 40 and 7 km; and
- a reflection (PB4,2) that appears in the record section in distances between 71 and 57 km. This phase travels with an apparent velocity of 7.5 km/s.

IV.5 MODELING TRAVEL TIMES AND AMPLITUDES

IV.5.1 Methodology

We did the forward modeling according to Ramírez-Ramos *et al.* (2015); which used the RAYGUI software (by Song and ten Brink, 2005), which is a graphical environment of the RAYINV scripts (Zelt and Smith, 1992). We started the modeling process by using the Nava and Brune (1982) flat-layered velocity model (NB82, Table 4) with the topography added along the top of the profile (Fig. 2a). This initial model is a three-layer model with P-wave velocities of 5.6, 6.6, and 7.0 km/s with depth discontinuities at 5.0 km and 19.8 km, respectively. In the NB82 model the Moho is at \sim 42 km and the half-space velocity below it is 8.0 km/s. In the modeling process, we considered the low velocities of the Laguna Salada basin and the basement depth (between 80 to 100 km distance and at \sim 3 km depth) reported by Ramírez-Ramos *et al.* (2015) and Garca-Abdeslem *et al.* (2001). We performed the forward modeling by adjusting velocity and topography of each velocity interphase (modifying the number, position, and velocity of boundary nodes, Fig. 3a and 4a) to reduce the travel time residuals (calculated minus observed, Fig. 3b and 4b). An arrival time reading error of $+/-$ 0.01 s was considered in the modeling process. By modeling all the observed phases in the direct and reverse shot (Fig. 2b and c, respectively), we produced a three-layer velocity model between \sim 25 and 88 km of distance: Ojos Negros Valley and SJ region. We also produced a four-layer velocity model for the Ensenada Mountains and LS regions. We computed the relative amplitudes of synthetic seismograms of the two blasts (Fig. 3c and 4c) using TRAMP and then plotted them using PLTSYN, both programs were

written by Zelt and Smith (1992). The normalized amplitudes of the synthetic data (Fig. 3c and 4c) were compared to the record sections of the direct and reverse shot (Fig. 2b and c, respectively). To reproduce the average behavior observed in the two recorded sections, we adjusted the amplitudes of the synthetic phases by modifying the velocity contrast and gradient of the nodes. Using DMPLSTSQR (from the RAYINVR software package; Zelt and Smith, 1992) we calculated the root mean square of the adjusted travel-time residual model: 0.093.

IV.5.2 Modeling Results

Raytracing of direct and reverse shot models are shown in Figures 3a and 4a, respectively. In the direct shot, the lack of arrival readings (for distances > 65 km and only two for distances > 50 km) corresponds to the loss of records due to failure of the power supply (the batteries discharged before the blast took place) or the loss of the Global Positioning System time connection.

Because of significant changes in depth in the last interface and the presence of a low-velocity layer at EM and LS in the southwestnortheast direction of the profile (Fig. 5), our crustal velocity model (VM18) was divided as follows:

- 1) EM18: We got a 4-layer velocity model for the Ensenada Mountains region (distances < 22 km), in which the first layer has a mean velocity of 4.1 km/s. The first interface of this section is located at ~ 1.4 km depth, with a 5.3 and 6.4 km/s velocity at top and bottom, respectively. The second layer extends of ~ 6.6 km depth and has a mean velocity of 6.5 km/s. The second interface has velocities of 6.6 and 6.8 km/s at the top and bottom, respectively. The third layer has a mean velocity of 6.9 km/s and reaches ~ 10.9 km depth. The third interface has velocity at the top and bottom of 7.0 and 7.2

km/s, respectively. The fourth layer has a mean velocity of 7.3 km/s. The interface between the fourth layer and the half-space (velocity of 8.0 km/s) was inferred and is located at \sim 35.4 km.

2) SJ18: For the Ojos Negros Valley and Sierra Juárez region, distances from 22 to 87 km, we modeled three layers. The first one, down to \sim 4.5 km depth, has velocities of 5.3 and 6.0 km/s at top and bottom, respectively, with a mean velocity of 5.6 km/s. The second layer is located from \sim 4.5 to \sim 9.5 km depth and has a mean velocity of 6.8 km/s, with top and bottom velocities of 6.6 and 7.0, respectively. The third layer has a mean velocity of 7.3 km/s, and extends from \sim 9.5 to 18.2 km depth; it has a velocity of 7.2 and 7.5 km/s at top and bottom, respectively. This last layer is over a half-space with a mean velocity of 7.9 km/s.

3) LS18: For the Laguna Salada region, at a distances $>$ 87 km, we modeled the LS basin with a mean velocity of 3.0 km/s at \sim 1.6 km depth. The first interface (basement) has a velocity, at the top, of 3.7 and 4.6 km/s at its lower part. This basement depth (\sim 1.6 km) is similar to the results from previous seismic reflection studies (between 0.7 and 1.5 km depth; González-Escobar *et al.*, 2016). The second interface, \sim 4.8 km depth, has an upper and lower velocity of 5.4 and 6.3 km/s, respectively, the mean velocity in the second layer is 5.0 km/s. The third interface is at \sim 8.0 km in depth and has velocities at the top and bottom of 7.0 and 7.3, respectively, the mean velocity of the third layer is 6.6 km/s. The fourth layer has a mean velocity of 7.4 km/s; this layer has a velocity of 7.5 at the bottom. The half-space begins at \sim 11.3 km depth and has a velocity of 7.8 km/s.

IV.6 DISCUSSION

A comparison of crustal velocity models for the two main geological regions of northern BC is as follows:

- 1) For the PRBC region, we compared the NB82 model with the EM18 and SJ18 models that we obtained (Fig. 6a). The EM18 is 1.5 km/s slower than the NB82 between 0 and 1.4 km depth, and \sim 1.0 km/s faster between depths of 1.4 and 6.6 km. Velocities of EM18 and SJ18 are \sim 0.3 km/s faster than those of NB82 between the depths of \sim 5 and 10 km, whereas from 10 to 18 km, the two models are \sim 1 km/s faster than NB82. The velocity model EM18 is 0.3 km/s higher than NB82 between depths of 20 and 35 km.
- 2) For the MV region, we compared LS18 with the regional velocity model (Fig. 6b), also known as the Mexicali Valley model (MVM, Fabriol and Mungua, 1997). The LS18 is 1.30.7 km/s higher than the MVM in depths between 0 and 1.8 km. For depths between 1.8 and 11.3 km, the crustal velocities of LS18 are \sim 2 km/s higher than the MVM. Compared with the crustal velocity model for the southern Mexicali Valley model (SMVM, Ramrez-Ramos *et al.*, 2015), the velocities are more similar to those of the LS18 velocity model, with the difference that the last layer interface in the SMVM is \sim 4 km deeper than is the case with the LS18.

For the interface between the PRBC and southwestern LS the resulting model shows a contrasting difference both in depth and in velocity structure: for the southwestern LS we have a low-velocity layer at the top of the model (\sim 2.5 km/s, reaching \sim 3 km depth), since we are in the sedimentary environment, while the velocity structure for the PRBC presents higher velocities (\sim 5.5 km/s) at \sim 5 km depth. In addition, the LS18 model has the last layer boundary at a shallower depth (\sim 11 km) than the last layer of the EM18 and SJ18 velocity models (\sim 35 and \sim 18 km, respectively).

The lack of Pn -arrivals in the seismograms of direct and reverse shots does not allow us to estimate the Moho discontinuity. To have an appropriate crustal velocity model for the PRBC, a receiver function study is in progress. Combining the results of this study with those from receiver functions will allow for the development of a more complete velocity model for PRBC-southwestern LS region. Some recent studies, using the receiver function technique, by Persaud *et al.* (2007) and Fernández and Pérez-Campos (2017), have reported results of the Moho depth in a wider area of study (Southern California, Gulf of California and Sonora, Mexico). Although it is a good initial point to constrain our velocity model in northern Baja California, we consider that a receiver function study will give a detailed variation of the Moho depth (from west to east).

IV.7 CONCLUSIONS

Using a refraction study, we determined a P -wave velocity model for the PRBC and southwestern LS, Mexico. To record two time-controlled blasts (one located in southern the city of Ensenada and the other in southwestern LS, BC, Mexico), we installed 30 portable seismic stations, complemented with two permanent stations along a profile. Our modeling of the travel time of P -wave arrivals and normalized amplitudes using asymptotic ray theory resulted in the formation of a 2D crustal velocity model. Our resulting model provides a good fit to the arrival times and relative amplitudes of the seismograms generated by the two blasts.

Because of the complexity of the region (mountain ranges adjacent to sedimentary basins), we divided our model into three flat-layer velocity models; these were EM18 (for city of southern the city of Ensenada to the western side of Ojos Negros Valley), SJ18 (for the Ojos Negros Valley to the eastern side of SJ mountain range [Main Gulf

Escarpment]), and LS18 (for the Main Gulf Escarpment to the southwestern LS). These models differ primarily in the depths of the last layer boundaries, which increase in the southwestern direction, from \sim 11 km (LS) to an inferred \sim 35 km (south of the city of Ensenada). Another difference between the three models is the low-velocity upper layer of LS18 and EM18 that is not present in the SJ18. Regarding the velocity differences, EM18 and SJ18 models have values \sim 1 km/s higher than those of the NB82 model, and the LS18 model has values \sim 2 km/s higher than those of the MVM.

Although we did not have Pn arrivals in any of the record sections, depths of the lowermost boundaries of the three velocity models become shallower from the southwest Ensenada Mountains to the southwestern part of LS, suggesting a decrease of the Moho depth. This is in concordance with results reported from receiver function profiles at \sim 33° N (Ichinose *et al.*, 1996), \sim 31° N (Lewis *et al.*, 2001), and for the Baja California peninsula (Persaud *et al.*, 2007, and Fernández and Pérez-Campos, 2017).

The velocity models reported in this study improve the existing models for Northern BC. We hope that, as a consequence, their use will allow better locations of the regional seismicity.

IV.8 DATA AND RESOURCES

The map was made using the Generic Mapping Tools version 5.3.1, <http://gmt.soest.hawaii.edu/> (last accessed on August 2018).

Some plots were made using the RAYINVR software <http://terra.rice.edu/department/faculty/zelt/rayinvr.html> (last accessed on August 2018).

Data from the Northwestern Mexico Seismic Network are available, since September 10, 2014, from the Incorporated Research Institutions for Seismology Data Management Center (IRISDMC) at <http://ds.iris.edu/mda/BC> (last accessed on November 2018).

The data used in this study are available upon request to María Alejandra Nuñez-Leal. (anunez@cicese.mx).

IV.9 ACKNOWLEDGMENTS

The first author worked thanks to the support of the National Council of Science and Technology of Mexico (CONACYT) under the scholarship no. 254218. The CONACYT provided financial support for this project (CB-2009-133019 SEP-CONACYT). Financial support and facilities were also provided by: The Centro de Investigación Científica y de Educación Superior de Ensenada (CICESE), via the Earth Sciences Division and the Department of Seismology; Autonomous University of Baja California, México (UABC), and its Engineering Institute. The publishing charges were funded by PRODEP 2019 program at the Universidad Autónoma de Baja California, Instituto de Ingeniería, and by CICESE, of the Earth Science Division and the Department of Seismology. José Acosta Chang provided the temporary short-period seismic stations for the project, Gustavo Arellano and Euclides Ruiz provided technical support and

helped during the installation of the temporary stations. For the installation of instrumentation along the profiles we acknowledge: Rogelio Arce, Ignacio Méndez, Oscar Gálvez, Luis Orozco, Rogelio Reyes, German Martínez, Miguel Oliver, Leandro John, and Martín Pacheco, from the Earth Sciences Division of CICESE; Frida Cital, Agustín Oropeza, Erick Jonathan Ramírez, and Iván Ramírez, from the Engineering Institute of the UABC; Jovanny Morán, from the Technical Institute of Ensenada (ITE), BC, México. Sergio Arregui provided the main script used for generating maps in Generic Mapping Tools (<http://gmt.soest.hawaii.edu/>, last accessed May 2016), and he also wrote the programs to download seismic time series from the RESNOM database. Mr. Rafael Barajas-Angulo provided off-road vehicles for the installation of the temporary stations in Mexicali Valley region. Mr. Victor Dukes allowed us to perform the LS-blast on his property. We acknowledge the explosives company (Rivada), especially Glenda Vazquez and Engineer Dagguer, for their support and help during the blast in Laguna Salada. The Ministry of Environmental and Natural Resources (SEMARNAT), the Mexican Secretariat of National Defense (SEDENA), the Government of the State of Baja California, and the Municipality of Mexicali, BC, granted the permits required to perform the blast in Laguna Salada, BC.

IV.10 REFERENCES

Angelier, J., B. Colletta, J. Chorowicz, L. Ortlieb, and C. Rangin (1981). Fault tectonics of the Baja California Peninsula and the opening of the Sea of Cortez, Mexico, J. of Struct. Geol. 3 (4) 347-357, doi: 10.1016/0191-8141(81)90035-3.

Armstrong, P. A., R. R. Perez, L. A. Owen, and R. C. Finkel (2010). Timing and

controls on late Quaternary landscape development along the eastern sierra El Mayor range front in northern Baja California, Mexico, *Geomorphology* 114 (3) 415-430, doi: 10.1016/j.geomorph.2009.08.005.

Axen, G. J. and J. M. Fletcher (1998). Late Miocene-Pleistocene extensional faulting, northern Gulf of California, México, and Salton trough, California, *Int. Geol. Rev.* 40 (3) 217-244, doi: 10.1080/00206819809465207.

Fabriol, H. and L. Munguía (1997). Seismic activity at the Cerro Prieto geothermal area (México) from August 1994 to December 1995, and its relationship with tectonics and fluid exploitation, *Geophys. Res. Lett.* 24 (14) 1807-1810, doi: 10.1029/97GL01669.

Fernández, A. and X. Pérez-Campos (2017). Lithosphere thickness in the Gulf of California region, *Tectonophysics* 719 17-26, <https://doi.org/10.1016/j.tecto.2017.06.016>.

García-Abdeslem, J., J. M. Espinosa-Cardea, L. Munguía-Orozco, V. M. Wong-Ortega, and J. Ramírez-Hernández (2001). Crustal structure from 2-d gravity and magnetic data modeling, magnetic power spectrum inversion, and seismotectonics in the Laguna Salada basin, northern Baja California, Mexico, *Geofís. Int.* 40 (2) 67-86.

González-Escobar, M, C. G. Gallardo-Mata, A. Martín, L. Munguia, and F. Surez-Vidal (2016). Subsurface constraints of an active detachment fault in Laguna Salada Basin, Baja California, México, from interpretation of seismic-reflection profiles, *Geosphere* 12 (4) 1283-1299, <https://doi.org/10.1130/GES01261.1>.

Gonzalez-Ortega, A., Y. Fialko, D. Sandwell, F. A. Nava-Pichardo, J. Fletcher, J.

Gonzalez-Garcia, B. Lipovsky, M. Floyd, and G. Funning (2014). El Mayor-Cucapah (Mw 7.2) earthquake: Early near-field postseismic deformation from InSAR and GPS observations, *J. Geophys. Res.: Solid Earth* 119 (2) 1482-1497, <https://doi.org/10.1002/2013JB010193>.

Hauksson, E., J. Stock, K. Hutton, W. Yang, J. A. Vidal-Villegas, and H. Kanamori (2011). The 2010 Mw 7.2 El Mayor-Cucapah Earthquake Sequence, Baja California, Mexico and Southernmost California, USA: Active Seismotectonics along the Mexican Pacific Margin, *Pure Appl. Geophys.* 168 (8-9) 1255-1277.

Henry, C. D. (1989). Late Cenozoic basin and range structure in western Mexico adjacent to the Gulf of California, *Geol. Soc. Am. Bull.* 101 (9) 11471156, doi: 10.1130/0016-7606(1989)101<1147:LCBARS>2.3.CO;2.

Ichinose, G., S. Day, H. Magistrale, T. Prush, F. Vernon, and A. Edelman (1996). Crustal thickness variations beneath the Peninsular Ranges, southern California, *Geophys. Res. Lett.* 23 (22) 3095-3098, <https://doi.org/10.1029/96GL03020>.

Lewis, J. L., S. M. Day, H. Magistrale, R. R. Castro, C. Rebollar, L. Astiz, J. Eakins, F. L. Vernon, and J. N. Brune (2001). Crustal thickness of the peninsular ranges and gulf extensional province in the Californias, *J. Geophys. Res.* 106 (B7) 13-599, doi: 10.1029/2001JB000178.

Lomnitz, C., F. Mooser, C. R., Allen, J. N. Brune, and W. Thatcher (1970). Seismicity and tectonics of the northern Gulf of California region, México, preliminary results, *Geofís. Int.* 10 3748.

Nava, F. A. and J. N. Brune (1982). An earthquake-explosion reversed refraction line in the Peninsular Ranges of southern California and Baja California Norte, Bull. Seismolo. Soc. Am. 72 (4) 1195-1206.

Nuñez-Cornú, F., J. Frez-Cárdenas, C. Montana, L. Munguía, F. A. Nava, J. J. González-García, L. Mendoza, M. Aragón, C. Sánchez-Mora, M. Morandi, J. Madrid, and Grupo de Perfiles Sísmicos del CICESE (1996). Un modelo de la estructura de corteza para el sistema de fallas de San Andrés en la zona fronteriza México-EEUU, Geotermia, Revista Mexicana de Geoenergía, 12(1) 43-51.

Oskin, M. E., J. R. Arrowsmith, A. Hinojosa-Corona, A. J. Elliott, J. M. Fletcher, E. J. Fielding, P.O. Gold, J. J Gonzalez-Garcia, K. W. Hudnut, J. Liu-Zeng, and O. J. Tern (2012). Near-field deformation from the El Mayor-Cucapah earthquake revealed by differential LIDAR, Science 335 (6069) 702-705, doi: 10.1126/science.1213778 .

Persaud P., X. Pérez-Campos, and R. W. Clayton (2007) Crustal thickness variations in the margins of the Gulf of California from receiver functions, Geophys. J. Int. 170 (2) 687-699, <https://doi.org/10.1111/j.1365-246X.2007.03412.x>.

Ramírez-Ramos, E. E., A. Vidal-Villegas, A. González-Fernández, and J. Stock (2015). A crustal velocity model for the southern Mexicali Valley, Baja California, Mexico, Seismol. Res. Lett. 86 (1) 181-191, doi: 10.1785/0220140007.

Seiler, C., J. M. Fletcher, M. C. Quigley, A. J. Gleadow, and B. P. Kohn (2010). Neogene structural evolution of the Sierra San Felipe, Baja California: Evidence for

proto-gulf transtension in the Gulf Extensional Province?, *Tectonophysics* 488 (1) 87-109, doi: 10.1016/j.tecto.2009.09.026.

Song, J., and T. U. Brink (2005). Graphical user interface for interactive seismic ray tracing, *Eos, Transactions American Geophysical Union* 86 (9) 90-90, <https://doi.org/10.1029/2005EO090004>.

Stock, J. M., A. Martín-Barajas, F. Suárez-Vidal, and M. M. Miller (1991). Miocene to Holocene extensional tectonics and volcanic stratigraphy of NE Baja California, Mexico, in geological excursions in southern California and Mexico, Geological excursions in Southern California and Mexico: guide book, 1991 Annual Meeting, Geological Society of America, San Diego, California, October 21-24, 1991. San Diego State University, San Diego, CA, 44-67.

Suárez-Vidal, F., L. Munguía-Orozco, M. González-Escobar, J. González-García, and E. Glowacka (2007). Surface rupture of the Morelia fault near the Cerro Prieto geothermal field, Mexicali, Baja California, Mexico, during the Mw 5.4 earthquake of 24 may 2006, *Seismol. Res. Lett.* 78 (3) 394-399, doi: 10.1785/gssrl.78.3.394.

Suárez-Vidal, F., R. Mendoza-Borunda, L. M. Nafarrete-Zamarripa, J. Ramírez, and E. Glowacka (2008). Shape and dimensions of the Cerro Prieto pull-apart basin, Mexicali, Baja California, Mexico, based on the regional seismic record and surface structures, *Int. Geol. Rev.* 50 636-649, doi: 10.2747/0020-6814.50.7.636.

Wei, S., E. Fielding, S. Leprince, A. Sladen, J. P. Avouac, D. Helmberger, E. Hauksson, R. Chu, M. Simons, K. Hudnut, T. Herring, and R. Briggs (2011). Superficial simplic-

ity of the 2010 El Mayor-Cucapah earthquake of Baja California in Mexico, *Nature Geoscience* 4 (9) 615-618, doi: 10.1038/ngeo1213.

Zelt, C. A. and R. B. Smith (1992). Seismic travelttime inversion for 2-D crustal velocity structure, *Geophys. J. Int.* 108 16-34, <https://doi.org/10.1111/j.1365-246X.1992.tb00836.x>.

IV.11 MAILING ADDRESS

Erik E. Ramírez - ramirez.erik@uabc.edu.mx

Universidad Autónoma de Baja California (UABC), Instituto de Ingeniería. Calle de la Normal S/N, Insurgentes Este, 21280, Mexicali, Baja California, México.

J. Antonio Vidal-Villegas - vidalv@cicese.mx

Centro de Investigación Científica y de Educación Superior de Ensenada, Baja California (CICESE), Departamento de Sismología, División Ciencias de la Tierra. Carretera Ensenada-Tijuana 3918, Zona Playitas, 22860, Ensenada, Baja California, México.

Jorge Ramíez-Hernandez - jorger@uabc.edu.mx

Universidad Autónoma de Baja California (UABC), Instituto de Ingeniería. Calle de la Normal S/N, Insurgentes Este, 21280, Mexicali, Baja California, México.

Antonio González-Fernández - minmundi@cicese.mx

Centro de Investigación Científica y de Educación Superior de Ensenada, Baja California (CICESE), Departamento de Geología, División Ciencias de la Tierra. Carretera

Ensenada-Tijuana 3918, Zona Playitas, 22860, Ensenada, Baja California, México.

Joann M. Stock - jstock@gps.caltech.edu

California Institute of Technology, Seismological Laboratory, Division of Geological and
Planetary Sciences. Pasadena California 91125 U.S.A.

IV.12 TABLES

Tabla I: Location, time, and weight of explosives for the refraction study of the PRBC.

Blast	Load of explosives (kg)	Latitude (°)	Longitude (°)	Origin time, UTC (yyyy/mm/dd hh:mm:ss.ss)
(A) South Ensenada, B.C., Mexico.	2900	31.7689	-116.5462	19/05/2015 21:51:07.46
(B) Laguna Salada, B.C., B.C., Mexico.	380	32.0251	-115.6406	06/12/2016 13:06:10.07

Tabla II: Coordinates of stations that recorded the blast A.

Station	Latitude (°)	Longitude (°)	Elevation (m)	Distance from blast A (km)
B081	31.7655	-116.5575	30	-0.94
B082	31.7709	-116.5549	84	-0.61
B080	31.7439	-116.5441	35	0.68
B086	31.765	-116.5368	38	1.13
QS145	31.7865	-116.5058	77	4.48
QS156	31.7976	-116.4435	196	10.44
QS157	31.8424	-116.303	825	24.68
QS147*	31.8423	-116.2716	760	27.47
QS148*	31.8581	-116.2232	737	32.38
QS133*	31.8787	-116.195	757	35.64
QS126	31.8809	-116.1492	854	39.82
QS146	31.8889	-116.1099	973	43.64
QS152*	31.9059	-116.0824	1221	49.66
QS151	31.9108	-116.0456	1323	50.17
QS138*	31.9218	-116.0001	1564	54.65
QS153	31.9256	-115.986	1530	56.05
QS154*	31.9329	-115.9721	1536	57.55
SJX†	32.0047	-115.9476	1611	62.3
QS140*	31.9491	-115.8998	1755	64.61
QS131*	31.97	-115.8278	1558	70.91

The first two digits in the station code indicate the type of sensor: B0, ES-T accelerometers; QS, short period SARA stations. The last 3 digits are the last 3 numbers of the digitizer used. Negative distance values indicate western location from the blast A.

* Stations deployed for the seismic refraction profile but not recorded the blast A.

† Station belonging to RESNOM.

IV.13 FIGURE CAPTIONS

Figure 1: The two main geological provinces of northern BC, México, and, in the inset, the tectonic context of the interaction and boundary of the North America and Pacific plates; dark-gray area represents the Gulf Extensional Province. The detailed map shows the locations of the shots A (yellow star) and B (blue star) that were used for the seismic refraction profile (thin white line). Temporary stations used in the modeling

Tabla III: Coordinates of stations that recorded the blast B.

Station	Latitude (°)	Longitude (°)	Elevation (m)	Distance from blast A (km)
SJPMD	31.7944	-116.4723	151	7.41
SN553	31.8305	-116.3948	320	15.61
SN552*	31.843	-116.303	820	24.29
SN546	31.8421	-116.2709	764	27.14
SS126	31.8622	-116.2255	727	31.91
SS142	31.878	-116.1955	752	35.15
SS136	31.881	-116.1492	857	39.41
SS156	31.906	-116.0824	1218	46.27
SS147*	31.9107	-116.0456	1319	49.73
SS150	31.9218	-115.9999	1581	54.22
SS146	31.9328	-115.9722	1535	57.08
SS137	31.9435	-115.9288	1705	61.34
SS157	31.9491	-115.8998	1750	64.13
SS149	31.9699	-115.8278	1552	71.04
ALAMX	32.0068	-115.709	320	83.24
VN152	32.0248	-115.6825	268	86.25
VN362	32.0251	-115.6404	166	90.02

The first two letters in the station code indicate the type of sensor: SN, Nanometrics Trillium Compact with Taurus recorder; SS, short period SARA stations; VN, Nanometrics Titan accelerometers with Centaur recorders. SJPMD is the intermediate-band PMD sensor. The last 3 digits are the last 3 numbers of the digitizer used.

* Stations deployed for the seismic refraction profile but not recorded the blast B.

† Station belonging to RESNOM.

Tabla IV: Coordinates of stations that recorded the blast B.

Models														
PRBC region						MV region								
EM18			SJ18			NB82			LS18			MVM	P-wave	SMVM
Depth (km)	Mean P-wave velocity (km/s)	Depth (km)	Mean P-wave velocity (km/s)	Depth (km)	Mean P-wave velocity (km/s)	Depth (km)	Mean P-wave velocity (km/s)	Depth (km)	Mean P-wave velocity (km/s)	Depth (km)	Mean P-wave velocity (km/s)	Depth (km)	P-wave velocity (km/s)	
0 -	4.1	-1.8*	5.6	0.0 -	5.6	0 -	3	0.0 -	1.7	0.00 -	1.90 -			
1.4		4.5		5		1.6		0.1		1.23	3.81			
1.4 -	6.5	4.5 -	6.8	5.0 -	6.6	1.6 -	5	0.1 -	2	1.23 -	4.77 -			
6.6		9.5		19.8		4.8		0.7		5.60	6.30			
6.6 -	6.9	9.5 -	7.3	19.8 -	7	4.8 -	6.6	0.7 -	2.3	5.60 -	6.54 -			
10.9		18.2		41.8		8.0		1.8		15.25	7.18			
10.9 -	7.3	18.2 -	7.9	41.8 -	8	8.0 -	7.4	1.8 -	2.6	15.27 -	7.65 -			
35.4						11.3		2.9						
35.4 -	8	-	-	-	-	11.3 -	7.8	2.9 -	3					
								5.6						
								5.6 -	5					
								10.0						
								10.0 -	6					
								20.0						
								20 -	7.8					

* This value represents the altitude a.m.s.l. due the consideration of topography of the PRBC.

process (black inverted triangles), and permanent broadband stations (white diamonds) belonging to the RESNOM are also shown. The gray circle indicates the ELS-3 well, and the black line below 4965 indicates a seismic reflection profile (González-Escobar et al., 2016). Previous refraction studies in the region are shown as: purple line, Nava and Brune (1982); blue line, Nuñez-Cornú et al. (1996); orange line, Ramírez-Ramos *et al.* (2015). The dashed black line represents the limit of the Main Gulf Escarpment in northern BC. Gray star indicates the location of the 2010 Mw 7.2 El Mayor-Cucapah earthquake. Gray circles show the seismicity $M > 3.4$ since 1990 reported by RESNOM. Regions or sites: PRBC, Peninsular Ranges of Baja California; MV, Mexicali Valley; LS, Laguna Salada; SLRC, San Luis Río Colorado; EMM, El Mayor Mountains; CM, Cucapah Mountains; SJM, Sierra Juárez Mountains, SPM, Sierra San Pedro Martir; ONV, Ojos Negros Valley; EM, Ensenada Mountains. The main faults (red labels), that crosses the refraction profiles, of northern Baja California and southern California regions shown are: SPMF, San Pedro Martir fault; ABF, Agua Blanca fault; SDF, San Diego fault; SCF, San Clemente, fault; THF, Tres Hermanos fault; SMF, San Miguel fault; VF, Vallecitos fault; SJF, Sierra Juárez fault; CDDF, Cañada David detachment fault; LSF, Laguna Salada fault; CF, Cucapah fault; CPF, Cerro Prieto fault; IF, Imperial fault; AF, Algodones fault; EF, Elsinore fault; CRF, Cañon Rojo fault; InF, Indiviso fault. Locations of plotted faults (red lines) were obtained from Seiler *et al.* (2010).

Figure 2: (a) Elevations along the Ensenada - southwestern LS profile (thin white line of Fig. 1). Both record sections have a travel-time reduction and are shown with offset distance relative to blast A. (b) Record section that recorded the blast A (Table 2). (c) Record section from station SJPMD to VN362 (Table 3) that recorded the blast B. Notation of interpreted phases that are also explained in the INTERPRETED

PHASES section: PS_{n,m}, where: S can be A or B for blasts; n indicates the number of the phase; m can be 1 or 2, which means a refraction or reflection phase, respectively.

Figure 3: Plots that illustrate the process of forward modeling using the direct blast (A, Table 1). (a) Ray tracing through the proposed velocity model. (b) Calculated travel times (black lines) and readings of interpreted phases (vertical bars), both plotted with travel-time reduction. (c) Synthetic seismograms of normalized amplitudes plotted with travel-time reduction. Interpreted phases are labeled for comparison to the ones observed in the record section of the blast A (Fig. 2b).

Figure 4: Plots that illustrate the process of forward modeling using the reverse blast (B, Table 1). (a) Ray tracing through the proposed velocity model. (b) Calculated travel times (black lines) and readings of interpreted phases (vertical bars), both plotted with travel-time reduction. (c) Synthetic seismograms of normalized amplitudes plotted with travel-time reduction. Interpreted phases are labeled for comparison to the ones observed in the record section of the blast B (Fig. 2c).

Figure 5: (a) Crustal velocity model for the PRBC and the southwestern part of LS of the refraction profile (thin line Fig. 1). This model was obtained by forward modeling using a direct and reverse blast (Fig. 2 to 4). Thick black lines indicate from top to bottom: elevation; basement of the low-velocity layers in the Ensenada Mountains and LS model sections; the last velocity gradient interface proposed. Dashed lines indicated the inferred layer boundaries. Color bar to the right indicates the *P*-wave velocity in km/s. (b) and (c) detailed insets of the dashed-line rectangles of (a) with the same velocity color code of (a).

Figure 6: Comparison of the velocity models resulting from this work with previous crustal velocity models. (a) Comparison of our EM18 and SJ18 velocity models with NB82 (Nava and Brune, 1982). The main difference is SJ18 and EM18 have velocities that are ~ 1 km/s higher than the NB82 model. (b) Comparison of our LS18 velocity model with the one used in the MV region (MVM; Fabriol and Munguía, 1997). The velocities in LS18 are ~ 2 km/s higher than those of MVM.

IV.14 FIGURES

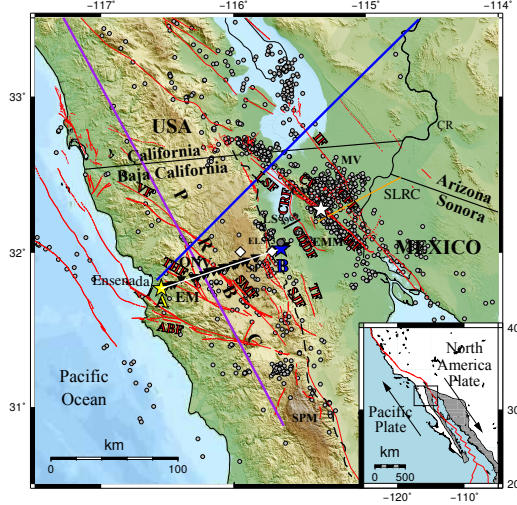


Figura 1: The two main geological provinces of northern BC, México, and, in the inset, the tectonic context of the interaction and boundary of the North America and Pacific plates; dark-gray area represents the Gulf Extensional Province. The detailed map shows the locations of the shots A (yellow star) and B (blue star) that were used for the seismic refraction profile (thin white line). Temporary stations used in the modeling process (black inverted triangles), and permanent broadband stations (white diamonds) belonging to the RESNOM are also shown. The gray circle indicates the ELS-3 well, and the black line below 4965 indicates a seismic reflection profile (González-Escobar et al., 2016). Previous refraction studies in the region are shown as: purple line, Nava and Brune (1982); blue line, Nuñez-Cornú et al. (1996); orange line, Ramírez-Ramos et al. (2015). The dashed black line represents the limit of the Main Gulf Escarpment in northern BC. Gray star indicates the location of the 2010 Mw 7.2 El Mayor-Cucapah earthquake. Gray circles show the seismicity $M > 3.4$ since 1990 reported by RESNOM. Regions or sites: PRBC, Peninsular Ranges of Baja California; MV, Mexicali Valley; LS, Laguna Salada; SLRC, San Luis Río Colorado; EMM, El Mayor Mountains; CM, Cucapah Mountains; SJM, Sierra Juárez Mountains, SPM, Sierra San Pedro Martir; ONV, Ojos Negros Valley; EM, Ensenada Mountains. The main faults (red labels), that crosses the refraction profiles, of northern Baja California and southern California regions shown are: SPMF, San Pedro Martir fault; ABF, Agua Blanca fault; SDF, San Diego fault; SCF, San Clemente, fault; THF, Tres Hermanos fault; SMF, San Miguel fault; VF, Vallecitos fault; SJF, Sierra Juárez fault; CDDF, Cañada David detachment fault; LSF, Laguna Salada fault; CF, Cucapah fault; CPF, Cerro Prieto fault; IF, Imperial fault; AF, Algodones fault; EF, Elsinore fault; CRF, Cañon Rojo fault; InF, Indiviso fault. Locations of plotted faults (red lines) were obtained from Seiler et al. (2010).

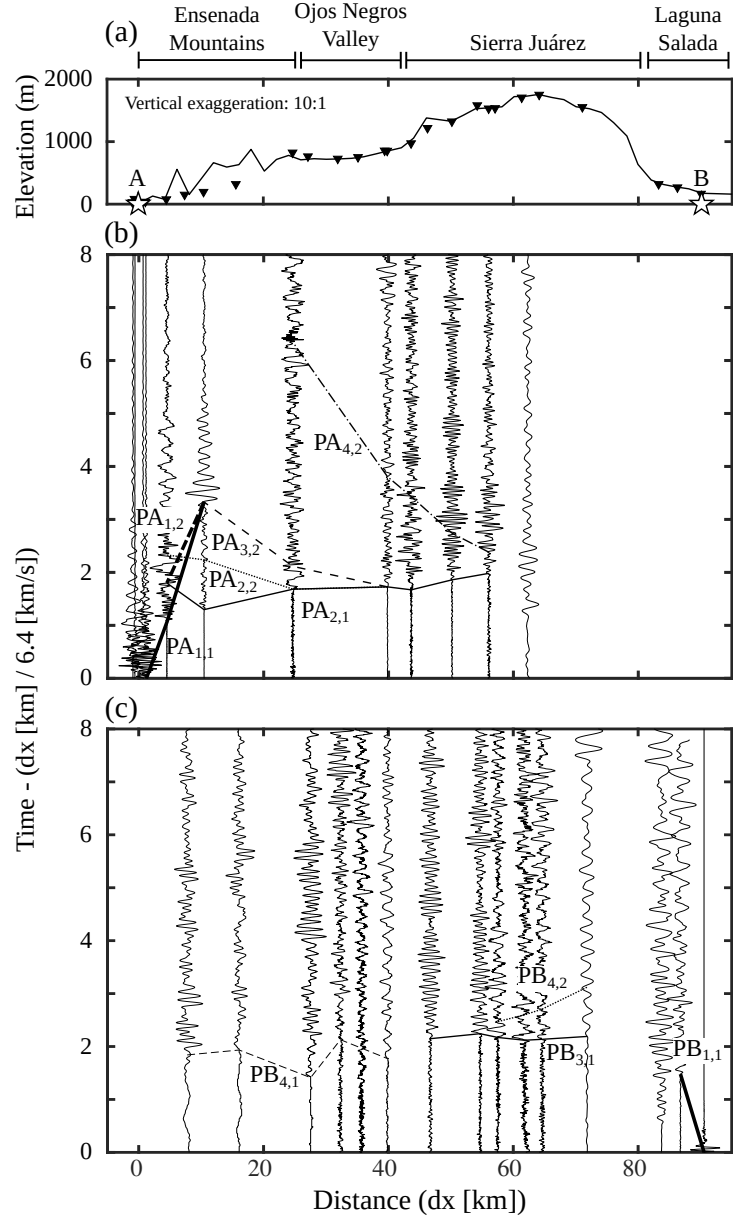


Figura 2: (a) Elevations along the Ensenada - southwestern LS profile (thin white line of Fig. 1). Both record sections have a travel-time reduction and are shown with offset distance relative to blast A. (b) Record section that recorded the blast A (Table 2). (c) Record section from station SJPMD to VN362 (Table 3) that recorded the blast B. Notation of interpreted phases that are also explained in the INTERPRETED PHASES section: PSn,m, where: S can be A or B for blasts; n indicates the number of the phase; m can be 1 or 2, which means a refraction or reflection phase, respectively.

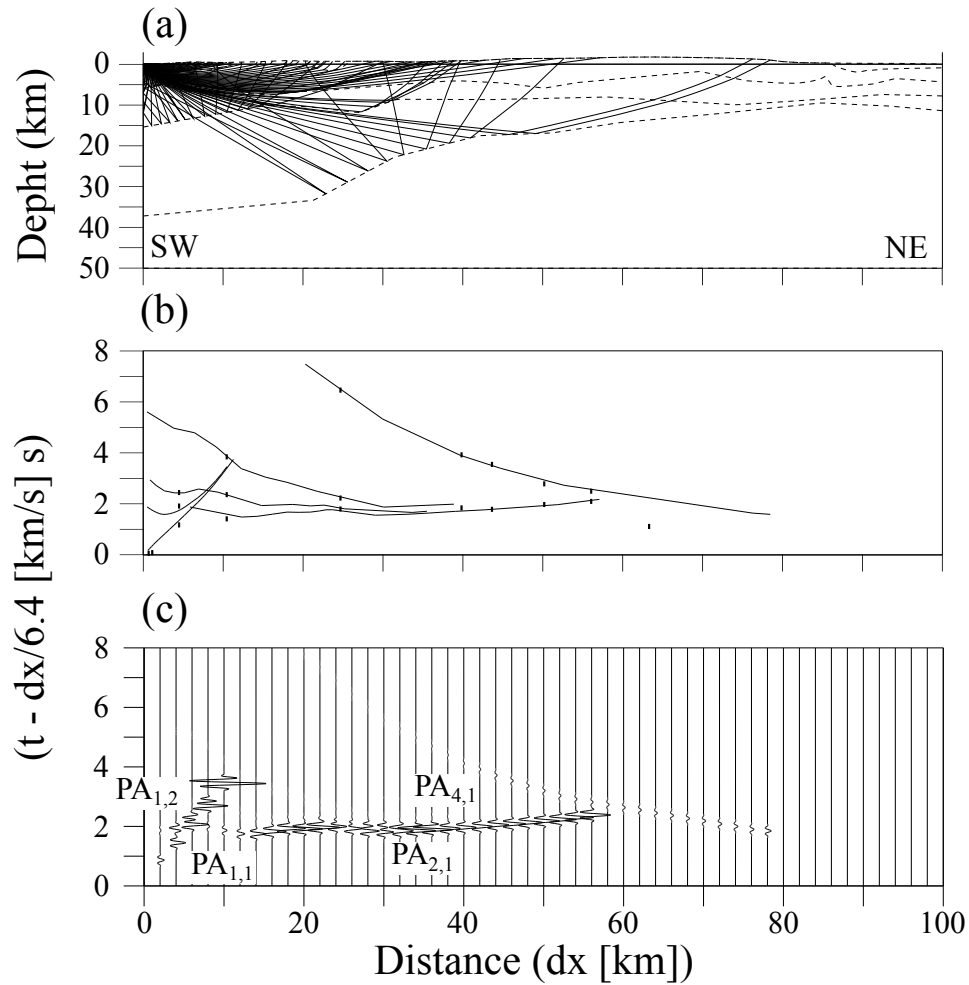


Figura 3: Plots that illustrate the process of forward modeling using the direct blast (A, Table 1). (a) Ray tracing through the proposed velocity model. (b) Calculated travel times (black lines) and readings of interpreted phases (vertical bars), both plotted with travel-time reduction. (c) Synthetic seismograms of normalized amplitudes plotted with travel-time reduction. Interpreted phases are labeled for comparison to the ones observed in the record section of the blast A (Fig. 2b).

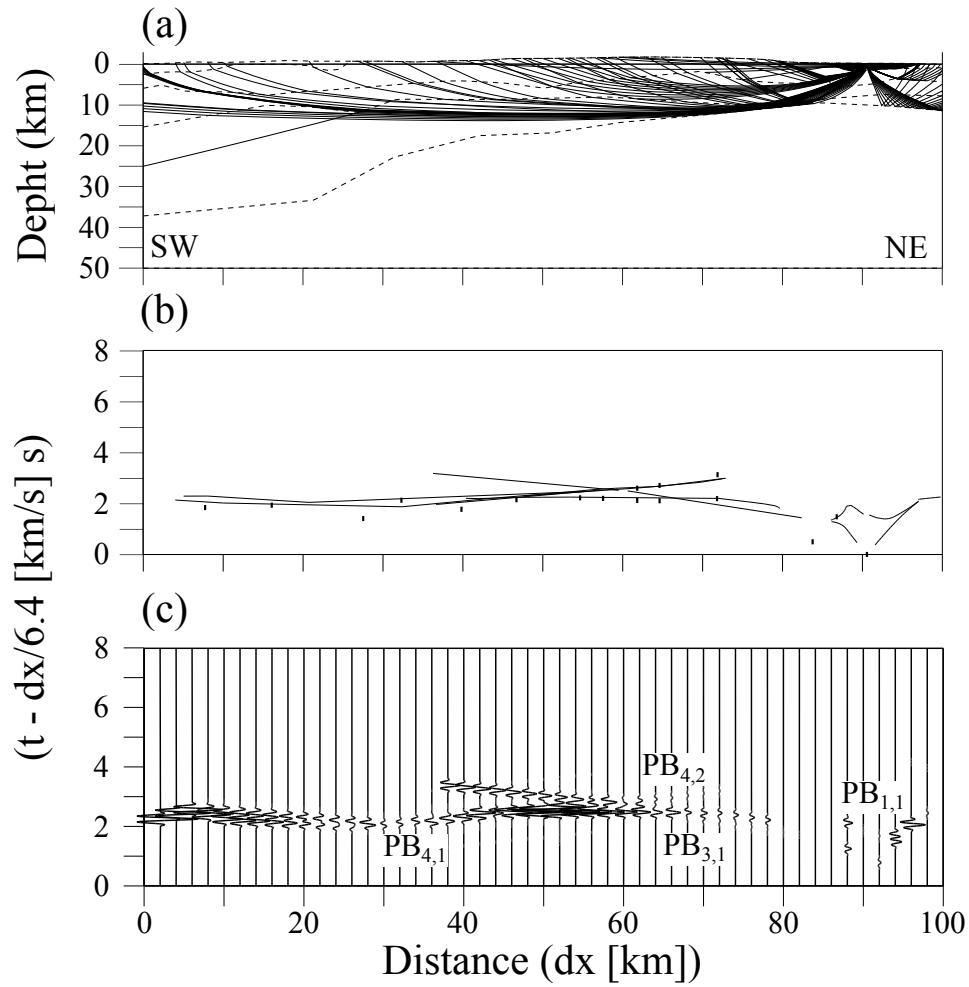


Figura 4: Plots that illustrate the process of forward modeling using the reverse blast (B, Table 1). (a) Ray tracing through the proposed velocity model. (b) Calculated travel times (black lines) and readings of interpreted phases (vertical bars), both plotted with travel-time reduction. (c) Synthetic seismograms of normalized amplitudes plotted with travel-time reduction. Interpreted phases are labeled for comparison to the ones observed in the record section of the blast B (Fig. 2c).

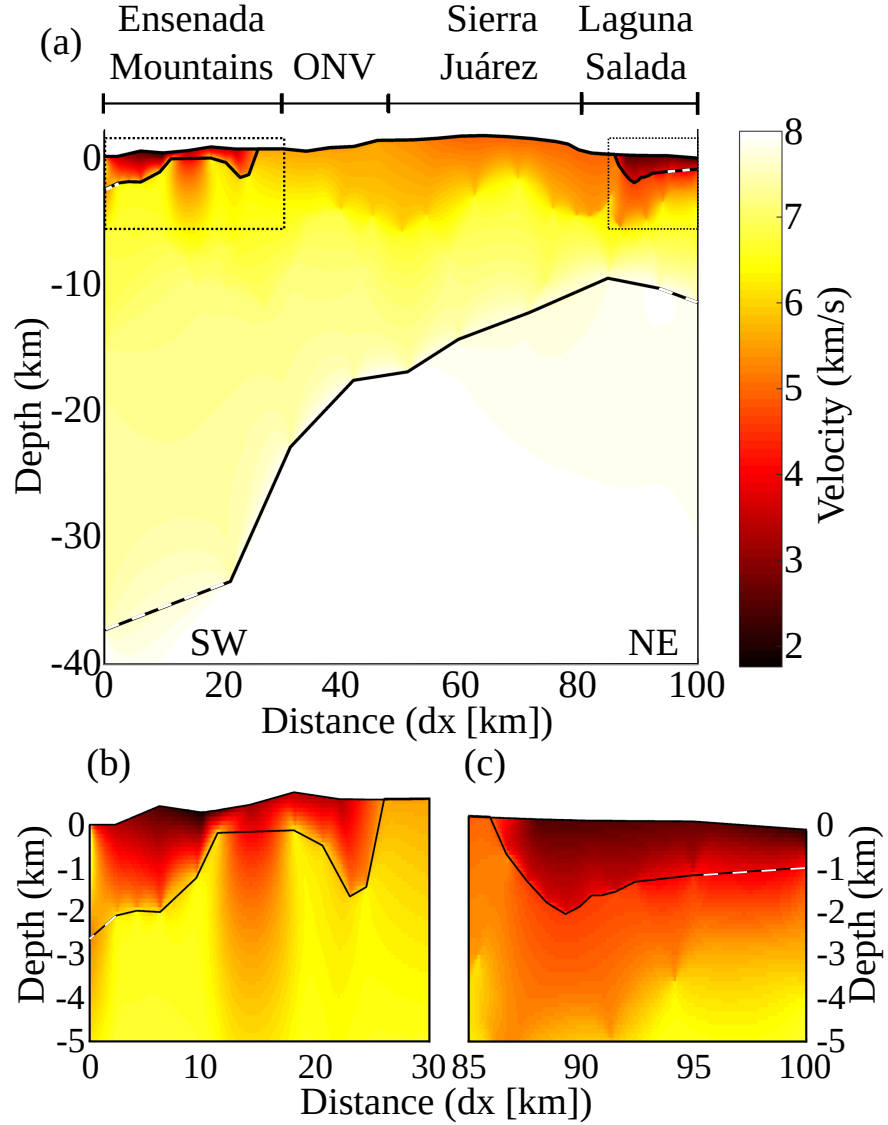


Figura 5: (a) Crustal velocity model for the PRBC and the southwestern part of LS of the refraction profile (thin line Fig. 1). This model was obtained by forward modeling using a direct and reverse blast (Fig. 2 to 4). Thick black lines indicate from top to bottom: elevation; basement of the low-velocity layers in the Ensenada Mountains and LS model sections; the last velocity gradient interface proposed. Dashed lines indicated the inferred layer boundaries. Color bar to the right indicates the P -wave velocity in km/s. (b) and (c) detailed insets of the dashed-line rectangles of (a) with the same velocity color code of (a).

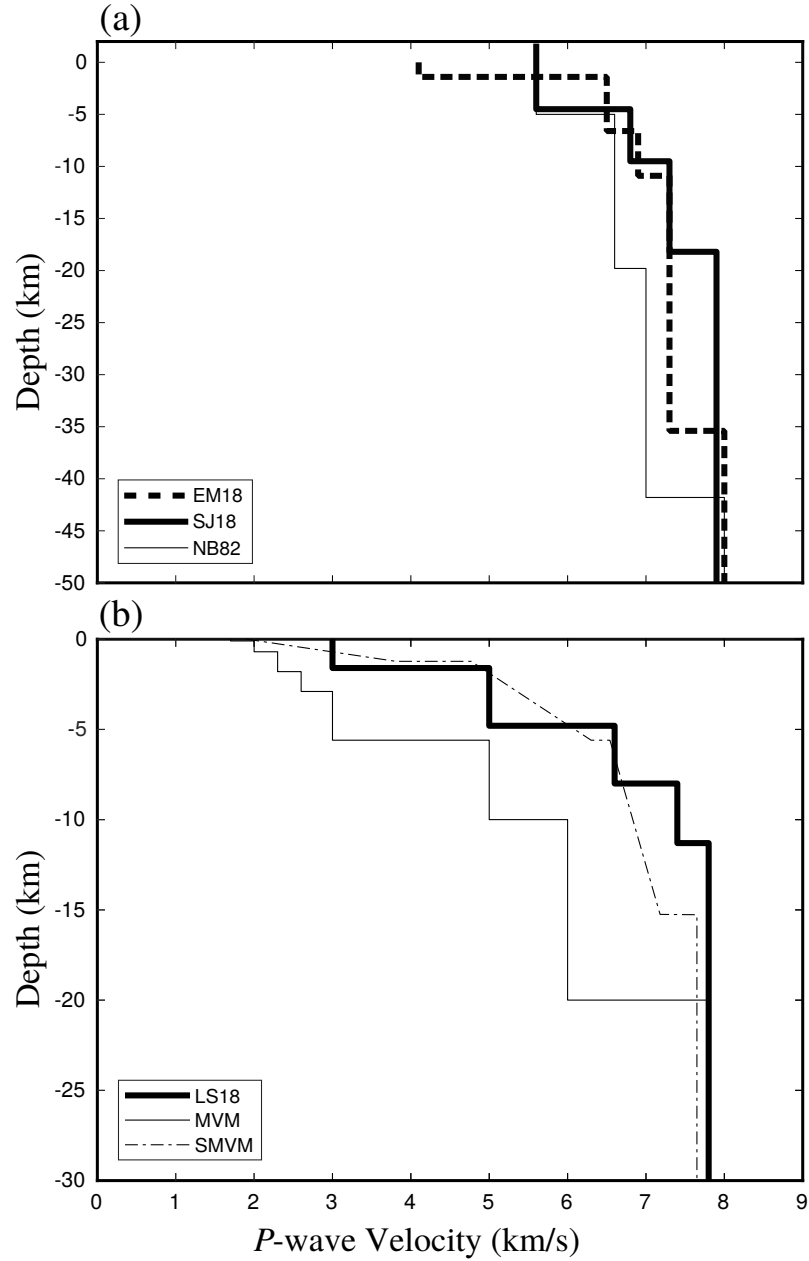


Figura 6: Comparison of the velocity models resulting from this work with previous crustal velocity models. (a) Comparison of our EM18 and SJ18 velocity models with NB82 (Nava and Brune, 1982). The main difference is SJ18 and EM18 have velocities that are ~ 1 km/s higher than the NB82 model. (b) Comparison of our LS18 velocity model with the one used in the MV region (MVM; Fabriol and Munguía, 1997). The velocities in LS18 are ~ 2 km/s higher than those of MVM.